ECOLE DOCTORALE SCIENCES DE L'INGÉNIEUR DE LILLE EDSPI no. d'ordre: 41801

UNIVERSITÉ DE LILLE 1

LABORATOIRE CRIStAL - UMR 9189

Contribution à l'Estimation et au Diagnostic robuste des Piles à Combustibles basse température

---

Thèse

Présentée en vue d'obtenir le titre de Docteur

(Spécialité Automatique, Génie Informatique et Traitement de Signal)

par

Severus Constantin OLTEANU

Soutenue le 06 Novembre 2015

Rapporteurs:	Dominique SAUTER	Professeur, Université de Lorraine
	Mohamed BECHERIF	MdC-HDR, Université de Technologie de Belfort-Montbéliard
Examinateurs:	Jérôme BOSCHE	MdC, Université de Picardie Jules Verne
	Nicolaï CHRISTOV	Professeur, Université de Lille 1
Superviseurs:	Lotfi BELKOURA	Professeur, Université de Lille 1
	Abdel AITOUCHE	Professeur, HEI Lille

ECOLE DOCTORALE SCIENCES DE L'INGÉNIEUR DE LILLE EDSPI order no.: 41801

UNIVERSITY OF LILLE 1

CRISTAL LABORATORY - UMR 9189

Contribution to robust State Estimation and Diagnostic of low temperature Fuel Cell systems

---

Dissertation

Submitted for the degree of Doctor of Philosophy

(Specialty Automatics, Computer Engineering and Signal Processing)

by

Severus Constantin OLTEANU

Reporters:	Dominique SAUTER	Professor, University of Lorraine
	Mohamed BECHERIF	Associate Professor, University of Technology of Belfort-Montbéliard
Examiners:	Jérôme BOSCHE	Associate Professor, University of Picardie Jules Verne
	Nicolaï CHRISTOV	Professor, University of Lille 1
Supervisors:	Lotfi BELKOURA	Professor, University of Lille 1
	Abdel AITOUCHE	Professor, HEI Lille

Acknowledgment

Firstly I would like to extend my wholehearted appreciation to Prof. Aitouche, that has been for me not only a supervisor, but also a mentor during this three year journey of research. I express my thanks for his continuous and invaluable support.

I also owe my sincerest gratitude to Prof. Belkoura, for giving me the opportunity and the trust to carry on the thesis.

It is with the utmost respect that I acknowledge the immeasurable help of Prof. Sauter and Dr. Becherif for accepting to analyze this manuscript.

Also, I recognize with esteem the affability of Prof. Christov and Dr. Bosche for approving to examine this thesis.

I undoubtedly have to mention my professors, colleagues and friends from the CRIStAL laboratory, whose pleasant technical interactions have always helped me to get unstuck from difficulties and encouraged my thirst for knowledge.

This period would have been more difficult without the support from my dearest friends, to whom I send my warmest 'thank you'.

Finally, my heartfelt thanks and gratitude goes to my parents and brother for their continual support and encouragement. Their presence acted as an anchor in the stormy and foggy reality of the PhD years.

Contents

List of publications i

Abbreviations and Acronyms iii

1 Introduction 1

2 On Takagi-Sugeno State Estimation 11

3 Fault Detection and Isolation 45

4 On nonlinear embedded system development 65

5 Application: Fuel Cell System 103

6 Conclusions and Perspectives 153

Appendices 157

A Significance of Fuel Cell parameters 159

B Physical Fuel Cell platform 163

C Chapter Embedded 173

List of publications

International Journals:

1. Olteanu, S.C., Aitouche, A., Belkoura, L., Advanced embedded nonlinear observer design and HIL validation using a Takagi-Sugeno approach with unmeasurable premise variables, Journal of Physics: Conference Series, vol 570, no. 2, 2014.
2. Olteanu, S.C., Aitouche, A., Belkoura, L., Embedded P.E.M fuel cell stack nonlinear observer by means of a Takagi-Sugeno approach, Studies in Informatics and Controls, ICI Publishing House, vol . 24, no 1, pp. 61-70, 2015.

International Conference Articles:

1. Olteanu, S.C., Aitouche, A.,Oueidat, M., Jouni, A., Fuel Cell diagnosis using Takagi-Sugeno observer approach, Renewable Energies for Developing Countries (REDEC), 2012 International Conference on., IEEE, pp.1-7, Lebanon, Beirut, November 2012.
2. Aitouche, A., Olteanu, S.C., Ould Bouamama, B., A survey on diagnostic of Fuel Cell systems, IFAC Symposium SAFEPROCESS-2012: Fault Detection, Supervision and Safety, vol. 8, no 1, pp. 84-89, Mexico, Mexico City, August 2012.
3. Olteanu, S.C.; Gouni, W.; Aitouche, A.; Belkoura, L., Nonlinear observer for P.E.M. Fuel Cells using a Takagi-Sugeno approach with unmeasurable premise variables, Systems and Control (ICSC), 2013 3rd International Conference on , vol., no., pp.193,199, 29-31 Oct. 2013.

4. Olteanu, S.C., Aitouche, A., Belkoura, L., Advances in P.E.M. Fuel Cell stack observer design using Takagi-Sugeno approach with unmeasurable premise variables, ICREGA 2014 Renewable Energy: Generation and Applications, Springer Proceedings in Energy, Chapter 10, pp. 117-130, 2014.

5. Feingesicht, M., Olteanu, S.C., Aitouche, A.,Belkoura, L., HIL Validation of an Embedded System Acting as a Nonlinear Takagi-Sugeno State Observer on an Arduino Board, Education and Research Conference (EDERC), 2014 6th European Embedded Design in, pp. 250-254, Italy, Milan, September 2014.

Abbreviations and Acronyms

TS	Takagi-Sugeno
FC	Fuel Cell
FCS	Fuel Cell System
PEM	Proton Exchange Membrane or Polymer Electrolyte Membrane
LMI	Linear Matrix Inequality
LME	Linear Matrix Equality
LPV	Linear Parameter Varying
BME	Bilinear Matrix Equality
PDC	Parallel Distributed Compensation
MIMO	Multi Input Multi Output
FDI	Fault Detection and Isolation
FDD	Fault Detection and Diagnostic
PIO	Proportional Integral Observer
DOS	Dedicated Observer Scheme
HIL	Hardware In the Loop
UIO	Unknown Integral Observer

List of Figures

1.1 Classification of different approaches for Diagnostics of FCSS 7

2.1 Observer block diagaram 12
2.2 Sector Nonlinearity - one dimensional Membership Function example 19
2.3 Min / Max, membership function example 20

3.1 Fault in the sensor return pressure manifold and its reconstruction 47

4.1 Entire Arduino system with Ethernet shield and LCD . . . 72
4.2 IEEE754 floating point format in 16 and 32 bit configuration 73
4.3 An example of 0b01010101 signal TTL and RS-232 77
4.4 a) One on One connection b) One master, multiple slaves connection 78
4.5 Proteus simulation showing 8 bit communication 79
4.6 Physical implementation of the parallel configuration . . . 80
4.7 Schematic of parallel computation 83
4.8 Arduino Ethernet shield 84

4.9 HIL connection diagram for testing 84
4.10 Logical diagram of the Arduino pseudo-code 85
4.11 Simulation Configuration Parameters 87
4.12 Interface for the Stream Input block || Interface for the Stream Output block 88
4.13 Hardware implementation 89
4.14 Logical diagram of Arduino code 90
4.15 Three tanks system representation 91
4.16 Simulink diagram including co-simulation block 94
4.17 AMESim implementation of the three tank system 95
4.18 Estimation error dynamics of the 3 heights (tank 1, 2 and 3) 96
4.19 Real/Estimated water levels evolution 96
4.20 Missed ticks for the measured premise variables observer calculated by Arduino in real-time 97
4.21 AMIRA DTS 200 system 97
4.22 AMIRA DTS 200 estimation error dynamics in time 98
4.23 AMIRA DTS 200 with faults injected in time 99
4.24 PCI 6024 E acquisition board 100

5.1 Functional behavior of a hydrogen Fuel Cell 105
5.2 Block view of fuel cell stack with auxiliary elements 108
5.3 General Observer Schema adapted to our FC System . . . 115
5.4 The evolution of the real and estimated values of the Oxygen Pressure in the cathode 122

5.5 The evolution of the estimation error for all the states (Lipschitz method) 123

5.6 Stabilization of the estimation error, for Return Manifold/Supply Manifold Pressures(Lipschitz method) 124

5.7 The vapor Pressure present inside the cathode volume . . 125

5.8 The estimation error dynamics of the states (bounded observer) 126

5.9 The estimation in parallel with the real value for Pressure O2 126

5.10 General Observer logic adapted to our FC system 127

5.11 Evolution of the Pressure in the Supply Manifold 131

5.12 Supply Manifold pressure estimation, in robust and non-robust cases 131

5.13 Cathode mass evolution 132

5.14 Cathode mass estimation error 132

5.15 The Amesim model of the PEM FC 133

5.16 Unmeasured premise variables observer error(difference between real and estimated value) for the gas masses of the oxygen supply of the PEMFC 134

5.17 Pressure estimation error of the oxygen supply of the PEMFC135

5.18 Real time observer values for the pressures of the oxygen supply of the PEMFC 135

5.19 Fault trees of Fuel Cell Stack System 137

5.20 Fault in Supply Manifold Pressure Sensor 145

5.21 Fault estim/real in the Supply Manifold pressure sensor . 145

5.22 Cathode mass estimation 146

5.23 Cathode mass estimation 146

5.24 The 3 rd derivative of the fault 147

5.25 Real and estimated fault acting on the SM pressure 148

5.26 SM pressure affected by the fault 148

5.27 SM pressure affected by the fault 148

5.28 Cathode side mass estimation error dynamics 149

5.29 Cathode side pressure estimation error dynamics 149

5.30 Cathode side mass estimated / real 150

5.31 Cathode side pressure estimated / real 150

A.1 List 1 of Fuel Cell Parameters 159

A.2 List 2 of Fuel Cell Parameters 159

A.3 List 3 of Fuel Cell Parameters 160

B.1 Heliocentris FC-42 platform 163

B.2 Block view of the platform with characteristic parameters 165

B.3 (low capacity H2 tank) Time evolution of FC/load power, voltage and current 166

B.4 (high capacity H2 tank) Voltage, temperature and current dynamics 167

B.5 (small H2 tank) Power and hydrogen Pressure 167

B.6 (big H2 tank) FC power and air excess 168

B.7 (small H2 tank) FC power and air excess 168

B.8 Labview program 169

B.9 Data received by the dedicated software 170

B.10 Obtained graphics from the data 171

B.11 Block view of fuel cell stack with auxiliary elements 171

C.1 Communication timing 175

C.2 Interface for the Packet Input block || Interface for the Packet Output block 175

List of Tables

4.1 Microcontroller boards 70
4.2 Atmega2560 characteristics 76
4.3 Distributed computation code 82

5.1 Premise variables's min/max values 113

A.1 Parameter values of the FC 160

Chapter 1

Introduction

1.1 Motivation and background 1
1.2 Literature review 3
1.2.1 Fuel Cell State Estimation approaches 4
1.2.2 Fuel Cell Diagnostic approaches 6
1.2.2.1 *Classification of Diagnostics methods for FCS* 6
1.2.2.2 *Observer based diagnostic* 8
1.3 Contribution 9
1.4 Dissertation stucture 10

1.1 Motivation and background

This thesis was carried out in the CRIStAL laboratory (Center for Research in Informatics, Signal and Automatics of Lille) CNRS-UMR 9189, at the University of Lille 1. The work was partly carried out in the framework of PN-7-022-BE i-MOCCA (Interregional Mobility and Competence Centres in Automation), an European territorial cooperation project part-funded by the European Regional Development Fund (ERDF) through the INTERREG IV A 2 Seas Programme and the Ministry of Education and Research, France.

Three major inter-correlated objectives/thematics are targeted in the thesis, these being:

- the problematic of nonlinear Takagi-Sugeno (TS) approach which is a method that is still open to testing and improvements
- the problematic of implementing nonlinear algorithms on small scale embedded systems
- the application of these aspects on mobile Fuel Cell Systems (FCSs)

These aspects, seen as a whole with their interrelations and raised difficulties, come as the contribution of the thesis.

Analyzing each of the three in part, we start by the Takagi-Sugeno approach of treating nonlinear systems. This methodology, still in development and testing, proves its efficiency, especially taken in the context of embedded nonlinear algorithms as it presents a structured form and development procedure as well as an easiness in implementation for both state estimation and diagnostics. The TS method has started with Sugeno's work in the 1980s from a fuzzy point of view and passing to its nonlinear state space expression in the end of 1990s (the work of Tanaka in 2001 being conclusive Tanaka and Wang (2001)). Also concerning the implementation of complex model based algorithms on embedded systems there are papers since the end of the 1980's as Sinha (1986).

Fuel Cells are electrochemical energy conversion devices that convert hydrogen and oxygen into water, producing electricity and heat in the process. Hydrogen is one of the best alternatives for fossil energy in the international context of pollution reduction, being targeted as the energy vector of the future. Thus it can be used for managing the energy in renewable energy generation, storing then re-generating energy when required and also for acting as high density fuel in the automotive industry. For vehicle applications, a Fuel Cell (FC) brings a high power density and low weight, no direct pollution and a fast recharging rate by means of hydrogen fuel stations.

Recently, the research community of fuel cells has shown a considerable interest for automatics, both for its role as system integrator, as well as for developing diagnosis tools in view to ensure safety, security, and availability when faults occur in the process, or for parameter estimation as a cost reduction method. These faults must be detected early on and be estimated in order to accommodate the system response. They are extremely vulnerable to faults that can cause the stop or the permanent damage of the fuel cell. To guarantee the safe operation of the fuel cell systems, it is necessary to use systematic techniques to detect and isolate faults.

The thesis is done in a time frame when Fuel Cells are showing their potential and their unavoidable adoption as common industrial energy converters. The fact that there are still variations in the types and materials used for the Fuel Cell construction (therefore a still varying behavioral model), emphasizes an imperative need to prepare the way for numerical techniques that can be adopted to different general models of FC stacks. These numerical techniques have to present themselves not only generally adaptable to different models but also capable of being implemented on embedded systems.

A Fuel Cell has been used to configure the simulated testing. The Fuel Cell itself and the testing results are presented in the Appendix B.

1.2 Literature review

FC science and technology cuts across multiple disciplines, including materials science, transport phenomena, electro-chemistry and catalysis science. It is always a major challenge to fully understand the thermodynamics, fluid mechanics, FC dynamics, and electrochemical processes within a FC. Even at this date, the industrial Fuel Cells developed do not manifest a perfectly constant behavior, still presenting a certain variation in the model for any same FCs produced at different times. These are the reasons why the energy generation systems based on FCs are so complex.

Moreover, these systems need a set of auxiliary elements (valves, compressor, sensors, controllers, etc.) to make the FC work at the pre-established optimal operating point. As such, they are vulnerable to faults that can cause the stop or the permanent damage of the FC. To guarantee the safe operation of the FCS, it is necessary to use systematic techniques to detect and isolate faults for the purpose of diagnostic.

To measure the physical variables of a fuel cell system (FCS), several sensors were installed: flow and pressure of hydrogen, air flow, current and velocity of compressor, water pressure coming out of stack current, voltage and temperature of the stack. Sometimes, electrical storage devices are used to prevent any stiff electrical transient on the FC stack and to enable braking energy recovery in case of use in transportation. Most of details of the description of FCS can be found in Spiegel (2008), Pukrushpan et al. (2004).

Regarding fault management, first of all the diagnostic tools can help to analyze the relationship between the structure, its properties and the performance of a FC and its components. Secondly, the results of diagnostics also provide qualitative data for general models, which can be used in prediction, optimization and control of different electrochemical and transport processes in fuel cells. In what follows in this section, a review and analysis of different techniques used for estimation and diagnostic of Fuel Cell Stack System (FCSS) will be presented.

1.2.1 Fuel Cell State Estimation approaches

As mentioned, the interest for fuel cell observer development is quite high considering the physical and cost related constraints, thus a significant number of papers treat this subject. Different methods are shown, each with certain advantages and disadvantages, acting upon a certain aspect related to the complex entity that is the Fuel Cell System.

Of course when talking about state estimation we talk about mathematical modeling, for the great majority of existing approaches. Chadli et al. (2008) worked on the problem of state estimation and diagnosis of TS systems. This approach deals with the generalization of the classical observers (Luenberger Observer), Unknown Input Observer (UIO) Darouach et al. (1994), *etc.* to the nonlinear system as in Chadli (2010). The proposed approaches are formulated as optimization problems under LMI (Linear Matrix Inequalities) constraints.

In the literature, among the work using observer development in fuel cell systems, most concentrate on using the observer for diagnostic and not just state estimation, thus the models used are mostly adapted for such purposes and not to create virtual sensors. In this sense many models for the gaseous part do not consider the valves at the cathode input and output *etc.*. Indeed the role of diagnostic is of high importance to the sensitivity of different parameters in the fuel cell, but the parameter estimation is as well.

An observer design to estimate the partial pressure of hydrogen in the anode channel of a fuel cell is presented by Arcak et al. (2004). The authors use a monotonic nonlinear growth property of the voltage output on hydrogen partial pressures at the inlet and at the exit of the channel. They considered that the inlet partial pressure is an unknown parameter, and an adaptive observer is developed that employs a nonlinear voltage injection term. The weakness of this method is the utilization of an electrical model which is directed more towards fast dynamics excluding thus some gaseous phenomena. The work of Kim et al. (2007) deals with the robust nonlinear observer developed for PEM fuel cell system. They choose a sliding mode observers using Lyapunov's stability analysis method to estimate the cathode and anode pressures, the manifold, oxygen and hydrogen pressure of PEMFC system. This method is not able to estimate the oxygen and hydrogen mass flow which are generally not measured and useful for the problem of the safety of the fuel cell. In the recent work of Pilloni et al. (2015), the main problematic is to estimate the oxygen excess ratio since its accurate regulation can increase the efficiency significantly. This work is based on a high-order sliding-mode approach to the observer-based output feedback control of a PEM fuel cell system comprising a compressor, a supply manifold, the fuel-cell stack and the return manifold. Sliding mode observers (SMO) do not need the process model to be linear, and are robust with respect to matched modeling errors and uncertainties as well. Furthermore, they can be implemented to estimate both the state variables and system parameters. A result on State Estimation with Application to Fuel Cell Stacks has been proposed by Benallouch et al. (2008) in order to estimate the partial pressure of oxygen and nitrogen and the mass flow rate of dry air in the cathode channel. The observer design is based on LMI and considers the mass flow rate of dry air as an unknown input and uses the voltage and the total pressure as measurements. This work does not consider some auxiliary elements as some valves and others. In the work of De Lira et al. (2011), an LPV (Linear Parameter Varying) approach is used for the development of an estimator, where the model is build using a Jacobian linearization technique. In Gorgun et al. (2005a), a voltage based observer was developed to estimate membrane water content in PEM fuel cells. In Kazmi et al. (2009), a nonlinear observer is designed for the estimation of the mass flow rates of reactant gases. Their precise estimation is necessary and plays an important role for diagnostics and then maintenance of FCS. In regards to the inlet manifolds of the FCS, a corresponding mass flow of air is extremely critical for proper maintenance of chemical reactions in the cathode. The work of Vepa (2012) considers an interesting approach for the estimation of a PEM fuel cell parameters, by means of adaptive observers.

1.2.2 Fuel Cell Diagnostic approaches

1.2.2.1 *Classification of Diagnostics methods for FCS*

The proposed logic is illustrated in figure 1.1. This classification of different approaches for Diagnosis is based on some of the predominant existing literature. These are classified in two types of methods: model-based approaches and knowledge-based or non model-based approaches.

- *Model based approaches*

  Model based approaches are classified generally in two categories: qualitative model based and quantitative model based. Reviews

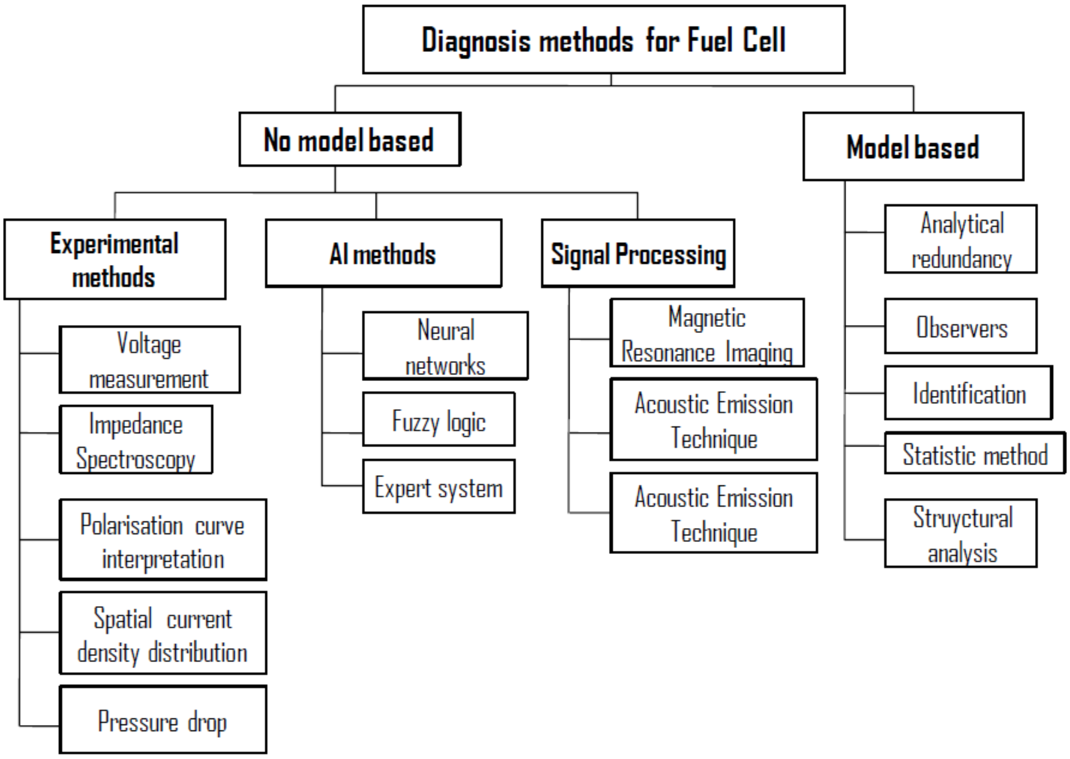

Figure 1.1: Classification of different approaches for Diagnostics of FCSS

of qualitative methods and quantitative methods respectively up to 2003 are given in Venkatasubramanian et al. (2003) in parts one and two. Most qualitative model-based approaches include: abstraction hierarchy (functional and structural analysis), causal models (signed direct graphs Maurya et al. (2006), fault tree analysis Jung et al. (2004), qualitative physics). Most quantitative model-based approaches include Analytical Redundancy Relations (ARRs) or parity space relations, observers, Kalman filters and parameter estimation methods. The performances of the quantitative model-based methods depend essentially on the model accuracy. The model of FC system is very complex containing nonlinearities and involving coupling between several energy areas: electrical, thermodynamic and electrochemical. Recent reviews on model based diagnostic techniques can be found in papers like Salim et al. (2013) or the authors Aitouche et al. (2012).

- *Knowledge based approaches*

As opposed to model based methods, that require a-priori knowledge of the model of the system, in non model based approaches the requirement falls upon the existence of a sufficient amount of processing data (as in Venkatasubramanian et al. (2003)). Knowledge based methods are mainly built on the availability of a sufficient and well defined data base which is used to perform learning, pattern recognition, qualitative reasoning and statistical analysis. As shown on figure 1.1, the most encountered knowledge based approaches are: signal processing approaches (magnetic resonance imaging, acoustic emission, magnetic field, neutron radiography); artificial intelligence approaches (fuzzy logic, neural network, expert system); experimental methods (voltage measurement, impedance spectroscopy, polarization curve interpretation, spatial current density distribution, pressure drop and gas chromatography).

1.2.2.2 *Observer based diagnostic*

From the different Model based approaches that exist in diagnosis research, we will focus in this work on the Observer based methods.

In the literature, not many papers deal with fuel cell systems' diagnosis based on observers. There is a majority of work that concentrates on other techniques that do not imply a behavioral model. Since several parameters are seriously sensitive to failures in the system, the fault detection and isolation could be realized by monitoring the variations of these parameters. In Riascos et al. (2008), a voltage based Bayesian diagnostic technique is developed to estimate faults as hydrogen pressure drop, air fueling system failure and cooling system failure. Similarly, other nonlinear observers for fuel processing reactors in fuel cell systems were designed in Gorgun et al. (2005b) where hydrogen content can be estimated and then, the gas fluid faults can be detected.

In Benallouch et al. (2008), Arcak et al. (2004), it is considered the problem of flooding diagnosis based on liquid water volume and gaseous physical behavior model. In this work, the strategy employed for diagnosis is based on the state estimation of volume of liquid water and pressure. Since the goal is only to estimate the volume of liquid water and not all the state, the author proposes to solve the problem using a functional observer. Regarding the inlet manifold of FCS, appropriate air and hydrogen mass flows are very critical for proper maintenance of chemical reactions in the cathode. Ingimundarson et al. (2008) have shown the development of a fault estimation in the anode side by analyzing the hydrogen the mass flow.

Another interesting approach is adopted in de Lira et al. (2010), where a LPV observer was used in order to compute residuals. The algorithm developed is able to identify and estimate multiple sensor faults for PEM fuel cell.

1.3 Contribution

As presented previously, the majority of the work on FC diagnostics use experimental methods which, with the exception of signal based methods, usually imply an off-line implementation or an offline configuration that may alter in time as the Fuel Cell gets older and changes behavior. This means that intrusive and costly experiments are generally required for the development stage as the isolation performances of the methods based on experimental analysis depend on learned faulty modes. Also from a numerical viewpoint, these methodologies are not well suited for embedded applications. This is why FDD (Fault Detection and Diagnosis) model-based can be a viable alternative, of course, by taking into account the adjacent inconveniences.

Also the importance and the development of Fuel Cell parameter estimation especially in the context of small scale embedding of algorithms is not treated in an exhaustive manner in literature. This thesis tries to promote and to contribute to the model based techniques for estimation and diagnostics as well as to the TS methodology and finally to the implementability of such algorithms in small scale embedded systems.

The problem of PEM FC estimation and diagnostics can be summarized as follows: insufficient instrumentation architecture, costly pattern recognition of faulty modes, complex and non stationary dynamic models, partially unknown numerical values of parameters, cells in serial connection are taken as a whole (monitoring of each cell individually being to hard), disturbed environment (for example in transportation system).

This shows only a few elements that present the motivation and contribution of this thesis.

1.4 Dissertation stucture

The organization of the thesis is as follows:

The second chapter describes the Takagi Sugeno methodology, the background for state estimation and the development of different types of Takagi Sugeno observers.

Afterward, chapter three deals with the scientific state of the art of fault detection and isolation as well as its TS implementation. This is achieved by means of a modified Proportional Integral observer.

The fourth chapter explores the subject of real time embedded systems, working on the existent small scaled systems, the possibility to implement on them nonlinear algorithms, specifically by means of the Takagi Sugeno representation. Also a procedure of real time testing of the embedded device is developed by means of the Amesim simulator on a Windows platform. The chapter ends with a basic application on a 3 tank system.

Finally, the last main chapter develops the previously described subjects, by applying them to a PEM Fuel Cell Stack System.

The thesis ends with a set of conclusions that could be drawn from the work and the perspectives envisaged in accordance.

Chapter 2

On Takagi-Sugeno State Estimation

2.1 Introduction 11
2.2 Takagi Sugeno Representation 16
2.3 TS observer based on the Lipschitz constant 22
2.4 TS Bounded stability approach 27
2.4.1 Observer development 27
2.5 Mean value theorem based approach 31
2.5.1 Observer development 31
2.5.1.1 *Robust observer* 33
2.6 Dynamic observer in a TS form 36
2.7 Conclusions 42

2.1 Introduction

The state estimation represents a radical step in optimizing an industrial process both from a cost related point of view and also from a hardware perspective in the sense that a real sensor can be replaced by a virtual one (the estimation itself) thus eliminating physical constraints imposed by the placement of the sensor. Furthermore the observer plays a central role in the construction of observer based diagnostic methods.

When talking about state estimation or observer development, we generally refer to methods that are model based. The state observer is an important tool both for estimating parameters that are not directly measurable, and also for use in diagnostic techniques. The use of it as a virtual sensor becomes obvious if we take into account the price constraints that any additional sensor would imply as well as the physical constraints, considering that space and weight are to be optimized in any embedded system.

The implementation of any observer, generally follows the structure presented in figure 2.1, where we see the observer being shown in parallel with the real system, taking as inputs the real system's inputs u (a vector input) as well as the measurable vector outputs of the real system y_m (where y_n is the vector of non measurable system outputs), in order to do the estimation error correction and finally to arrive at a correct estimation of the outputs ($\hat{y}$ becoming equal to $y = \begin{pmatrix} y_n & y_m \end{pmatrix}^T$). In

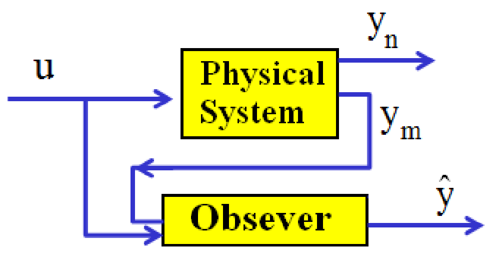

Figure 2.1: Observer block diagaram

the context of model based methods, the linear approaches are limited especially for complex systems where a linearisation would considerably affect the precision of the results. On the other hand, non-convex optimization problems (that appear when solving stability requirements in nonlinear systems) do not have a direct solution. Different types of approaches have been developed in order to arrive at a solution, even though a generally applicable result does not exist for the time being.

There are many observer design solutions for the nonlinear context, some in continuous form, and others in a discrete framework, both showing great interest in different industrial applications. But among the first works regarding state estimation for nonlinear systems, that of Thau (1973) is of reference. Here, the same as for the majority of the other papers that will follow, Lyapunov theory is used in order to apply stability to the estimation error. Regarding the observer form used, the solution is based on the work of Luenberger Luenberger (1971).

Let us begin with a nonlinear system, expressed in a general form as in (2.1).

$$\begin{cases} \dot{x}(t) = Ax(t) + g(x(t), u(t)) \\ y(t) = Cx(t) \end{cases}, \tag{2.1}$$

where $x(t) \in \mathbb{R}^{n_x}$ is the time varying state vector, $u(t) \in \mathbb{R}^{n_u}$ is the system input vector, $y(t) \in \mathbb{R}^{n_y}$ is the output vector, $A \in \mathbb{R}^{n_x \times n_x}$ is the state matrix, $C \in \mathbb{R}^{n_y \times n_x}$ is the output matrix and finally $g(x,u) \in \mathbb{R}^{n_x}$ is a nonlinear function dependent of states and inputs.

The Luenberger observer as presented in the previous work is of the form (2.2).

$$\begin{cases} \dot{\hat{x}}(t) = A\hat{x}(t) + g(\hat{x}(t), u(t)) + L(y(t) - \hat{y}(t)) \\ \hat{y}(t) = C\hat{x}(t) \end{cases}, \tag{2.2}$$

where the $\hat{x}(t)$ and $\hat{y}(t)$ are respectively, the estimation of the state vector and the estimation of the output vector. Here we see the L matrix represents the observer gain that acts upon the estimation error between the real and estimated output. From now on, for notation purposes we will ignore the time variable when writing state equations.

There exists a set of approaches that are worth mentioning for the observer design, which are constituted by methods based on observers with a variable structure. Previously the observer had a linear gain in order to adapt to the error dynamics, whereas these observers have a variable gain that varies according to the value of the estimation error. These methods are not as sensitive to the uncertainty of the model itself, yet come with the disadvantage of a noisy dynamics named often as chattering. Works based on such observers started in the 1980s with the works of Slotine et al. (1986), Walcott and Zak (1987) and have developed since as for example as the work on sliding mode observers of Edwards et al. (2007), based on the theory of VADIM (1977) or Utkin (1978) (the first such approach to MIMO systems although directed towards control and not necessarily observers).

In order to resolve numerically the stability problem that is demanded from the estimation error, since the years 2000s, because of the development of interior point methods for convex optimization Nesterov and Nemirovskii (1994), the resolution of Linear Matrix Inequalities (LMIs) becomes common practice. A good description is done in the book of Boyd et al. (1994). In order to treat the non convexity of the optimization problems that arise from the stability condition because of the nonlinear character of the system, different techniques are applied. The first and classical method as in Thau (1973) is to use the Lipschitz constant γ, which represents a scalar value, calculated offline, that satisfies the inequality (2.3).

$$\| g(x,u) - g(\hat{x},u) \| < \gamma \| x - \hat{x} \| \tag{2.3}$$

Here, the $\| \ \|$ stands for the Euclidean norm of the nonlinear function.

This method faces the problem of difficulty in finding the γ closest to the real value, as well as the numerical issues encountered when γ is too big. This constraint is somehow reduced in the work of Rajamani (1998), where the stability condition is presented in a more relaxed way.

A common method that has seen a strong advancement in the last two decades is to represent the nonlinear system in a polytopic form (can be seen also as a linear differential inclusion). In this category very common is the Linear Parameter Varying (LPV) form Shamma and Cloutier (1992). A newer interesting work oriented towards LPV observers is Trumpf (2007). In discrete time, for polytopic observers we can reference Zemouche and Boutayeb (2012) where after a state of the art for observers in Lipschitz nonlinear systems, a development is done for the Linear Parameter Varying (LPV) approach. This LPV method is further developed in Zemouche and Boutayeb (2013).

An interesting approach, that has seen an accelerated growth during the last two decades, is the construction of an equivalent system that achieves a perfect representation of the nonlinear model, entitled 'Takagi-Sugeno', after the two main researchers that contributed to this method. This method started as a fuzzy method Takagi and Sugeno (1985) where the system itself needed to be identified (Sugeno and Kang (1988)), but afterward caught a continuous model based form by constructing an equivalent model from a continuous (discrete) state space form Kang et al. (1998). A more modern work that encompasses all the aspects of the TS procedure for observation and control by using the notion of Linear Matrix Inequalities (LMI) is the book of Tanaka and Wang (2001). At that point in time the innovations in this technique started to lose in acceleration although the method became more robust, constraints were reduced, unmeasurable premise variables have been taken into account (as this thesis does). A good reference for observer development using this methodology is the book Lendek et al. (2011), where a detailed description of different existing observers is presented showing some performance comparison by means of a set of examples. Of course, there are other interesting newer works that build upon this method, as the work of Jamel et al. (2010). In constructing observers, a very common technique first employed for TS controller development is the so called Parallel Distributed Compensation (PDC) technique as in Wang et al. (1995). This methodology based on a Takagi-Sugeno approach, is the one that we have chosen to focus upon, as it proves to have a high potential for being applied to different types of systems, it permits robustness, it has a simple and accessible construction procedure, and finally it is attractive as it has a structured form that proves efficient for numerical implementability.

In this chapter we will begin with a section describing the TS modeling, followed by a section describing the TS observer, first by using the Lipschitz constant and then using a bounded stability approach. The next section, describes the implementation of an observer by means of a methodology similar to TS, based on the Mean Value theorem. The last section describes a different approach for the TS observer, that doesn't restrict the observer to a Luenberger form but instead expands it by means of a dynamic observer.

2.2 Takagi Sugeno Representation

This method can be found in literature, acting upon different types of industrial processes, like for example in Georg et al. (2014), many types of state observers being developed using it. This approach has an advantage over other nonlinear ones in that it has a relaxed and high degree of generality in the form of the nonlinear system, not forcing towards a certain class of systems.

The system in TS form can be seen as a blended sum of linear systems, where each system is weighted by a percentage describing how much the system belongs to a specific linear system at a certain point in time. This TS form is presented in equation (2.4).

$$\begin{cases} \dot{x} = \sum_{i=1}^{2^n} w_i(z)\left[A_i x + B_i u\right] \\ y = \sum_{i=1}^{2^n} w_i(z)\left[C_i x\right] \end{cases}, \tag{2.4}$$

where $x(t) \in \mathbb{R}^{n_x}$, $u(t) \in \mathbb{R}^{n_u}$, $y(t) \in \mathbb{R}^{n_y}$ represent respectively, the states vector, the inputs vector and the outputs vector, $z(x(t)) \in \mathbb{R}^n$ represents the vector of premise variables (nonlinear terms in number of n), $w_i(z(t)) : \mathbb{R}^n \rightarrow [0,1]$ represents a scalar function called the membership function, associated to the validity degree of each linear system and finally the matrices $A_i \in \mathbb{R}^{n_x \times n_x}$, $B_i \in \mathbb{R}^{n_x \times n_u}$, $C_i \in \mathbb{R}^{n_y \times n_x}$ are the linear system matrices representing the physical model.

From the previous equation one can notice the similarity to LPV systems, yet one important difference is that the nonlinear terms are no longer inside the matrices, but move in the weighting function $w(z)$.

In order to go from a nonlinear system form to a TS representation, a set of structured steps have to be followed:

1. Starting from the state-space model we separate the nonlinear terms.

2. We determine the maximum and minimum possible values of each nonlinear term.
3. We calculate the Weighting Functions starting from the nonlinear terms.
4. We write dynamically our system as a sum of linear models that have instead of the nonlinear terms, all the possible combinations of their maximum/minimum values. Each linear model in the sum being multiplied by its degree of truth called weighting function (the multiplication of the corresponding Membership Functions).

We will now develop around the previously mentioned steps:

1. Presenting in a more detailed manner the previous procedure, we note that one can arrive at a TS form by starting from a general form of the nonlinear system as in (2.5).

$$\begin{cases} \dot{x} = f(x) + g(x,u) \\ y = h(x) \end{cases}, \tag{2.5}$$

where $x(t) \in \mathbb{R}^{n_x}$ is the time varying state vector, $u(t) \in \mathbb{R}^{n_u}$ is the system input vector, $y(t) \in \mathbb{R}^{n_y}$ is the output vector, $f(x(t)) : \mathbb{R}^{n_x} \to \mathbb{R}^{n_x}$ is a vector of nonlinear functions dependent only on the system states, $h(x(t)) : \mathbb{R}^{n_x} \to \mathbb{R}^{n_y}$ is an output vector of nonlinear functions dependent only on the system states and finally $g(x(t), u(t)) : \mathbb{R}^{n_x} \times \mathbb{R}^{n_u} \to \mathbb{R}^{n_x}$ is also a vector of nonlinear functions dependent this time on states as well as on inputs.

In order to make the TS transformation, we separate the nonlinear terms (vector z) in the matrices as in the representation (2.6), operation that can be always be done, even though it may sometimes be cumbersome if the nonlinear term doesn't include one of the states directly multiplied.

$$\begin{cases} \dot{x} = A(z)x + B(z)u \\ y = C(z)x \end{cases} \tag{2.6}$$

We have considered $A \in \mathbb{R}^{n_x \times n_x}$ as the state matrix containing nonlinear terms, $C \in \mathbb{R}^{n_y \times n_x}$ as the output matrix containing nonlinear terms.

2. In the literature there are 2 major possibilities for determining the linear models inside the TS form (according to Lendek et al. (2011)).

    - The first one is the *'sector nonlinearity approach'* (presented in Tanaka and Wang (2001)), that is based on calculated minimum and maximum values for each nonlinear term z. Unfortunately this method comes with a major drawback, represented by the fact that the obtained linear models are not necessarily observable nor stable even if the initial system may be stable. The only solution to avoid this is to make another selection of the nonlinear terms, or to choose other values for the minimum and maximum values of the premise variables. Another disadvantage is that the number of fuzzy rules obtained is in fact growing as a power of 2, depending on the number of nonlinear terms.
    - The second approach is to apply a number of linearizations (their number has to be chosen by trying to balance the precision of the generated model and the complexity thus obtained) around a chosen set of operating points (not necessarily equilibrium points).

    Let us consider as an illustrative example the figure 2.2. Here it is drawn the evolution of a one dimensional vector $X(t)$, and a nonlinear function $f(X(t)) : \mathbb{R} \rightarrow \mathbb{R}$, and we can see that the time evolution of the nonlinear function can be bounded in a certain sector (therefore the name 'sector nonlinearity'), as long as $X(t)$ remains in the interval $[X_{min}, X_{Max}]$. To determine the upper and lower limit of each nonlinear term, we can use 2 methods:

    (a) experimental estimation of limits in certain intervals
    (b) if a nonlinear term depends on only maximum 2 states, then a 3-dimensional graph can be constructed of the form presented in Enrique et al. (2008)

3. As the first work related to TS was from a fuzzy perspective, many draw a parallel between any general TS form and a Fuzzy system. Thus, the effect of the weighting functions ($w_i(z)$) is seen as a defuzzyfication process. In this description we will focus on the sector

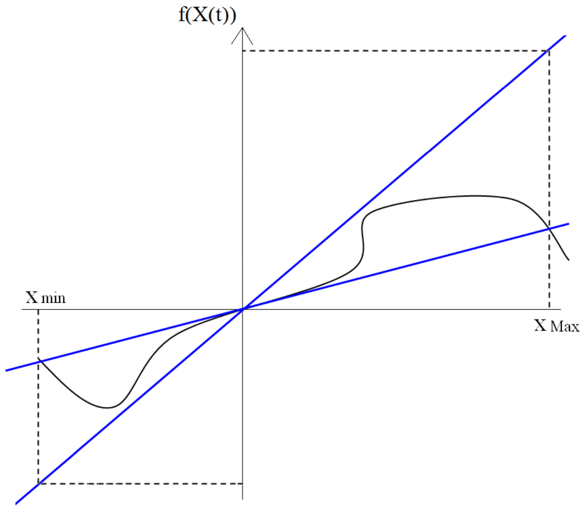

Figure 2.2: Sector Nonlinearity - one dimensional Membership Function example

nonlinearity technique presented previously, as this is the method utilized in the thesis' results. In order to obtain the weighting functions, one first needs the Membership functions (MF) which represent a pair of functions $MF_{min}(z_i)$, $MF_{Max}(z_i)$, which are associated to each nonlinearity (each z_i). Their significance is: $MF_{min}(z_i)$ gives the percentage at which the nonlinearity z_i at a current moment is close to its minimal value (we will note it as $z_{i,min}$); similarly $MF_{Max}(z_i)$ gives the percentage at which the nonlinearity z_i at a current moment is close to its maximal value (we will note it as $z_{i,Max}$).

There are different classical types of functions that can be chosen in order to obtain the membership functions, as triangular, trapezoidal, Gaussian, but we will limit to the triangular one. Thus the two adjacent membership functions can be obtained as in (2.7) for all $i = 1..n$.

$$\begin{aligned} MF_{min}(z_i) &= \frac{z_{i,Max} - z_i}{z_{i,Max} - z_{i,min}} \\ MF_{Max}(z_i) &= \frac{z_i - z_{i,min}}{z_{i,Max} - z_{i,min}} \end{aligned} \tag{2.7}$$

By considering another visual example in order to show graphically the membership functions, in figure 2.3 it is chosen a certain moment in time t_0, where Z_i is the value of the nonlinearity $z_i(x(t_0))$

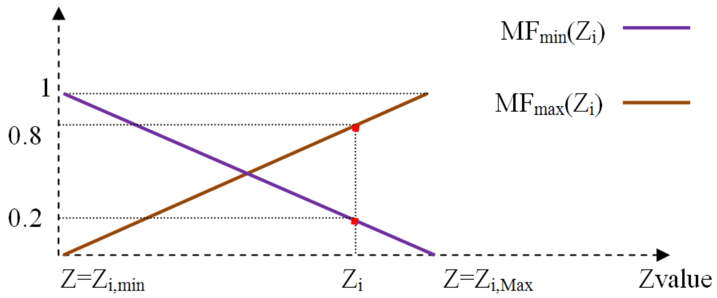

Figure 2.3: Min / Max, membership function example

at this certain point in time. Now, one can obtain the weighting functions $w_i(z)$ (being 2^n in number). As such one can realize that the weighting functions are constituted from all the combinations of minimal/maximal Membership Functions for all the nonlinearities. In order to calculate them, we use the equalities in (2.8), where after we obtain the h_i parameters, these values are to be normalized, in order to obtain positive and sub-unitary weighting functions.

$$\begin{aligned}
&h_1 = MF_{min}(z_1)\cdot MF_{min}(z_2)\cdot \ldots \cdot MF_{min}(z_n)\\
&h_2 = MF_{min}(z_1)\cdot MF_{min}(z_2)\cdot \ldots \cdot MF_{Max}(z_n)\\
&\ldots\ldots\\
&h_{2^n} = MF_{Max}(z_1)\cdot MF_{Max}(z_2)\ldots \cdot MF_{Max}(z_n)\\
&-----------------------\\
&w_1 = \frac{h_1}{\sum_{i=1}^{2^n} h_i};\ldots; w_{2^n} = \frac{h_{2^n}}{\sum_{i=1}^{2^n} h_i}
\end{aligned} \tag{2.8}$$

Therefore in this new representation, one can observe that the nonlinearities have moved into the membership functions w_i, where the convex sum property is satisfied $\sum w_i = 1$.

4. What remains to do now is to build each linear model and then to apply the weighting functions to their sum. The linear models can be visualized from a fuzzy perspective as a set of *'If Then' fuzzy rules*. Practically, one constructs from each nonlinear matrix, a set of constant matrices, replacing the nonlinear terms z_i with all the combinations of their minimal, maximal values $(z_{i,min}, z_{i,Max})$. Therefore one gets 2^n constant matrices of the form $A_{z_{1,k},\ldots,z_{n,k}}$, $B_{z_{1,k},\ldots,z_{n,k}}$, $C_{z_{1,k},\ldots,z_{n,k}}$ where k is either min or Max (of course, if one matrix

doesn't contain all the nonlinear terms some of the values will be identical, thus reducing their real number).

If Then fuzzy rules associated to the system:

If $[z_1$ **is** $(z_{1,min})]$ **and** $[z_2$ **is** $(z_{2,min})]$ **and...** $[z_n$ **is** $(z_{n,min})]$ **then**

$$\begin{cases} \dot{x} = A_{z_{1,min},\ldots,z_{n,min}} x + B_{z_{1,min},\ldots,z_{n,min}} u; \\ y = C_{z_{1,min},\ldots,z_{n,min}} x; \end{cases}$$

If $[z_1$ **is** $(z_{1,Max})]$ **and** $[z_2$ **is** $(z_{2,min})]$ **and...** $[z_n$ **is** $(z_{n,min})]$ **then**

$$\begin{cases} \dot{x} = A_{z_{1,Max},\ldots,z_{n,min}} x + B_{z_{1,Max},\ldots,z_{n,min}} u; \\ y = C_{z_{1,Max},\ldots,z_{n,min}} x; \end{cases}$$

....

If $[z_1$ **is** $(z_{1,Max})]$ **and** $[z_2$ **is** $(z_{2,Max})]$ **and...** $[z_n$ **is** $(z_{n,Max})]$ **then**

$$\begin{cases} \dot{x} = A_{z_{1,Max},\ldots,z_{n,Max}} x + B_{z_{1,min},\ldots,z_{n,Max}} u; \\ y = C_{z_{1,Max},\ldots,z_{n,Max}} x; \end{cases}$$

Instead of commuting between the linear models, the interest goes towards their blended summation as in (2.4).

This representation is a perfect mathematical representation of the initial system. The eventual impression and limitation when working with such system form, will appear when developing the observers, controllers and so on, because of the fact that we do not consider the evolution of the nonlinear terms, but instead we work with the bounded sector of the nonlinearity's dynamics. Therefore the more nonlinear the term is, the more of a limitation on the stable region of the system occurs. Also if the necessary operating regime of the system is too large, meaning the minimum and maximum values of the nonlinearities are too far apart, the resolution of the convex problems imposed by the stability conditions may not find any solutions. As a last note, a remark is to be made regarding the minimum and maximum values of the nonlinear terms. In the behavior of the system's nonlinear terms, there may be short instances when it's values are too close to 0 or too large; if this happens for a short enough period, we don't need to consider these values as the maximum and minimum, instead they will just be bounded out. Otherwise the optimization problem will not find reasonable solutions.

2.3 TS observer based on the Lipschitz constant

Although many papers consider the premise variables measurable Lendek et al. (2011), this case in many practical applications is unfortunately unattainable. Among those who have tackled the issue of unmeasurable premise variables, one can cite Yacine et al. (2012). Having the Takagi Sugeno model, we can now develop the observer. For this, based on the theory presented in Ichalal et al. (2007), we modify the TS system as follows:

$$\begin{cases} \dot{x} = \sum_{i=1}^{2^n} \left[w_i(x) \left(A_0 x + \bar{A}_i x + B_i u \right) \right] \\ y = Cx \end{cases} \tag{2.9}$$

We see as in the general TS form, a sum of 2^n (where n is the number of premise variables) combinations of linear system, only this time, we have one constant matrix A_0 that will play the role of dominant matrix of the system and all the other 2^n matrices are obtained as in the relation (2.10). Although here the dominant model is chosen simply as a medium numerical value it can be chosen specifically as a certain linear matrix A_i which experimentally is known to dominate the system behavior. This of course is easier done if the TS system is not constructed using the 'sector nonlinearity' technique but using Taylor series linearization (for obvious reasons, as the linearisation in precise operating regions would imply knowing these regions and the probability with which the system revolves around these points).

$$\begin{cases} A_i = \bar{A}_i + A_0 \\ A_0 = \frac{1}{2^n} \sum_{i=1}^{2^n} A_i \end{cases} \tag{2.10}$$

We will choose the model of the observer in a simple Luenberger like format as follows:

$$\begin{cases} \dot{\hat{x}} = \sum_{i=1}^{8}\left[w_i(\hat{x})\left(A_0\hat{x} + \bar{A}_i\hat{x} + B_i u + L_i\left(y-\hat{y}\right)\right)\right] \\ \hat{y} = C\hat{x} \end{cases} \tag{2.11}$$

The general procedure used for computing a TS system observer is to impose stability to the error dynamics of the estimation as in equation (2.12) addressing the state estimation error as $\dot{\tilde{x}}$.

$$\dot{\tilde{x}} = \dot{x} - \dot{\hat{x}} \tag{2.12}$$

By means of Lyapunov asymptotic stability theory we can obtain a set of Linear Matrix Inequalities (LMI) in order to calculate the gains of the observer matrix. These system of LMI is presented in (2.13).

$$\begin{array}{l} A_0^T P + PA_0 - C^T K_i^T - K_i C < Q \\ \begin{bmatrix} \left[Q + \lambda_1 M_i^2 I_4 + \lambda_2 N_i^2 I_4\right] & P\bar{A}_i & PB_i \\ \bar{A}_i P & -\lambda_1 M_i^2 I_4 & 0 \\ B_i^T P & 0 & -\lambda_2 N_i^2 I_3 \end{bmatrix} < 0 \end{array}, \tag{2.13}$$

where, using the notations employed until now, the system output matrix was chosen as constant C, $\lambda_1 > 0$ and $\lambda_2 > 0$ are two scalar positive values, the matrices $P \in \mathbb{R}^{n_x \times n_x}$ (having the vector of states $x \in \mathbb{R}^{n_x}$) and $Q \in \mathbb{R}^{n_x \times n_x}$ are two positive definite matrices that are unknown and to be found by solving the LMI. The observer gains that we need to find will be $L_i \in \mathbb{R}^{n_x \times n_y}$, and can be calculated by $L_i = P^{-1}K_i$ ($K_i \in \mathbb{R}^{n_x \times n_y}$). What remains is a set of three scalar terms N_i, M_i, β that can be calculated using the Lipschitz inequality of L_2 norms in relations (2.14).

$$\begin{array}{l} \| w_i(x)x - w_i(\hat{x})x \| \leq N_i \| x - \hat{x} \| \\ \| (w_i(x) - w_i(\hat{x})) \| \leq M_i \| x - \hat{x} \| \\ \| u \| \leq \beta \end{array} \tag{2.14}$$

What is to observe here is that we need the inputs to be bounded. In order to calculate N_i and M_i, as showed in Marx et al. (2010), a Taylor expansion at order zero with an integral remainder term of $f(x)$ around $\hat{x}$ is done as in (2.15), for any nonlinear function f of x.

$$\begin{cases} \| f(x) - f(\hat{x}) \| \leq J \| x - \hat{x} \| \\ J = \begin{bmatrix} a_{11} & \dots & a_{1n} \\ \dots & \dots & \dots \\ a_{n1} & \dots & a_{nn} \end{bmatrix} \\ a_{ij} = \max_{t \in [x_j, \hat{x}_j]} \left| \frac{\partial f_i}{\partial x_j} \right| \end{cases} \tag{2.15}$$

So for calculating N_i, we just consider the above function as being multiplied by x respectively $\hat{x}$, before doing the partial derivatives when calculating the Jacobian matrix J.

To calculate effectively the Lipchitz constant needed, after finding M_i and N_i as matrices, a simple singular value decomposition will generate the required value, although the LMIs work with M_i, N_i as constants or matrices.

In order to build a demonstration for the LMIs previously mentioned we start just from replacing (2.9) and (2.11) in (2.12). The aim for this is to impose stability conditions upon the system state estimation error.

$$\dot{\tilde{x}} = \sum_{i=1}^{5} \left[\left(\bar{A}_i (w_i(x)x - w_i(\hat{x})x) + B_i (w_i(x) - w_i(\hat{x}))u + (A_0 - L_i C) \tilde{x} \right) \right] \tag{2.16}$$

To impose a Lyapunov asymptotic stability to the system state estimation, it is required to choose an appropriate Lyapunov candidate function (in this case, a basic quadratic one) and if we find a set of observer gains that satisfy the condition that the Lyapunov function derivative is negative definite, then we will have an estimation error that converges asymptotically to 0.

Therefore for a quadratic Lyapunov function $V = \tilde{x}^T P \tilde{x}$, where $P \in \mathbb{R}^{n_x \times n_x}$ with P positive definite we will have V positive definite. The time derivative of the Lyapunov candidate function becomes therefore $\dot{V} = \dot{\tilde{x}}^T P\tilde{x} + \tilde{x}^T P\dot{\tilde{x}}$. Replacing (2.16) in the time derivative of the candidate function we obtain:

$$\left\{\sum_{i=1}^{2^n}\left[\begin{array}{l}\left(\bar{A}_i\left(w_i(x)x - w_i(\hat{x})x\right) + B_i\left(w_i(x) - w_i(\hat{x})\right)u\right) + \\ +\left(A_0 - L_iC\right)\tilde{x}\end{array}\right]\right\}^T P\tilde{x} + \\ +\tilde{x}^T P\left\{\sum_{i=1}^{2^n}\left[\begin{array}{l}\left(\bar{A}_i\left(w_i(x)x - w_i(\hat{x})x\right) + B_i\left(w_i(x) - w_i(\hat{x})\right)u\right) + \\ +\left(A_0 - L_iC\right)\tilde{x}\end{array}\right]\right\} < 0 \tag{2.17}$$

The equation can be rearranged so that we isolate the measured and estimated weighting functions:

$$\sum_{i=1}^{2^n}\left[\begin{array}{l}\left(w_i(x)x - w_i(\hat{x})x\right)^T\bar{A}_i^T P\tilde{x} + \tilde{x}^T P\bar{A}_i\left(w_i(x)x - w_i(\hat{x})x\right) + \\ +u^T\left(w_i(x) - w_i(\hat{x})\right)^T B_i^T P\tilde{x} + \tilde{x}^T PB_i\left(w_i(x) - w_i(\hat{x})\right)u\end{array}\right] + \\ +\sum_{i=1}^{5}\left[\tilde{x}^T\left(A_0 - L_iC\right)^T P\tilde{x} + \tilde{x}^T P\left(A_0 - L_iC\right)\tilde{x}\right] < 0 \tag{2.18}$$

As in the previously mentioned work Ichalal et al. (2007) we can use the following known matrix theorem :

Theorem 1 *For any X, Y square matrices of equal dimensions, the inequality $X^TY + Y^TX \leq \lambda X^TX + \lambda^{-1}Y^TY$ is always satisfied for any positive scalar λ.*

By applying this theorem to the terms inside the first sum in (2.18) we will arrive at the two following inequalities:

$$\left\{\begin{array}{l}\left(w_i(x)x - w_i(\hat{x})x\right)^T\bar{A}_i^T P\tilde{x} + \tilde{x}^T P\bar{A}_i\left(w_i(x)x - w_i(\hat{x})x\right) \leq \\ \lambda_1\left(w_i(x)x - w_i(\hat{x})x\right)^T\left(w_i(x)x - w_i(\hat{x})x\right) + \lambda_1^{-1}\tilde{x}^T P\bar{A}_i\bar{A}_i^T P\tilde{x} \\ u^T\left(w_i(x) - w_i(\hat{x})\right)^T B_i^T P\tilde{x} + \tilde{x}^T PB_i\left(w_i(x) - w_i(\hat{x})\right)u \leq \\ \lambda_2 u^T\left(w_i(x) - w_i(\hat{x})\right)^T\left(w_i(x) - w_i(\hat{x})\right)u + \lambda_2^{-1}\tilde{x}^T PB_iB_i^T P\tilde{x}\end{array}\right. \tag{2.19}$$

And by using the Lipschitz constants calculated in (2.14) we arrive at:

$$\begin{array}{l} (w_i(x)x - w_i(\hat{x})x)^T \bar{A}_i^T P\tilde{x} + \tilde{x}^T P\bar{A}_i (w_i(x)x - w_i(\hat{x})x) \leq \\ \lambda_1 \tilde{x}^T N_i^T N_i \tilde{x} + \lambda_1^{-1} \tilde{x}^T P\bar{A}_i \bar{A}_i^T P\tilde{x} \\ u^T (w_i(x) - w_i(\hat{x}))^T B_i^T P\tilde{x} + \tilde{x}^T PB_i (w_i(x) - w_i(\hat{x})) u \leq \\ \lambda_2 \tilde{x}^T M_i^T M_i \tilde{x} \beta^2 + \lambda_2^{-1} \tilde{x}^T PB_i B_i^T P\tilde{x} \end{array} \tag{2.20}$$

So from (2.20) and if we consider also each iteration in the sum in (2.14), we could write each as an inequality:

$$\begin{array}{l} \lambda_1 \tilde{x}^T N_i^T N_i \tilde{x} + \lambda_1^{-1} \tilde{x}^T P\bar{A}_i \bar{A}_i^T P\tilde{x} + \\ +\lambda_2 \tilde{x}^T M_i^T M_i \tilde{x} \beta^2 + \lambda_2^{-1} \tilde{x}^T PB_i B_i^T P\tilde{x} + \\ +\tilde{x}^T (A_0 - L_i C)^T P\tilde{x} + \tilde{x}^T P (A_0 - L_i C) \tilde{x} < 0 \end{array} \tag{2.21}$$

At this point we have obtained 2^n Matrix inequalities. Because we still are not in an LMI format, being unable to eliminate the inverses of the λ scalars, we modify (2.21). So by separating the last two terms in the inequality and by writing the Schur form for the other terms we obtain (2.13).

The conditions for asymptotic stability have been reached, but we have no conditions for imposing time response performances. For this we can see from Marx et al. (2010) that we can try to impose a faster response time by imposing restrictions over the eigenvalues of the $(A_0 - L_i C)$. By doing so, the LMIs (2.13) become:

$$\begin{cases} \left(A_0^T P + PA_0 - C^T K_i^T - K_i C + 2\nu_{\max} P\right) < Q \\ -\left(A_0^T P + PA_0 - C^T K_i^T - K_i C + 2\nu_{\min} P\right) < Q \\ \begin{bmatrix} \left[Q + \lambda_1 M_i^2 I_4 + \lambda_2 N_i^2 I_4\right] & P\bar{A}_i & PB_i \\ \bar{A}_i P & -\lambda_1 M_i^2 I_4 & 0 \\ B_i^T P & 0 & -\lambda_2 N_i^2 I_3 \end{bmatrix} < 0 \end{cases} \tag{2.22}$$

One observation we have to add is that if the system is very restrictive then we can separate the matrix LMI into 2 inequalities, one for terms containing M and A terms while the other N and B terms. Also we replace Q with Q_1 respectively Q_2 for each of the new ones.

2.4 TS Bounded stability approach

In order to further improve the implementability of the Observer, a solution is envisaged that eliminates the need for the Lipschitz constant, which is hard to obtain and problematic in the LMI resolution, if not chosen correctly. Thus, we have considered the characteristic of the studied system of having bounded states and bounded inputs. As a consequence, the notion of asymptotic stability has been replaced by the more general notion of bounded stability.

2.4.1 Observer development

Once the T-S representation has been obtained, the focus can now be directed towards the construction of the observer. The observer computation will materialize as an optimization problem that will deal with the resolution of a system of linear matrix inequalities (LMIs). It is considered that the premise variables z are not measurable. Although many cases in the literature deal with the simplifying supposition of measurable premise variables $w_i(\hat{z}) = w_i(z)$, in the current case this assumption cannot be satisfied. As a result, the Luenberger like observer is of the form (2.23).

$$\begin{cases} \dot{\hat{x}} = \sum_i w_i(\hat{z})\,(A_i\hat{x} + Bu + L_i(\hat{y} - y)) \\ \hat{y} = C\hat{x} \end{cases}, \tag{2.23}$$

where L_i are the observer gains attached to each linear sub-model. To obtain these gains, a numerical optimization problem should be resolved, with the aid of an LMI solver. This solution consists of the following LMIs (2.24) applied for all $i = 1..2^n$, where n is the number of nonlinearities, P is a symmetric and positive definite matrix, with the same dimension as A. Also α and λ are positive scalar and I denotes an identity matrix of appropriate dimensions. The set of unknown matrices $Q_i \in \mathbb{R}^{n_x \times n_y}$ need to be calculated by resolving the LMI. Once the Q_i matrices are found, the observer gains are obtained by $P^{-1}Q_i = L_i$.

$$\begin{pmatrix} A_i^T P - C^T Q_i + PA_i - Q_i C + 2\alpha P & P \\ P & -\lambda I \end{pmatrix} < 0 \tag{2.24}$$

In order to arrive at these LMIs, we apply the same technique as in the previous sub-chapter, by imposing asymptotic stability to the state estimation error.

The condition required for the observer to function correctly is to have an estimation error that converges towards zero $\tilde{x} = x - \hat{x}$. Using the Lyapunov stability method, it is demanded that a chosen Lyapunov function has a negative derivative. The Lyapunov function is chosen as $V = \tilde{x}^T P \tilde{x}$, where $P \in \mathbb{R}^{n_x \times n_x}$ is a square positive definite and symmetric matrix. Developing the derivative of the estimation errors we arrive at:

$$\dot{\tilde{x}} = \sum_{i=1}^{2^n} [w_i(x)A_i x - w_i(\hat{x})A_i x + w_i(x)B_i u - w_i(\hat{x})B_i u - w_i(\hat{x})L_i C x] \tag{2.25}$$

It can easily be noted that, without the simplifying hypotheses of measurable premise variables, there will be membership functions depending on state estimates. To solve this problem, the technique presented in Yacine et al. (2012) is applied. Therefore by adding and subtracting a $w_i(\hat{x}) \cdot A_i \cdot x$, and separating the two sums, the first one is seen as a perturbation (It is clear that $w_i(x) - w_i(\hat{x})$ converges to zero as the estimated state converge towards the real state values ($x \to \hat{x}$)).

The derivative of the estimation error can be rewritten so that the estimated and real membership functions multiplied by the states are isolated in a separate term. This is done in order to reduce complications that would appear in the construction of the LMIs. Therefore (2.26) is reached, where we use a notation Δ in order to isolate the weighting functions depending on estimated states and the real weighting functions.

$$\begin{aligned} \dot{\tilde{x}} &= \sum_i w_i(\hat{x})(A_i\tilde{x} + Bu - L_iC\tilde{x}) + \Delta \\ \Delta &= \sum_i (w_i(x) - w_i(\hat{x}))(A_ix + Bu) \end{aligned} \tag{2.26}$$

By replacing (2.26) into the Lyapunov function's derivative $\dot{V}$, it can be noticed in (2.27) that the multiplication with the state impedes obtaining a linear inequality. A usual workaround is to apply Lipschitz constants, but the method could prove restrictive, first of all because these values are hard to find and also high constants may have negative effects on the resolution of the LMIs.

$$\dot{V} = \tilde{x}^T \begin{pmatrix} \sum_i w_i(\hat{x})(A_i - L_iC)^T P + \\ + \sum_i w_i(\hat{x}) P (A_i - L_iC) \end{pmatrix} \tilde{x} + \Delta^T P\tilde{x} + \tilde{x}^T P\Delta \tag{2.27}$$

As such, the solution adopted here is to view Δ as a virtual perturbation, a parameter that converges towards zero. This would allow us to impose more relaxed conditions, by demanding a bounded stability instead of an asymptotic one, with a minimal bound. An article with a similar method is Yacine et al. (2012), employing the notion of Input to state stability Sontag (1995). Practically this translates into a problematic of stability with rejection of the symbolic perturbation Δ, as in (2.28), having R as a positive matrix (identity or not), and a positive scalar ξ representing a variable to be minimized.

$$\dot{V} + \tilde{x}^T R\tilde{x} - \xi^2\Delta^T\Delta < 0 \tag{2.28}$$

Therefore, using (2.27):

$$\begin{aligned} &\tilde{x}^T \left(\sum_i w_i(\hat{z}) \left[(A_i - L_iC)^T P + P(A_i - L_iC) \right] \right) \tilde{x} + \\ &+ \Delta^T P\tilde{x} + \tilde{x}^T P\Delta + \tilde{x}^T R\tilde{x} - \xi^2\Delta^T\Delta < 0 \end{aligned} \tag{2.29}$$

In order to eliminate the nonlinear terms that remain in the previous inequality, we make use of the theorem 1. What is important to note is that this is true for any positive x_i, which for (2.30) translates into:

$$\begin{aligned} &\Delta^T P\tilde{x} + \tilde{x}^T P\Delta + \tilde{x}^T R\tilde{x} - \xi^2\Delta^T\Delta \leq \\ &\lambda\Delta^T\Delta + \lambda^{-1}\tilde{x}^T PP\tilde{x} + \tilde{x}^T R\tilde{x} - \xi^2\Delta^T\Delta \end{aligned} \tag{2.30}$$

Adding this to (2.30) gives us the modified inequality (2.31).

$$\begin{aligned} &\tilde{x}^T\left(\sum_i w_i(\hat{z})\left[(A_i - L_iC)^T P + P(A_i - L_iC)\right] + I\right)\tilde{x} + \\ &+\lambda\Delta^T\Delta + \lambda^{-1}\tilde{x}^T PP\tilde{x} - \xi^2\Delta^T\Delta < 0 \end{aligned} \tag{2.31}$$

An interesting observation is that, because λ >0 can be any coefficient, it can be chosen as $\lambda = \xi^2$, which simplifies the relation; moreover, employing the convex sum property ($\sum_i^{2^n} w_i = 1$), we arrive at (2.32). A similar idea was used in Ghorbel et al. (2014).

$$\sum_i w_i(\hat{x})\left[(A_i - L_iC)^T P + P(A_i - L_iC) + I + \lambda^{-1}PP\right] < 0 \tag{2.32}$$

The following step is to use the hypothesis that the inequality is true if all the terms of the sum are negative. Although restrictive, this proves to bring small enough constraints to the stability regions of the solution. Thus, we arrive at the following set of LMI in (2.33) applied for all combinations of the linear systems $i = 1..2^n$.

$$(A_i - L_iC)^T P + P(A_i - L_iC) + I + \lambda^{-1}PP < 0 \tag{2.33}$$

In order to eliminate the Bilinear Matrix Inequalities (BMIs) forms, a notation $Q_i = PL_i$ can be made. Also using the Schur transformation, we end up with simple LMIs. One can improve upon the performances by asking for exponential stability, using relation (2.34), where α represents the exponential decay rate.

$$\dot{V} + \tilde{x}^T R \tilde{x} - \xi^2 \Delta^T \Delta + 2\alpha V < 0 \tag{2.34}$$

As for BMIs there are no standard solutions, a choice of α by trial can be made. Finally LMIs (2.24) were obtained.

2.5 Mean value theorem based approach

The Takagi Sugeno can be viewed also from another perspective, by using the Mean Value theorem described by Phanomchoeng et al. (2011).

2.5.1 Observer development

A general Luenberger observer form is adopted for this state estimator as well, observer for which it has been utilized the Mean Value Theorem (Bounded Jacobian) approach to integrate the nonlinearities. The system has to be of the special form, showed in parallel to the associated observer:

$$\begin{cases} \dot{\hat{x}} = A\hat{x} + \Phi(\hat{x}) + g(y,u) + L(y - \hat{y}) \\ \hat{y} = C\hat{x} \end{cases}, \tag{2.35}$$

$$\begin{cases} \dot{x} = Ax + \Phi(x) + g(y,u) \\ y = Cx \end{cases}, \tag{2.36}$$

where $\hat{x}$ represents the estimated states, L is the Observer's Gain Matrix, y is the real measured output vector, and $\hat{y}$ the estimated output.

To calculate the gain matrix L, we search for a P positive definite matrix, a K unknown temporary matrix, so that the following LMIs present a solution for all the combinations of $i = 1..n_x$ and $j = 1..n_x$, where $x \in \mathbb{R}^{n_x}$.

$$\begin{cases} P(A+H_{ij}^{\max})+(A+H_{ij}^{\max})^T P - C^T K^T - KC < 0 \\ P(A+H_{ij}^{\min})+(A+H_{ij}^{\min})^T P - C^T K^T - KC < 0 \end{cases}, \tag{2.37}$$

where we have:

$$\begin{cases} h_{ij}^{\max} \geq \max(\frac{\partial \Phi_i}{\partial x_j}); h_{ij}^{\min} \leq \min(\frac{\partial \Phi_i}{\partial x_j}) \\ H_{ij}^{\max} = Ze_{n_x}(i)e_{n_x}^T(j)h_{ij}^{\max}; H_{ij}^{\min} = Ze_{n_x}(i)e_{n_x}^T(j)h_{ij}^{\min} \\ e_{n_x}(i) = [0..1...0]^T; Z = nn \end{cases}, \tag{2.38}$$

In order to prove the previous LMIs, we start from the estimation error dynamics that becomes:

$$\dot{\tilde{x}} = (A - LC)\tilde{x} + \tilde{\Phi}(\hat{x}) \tag{2.39}$$

Here we have considered the notations for the state estimation error as $\dot{\tilde{x}} = x - \hat{x}$ and $\tilde{\Phi}(\hat{x}) = \Phi(x) - \Phi(\hat{x})$.

Applying the Lyapunov asymptotic stability criterion, we begin by choosing a Lyapunov candidate function that may be defined as:

$$V = \tilde{x}^T P \tilde{x} \tag{2.40}$$

Where $P \in^{n_x \times n_x}$ is, as before, a symmetric positive definite matrix, and n_x being the number of system states.

$$\dot{V} = \tilde{x}^T[(A-LC)^T P + P(A-LC)]\tilde{x} + \tilde{x}^T P \tilde{\Phi} + \tilde{\Phi}^T P \tilde{x} \tag{2.41}$$

We want $\dot{V} < 0$ yet we know from the Mean value theorem that:

$$[\Phi(x) - \Phi(\hat{x})] = \left[\left(\sum_{i,j}^{n,n} H_{ij}^{\max} \delta_{ij}^{\max} \right) + \left(\sum_{i,j}^{n,n} H_{ij}^{\min} \delta_{ij}^{\min} \right) \right] (x - \hat{x}), \tag{2.42}$$

where $\delta_{ij}^{\max} + \delta_{ij}^{\min} = 1$, each term being an unknown positive number.

So we can write (2.43) as:

$$\dot{V} = \tilde{x}^T[(A-LC)^T P + P(A-LC) + P\left(\sum_{i,j}^{n,n} H_{ij}^{\max}\delta_{ij}^{\max}\right) + \\ +P\left(\sum_{i,j}^{n,n} H_{ij}^{\min}\delta_{ij}^{\min}\right) + \left(\sum_{i,j}^{n,n} H_{ij}^{\max}\delta_{ij}^{\max}\right)^T P + \left(\sum_{i,j}^{n,n} H_{ij}^{\min}\delta_{ij}^{\min}\right)^T P]\tilde{x} \tag{2.43}$$

After some computations, we can write as sums all the terms in (2.43) because $\delta_{ij}^{\max} + \delta_{ij}^{\min} = 1$. Afterward, eliminating the $\delta_{ij}^{\max}, \delta_{ij}^{\min}$ terms that are unknown, we give the restrictive hypothesis that if all the terms in a sum are less than 0 then their sum is less than 0. We consider $K = PL$ (therefore to calculate the observer gain we have the relation $L = P^{-1}K$), reaching the LMIs mentioned in (2.37).

2.5.1.1 *Robust observer*

We can also take into consideration some additive perturbations both of the system dynamics and the output. This has been achieved in a similar manner with Zemouche and Boutayeb (2007) , by considering additive perturbations. This is resolved using H_{inf} performance requirement. The gain matrix can be reached by finding a matrix $P > 0$, $K > 0$ and a scalar $\lambda > 0$ so that the following LMIs converge to a solution:

$$\begin{aligned} &\begin{pmatrix} \left[H_{ij}^{\max}+A\right]^T P - C^T K^T + P\left[H_{ij}^{\max}+A\right] - KC + I & (PW_1 - KW_2) \\ (PW_1 - KW_2)^T & -\lambda^2 I \end{pmatrix} < 0 \\ &\begin{pmatrix} \left[H_{ij}^{\min}+A\right]^T P - C^T K^T + P\left[H_{ij}^{\min}+A\right] - KC + I & (PW_1 - KW_2) \\ (PW_1 - KW_2)^T & -\lambda^2 I \end{pmatrix} < 0 \\ &P > 0 \end{aligned} \tag{2.44}$$

We now develop the proof of the previous system of LMI. For this let us consider the following system:

$$\begin{cases} \dot{x} = Ax + \Phi(x) + g(y,u) + W_1 w(t) \\ y = Cx + W_2 w(t) \end{cases} \tag{2.45}$$

where $W_1 = [\ E \quad 0\ ], W_2 = [\ 0 \quad D\ ], w(t) = [\ w_1 \quad w_2\ ]^T$.

By using Lyapunov properties, the following conditions have to apply in order to reduce the effects of the perturbations upon the system:

$$\begin{array}{l} \lim_{t\to\infty} \tilde{x}(t) = 0, \text{ for } w(t) = 0 \\ \|\tilde{x}(t)\|_{L_2} \leq \lambda^2 \|w(t)\|_{L_2} \text{ for } w(t) \neq 0 \text{ and } x(0) = 0 \end{array}$$

So we have to find λ>0 respecting the following inequality:

$$\dot{V} + \tilde{x}^T \tilde{x} - \lambda^2 w^T w < 0 \tag{2.46}$$

The observer form remains (2.35), but the estimation error dynamics ($\dot{\tilde{x}} = \dot{x} - \dot{\hat{x}}$) becomes:

$$\dot{\tilde{x}} = (A - LC)\tilde{x} + \tilde{\Phi}(\hat{x}) + (W_1 - LW_2)w, \tag{2.47}$$

where $\tilde{\Phi}(\hat{x}) = \Phi(x) - \Phi(\hat{x})$.

The Lyapunov function candidate will be defined as $V = \tilde{x}^T P \tilde{x}$, for a square, symmetric and positive definite matrix $P > 0$ ($P \in^{n_x \times n_x}$). We can now calculate the derivative of the Lyapunov function:

$$\begin{array}{l} \dot{V} = \tilde{x}^T[(A-LC)^T P + P(A-LC)]\tilde{x} + \tilde{x}^T P \tilde{\Phi} + \tilde{\Phi}^T P \tilde{x} + \\ + w^T (W_1 - LW_2)^T P \tilde{x} + \tilde{x}^T P (W_1 - LW_2) w \end{array} \tag{2.48}$$

From (2.48) and (2.46), we arrive at the equation:

$$\begin{array}{l} \dot{V} + \tilde{x}^T \tilde{x} - \lambda^2 w^T w = \tilde{x}^T[(A-LC)^T P + P(A-LC) + I]\tilde{x} + \\ + \tilde{x}^T P \tilde{\Phi} + \tilde{\Phi}^T P \tilde{x} + w^T (W_1 - LW_2)^T P \tilde{x} + \tilde{x}^T P (W_1 - LW_2) w - \lambda^2 w^T w \end{array} \tag{2.49}$$

Writing it as a Matrix we will have:

$$\begin{pmatrix} \tilde{x}^T & w^T \end{pmatrix} \begin{pmatrix} [(A-LC)^T P + P(A-LC) + I] & [P(W_1 - LW_2)] \\ \left[(W_1 - LW_2)^T P\right] & -\lambda^2 I \end{pmatrix} \begin{pmatrix} \tilde{x} \\ w \end{pmatrix} + \\ + \tilde{x}^T P \tilde{\Phi} + \tilde{\Phi}^T P \tilde{x} \tag{2.50}$$

Yet from the mean value theorem , using (2.42) and knowing that $\delta_{ij}^{\max} + \delta_{ij}^{\min} = 1$ we conclude :

$$\begin{pmatrix} [\sum_{i,j=1}^{n,n} \left\{ \left[H_{ij}^{\max} + (A-LC)\right]^T P + P\left[H_{ij}^{\max} + (A-LC)\right] + I \right\} \delta_{ij}^{\max} + \\ + \sum_{i,j=1}^{n,n} \left\{ \left[H_{ij}^{\min} + (A-LC)\right]^T P + P\left[H_{ij}^{\min} + (A-LC)\right] + I \right\} \delta_{ij}^{\min}] & [P(W_1 - LW_2)] \\ \left[(W_1 - LW_2)^T P\right] & -\lambda^2 I \end{pmatrix} \\ < 0; \tag{2.51}$$

The nonlinear unknown terms that remain can be eliminated directly, but in order to demonstrate that, we use the Schur transformation of matrix inequalities. Also by doing some grouping of terms, we arrive at the inequality:

$$\begin{aligned} &\sum_{i,j=1}^{n,n} \left\{ \left[H_{ij}^{\max} + (A-LC)\right]^T P + P\left[H_{ij}^{\max} + (A-LC)\right] + I + \right. \\ &\left. + [P(W_1 - LW_2)] \tfrac{1}{\lambda^2} I \left[(W_1 - LW_2)^T P\right] \right\} \delta_{ij}^{\max} + \\ &+ \sum_{i,j=1}^{n,n} \left\{ \left[H_{ij}^{\min} + (A-LC)\right]^T P + P\left[H_{ij}^{\min} + (A-LC)\right] + I + \right. \\ &\left. + [P(W_1 - LW_2)] \tfrac{1}{\lambda^2} I \left[(W_1 - LW_2)^T P\right] \right\} \delta_{ij}^{\min} < 0 \end{aligned} \tag{2.52}$$

Assumption made by Phanomchoeng et al. (2011):

If each term in the upper sums is negative then the whole inequality becomes negative. Then we can transform the inequality in multiple inequalities.

Also taking into consideration $\bar{\delta}_{ij}^{\max}, \bar{\delta}_{ij}^{\min} \geq 0$, for all i, j, using the inverse Schur format, and *considering* $K = PL$ *and* $L = P^{-1}K$ we reach the wanted LMIs.

2.6 Dynamic observer in a TS form

In this section, a new type of observer, different than the simple Luenberger one, is developed. The Luneberger observer is a very powerful structure, but the static gain can add constraints to the stability region. Therefore other solutions are searched. There are different approaches that try to find alternatives to the classical observer, like sliding mode terms or the dynamic observer form (the focus of this section) but the approach is not employed in too many works. For example Golabi et al. (2013) also employed such a solution. There are different variations in the way these observers are constructed, but a common problem for them is the fact that we tend to arrive at BMI forms (Bilinear Matrix Inequality). So our contribution here lies in the way we avoided the BMI. We define the general TS system as in previous methods, followed by the proposed observer structure:

$$\begin{cases} \dot{x} = \sum_i w_i(z)(A_i x + B_i u) \\ y = Cx \end{cases}, \tag{2.53}$$

$$\begin{cases} \dot{\hat{x}} = \sum_i w_i(\hat{z})(A_i \hat{x} + B_i u) + \xi \\ \hat{y} = C\hat{x} \\ \dot{x}_d = A_d x_d + B_d \eta \\ \xi = C_d x_d + D_d \eta \\ \eta = y - \hat{y} = Ce \\ e = x - \hat{x} \end{cases} \tag{2.54}$$

We propose a change in variable $x_a = (e; x_d)^T$. The derivative of this new state becomes:

$$\dot{x}_a = \begin{pmatrix} \dot{e} \\ \dot{x}_d \end{pmatrix} = \begin{pmatrix} \sum_i w_i(z)(A_i x + B_i u) - \sum_i w_i(\hat{z})(A_i \hat{x} + B_i u) - C_d x_d - D_d C e \\ A_d x_d + B_d C e \end{pmatrix} \tag{2.55}$$

$$\dot{x}_a = \begin{pmatrix} \sum_i \{w_i(z) A_i x - w_i(\hat{z}) A_i x + w_i(z) B_i u - w_i(\hat{z}) B_i u\} - C_d x_d - D_d C e \\ A_d x_d + B_d C e \end{pmatrix} \tag{2.56}$$

It can easily be noted that, without the simplifying hypotheses of measurable premise variables, there will be membership functions depending on state estimates. To solve this problem, the technique presented in Yacine et al. (2012) is applied. Therefore by adding and subtracting a $w_i(\hat{x}) \cdot A_i \cdot x$, and separating the two sums, the first one is seen as a virtual perturbation (It is clear that when $x \to \hat{x}$, $(w_i(x) - w_i(\hat{x})) \to 0$). We rearrange the state derivative:

$$\dot{x}_a = \begin{pmatrix} \sum_i \left\{ \begin{array}{l} (w_i(z) - w_i(\hat{z})) A_i x + (w_i(z) - w_i(\hat{z})) B_i u + \\ + w_i(\hat{z})(A_i x - A_i x) \end{array} \right\} - C_d x_d - D_d C e \\ A_d x_d + B_d C e \end{pmatrix} \tag{2.57}$$

The terms dependent of $((\mathrm{w}_i(x) - \mathrm{w}_i(\hat{x}))$ can be separated, therefore we reach the following expression:

$$\left\{ \begin{array}{l} \dot{x}_a = \begin{pmatrix} \Delta + \sum_i \{w_i(\hat{z}) \cdot A_i \cdot e\} - C_d x_d - D_d C e \\ A_d x_d + B_d C e \end{pmatrix} \\ \Delta = \sum_{i=1}^{8} [(w_i(z) - w_i(\hat{z})) \cdot (B_i \cdot u + A_i \cdot x)] \end{array} \right. \tag{2.58}$$

As we know that $\sum_i w_i(z) = 1$ then the equality becomes:

$$\begin{cases} \dot{x}_a = \begin{pmatrix} \Delta \\ 0 \end{pmatrix} + \begin{pmatrix} \sum_i \{w_i(\hat{z})(A_i - D_d C)\} & -C_d \\ B_d C & A_d \end{pmatrix} \begin{pmatrix} e \\ x_d \end{pmatrix} \\ \Delta = \sum_{i=1}^{8} [(w_i(z) - w_i(\hat{z}))(B_i \cdot u + A_i x)] \end{cases} \tag{2.59}$$

By considering bounded states, bounded inputs as well as bounded membership functions, then Δ is clearly bounded as well. A quadratic Lyapunov function has been chosen $V = x_a^T P x_a$ with a square, positive definite and symmetric matrix $P > 0$. Applying H_{inf} stability in the presence of Δ, interpreted as as perturbation, we arrive at the expression:

$$\dot{V}(t) = \dot{x}_a^T P x_a + x_a^T P \dot{x}_a < -x_a^T G x_a + \gamma^2 \begin{pmatrix} \Delta \\ 0 \end{pmatrix}^T \begin{pmatrix} \Delta \\ 0 \end{pmatrix} \tag{2.60}$$

Differentiating the Lyapunov function, the next inequality arises:

$$\begin{cases} \dot{V}(t) = \begin{pmatrix} \Delta \\ 0 \end{pmatrix}^T P x_a + \begin{pmatrix} e \\ x_d \end{pmatrix}^T \begin{pmatrix} \sum_i \{w_i(\hat{z}) \cdot (A_i - D_d C)\} & -C_d \\ B_d C & A_d \end{pmatrix}^T P x_a + \\ + x_a^T P \begin{pmatrix} \Delta \\ 0 \end{pmatrix} + x_a^T P \begin{pmatrix} \sum_i \{w_i(\hat{z}) \cdot (A_i - D_d C)\} & -C_d \\ B_d C & A_d \end{pmatrix} \begin{pmatrix} e \\ x_d \end{pmatrix} < -x_a^T G x_a + \\ + \gamma^2 \begin{pmatrix} \Delta \\ 0 \end{pmatrix}^T \begin{pmatrix} \Delta \\ 0 \end{pmatrix} \\ \Delta =^{not} \sum_{i=1} [(w_i(z) - w_i(\hat{z})) \cdot (B_i \cdot u + A_i \cdot x)] \\ x_a = \begin{pmatrix} e \\ x_d \end{pmatrix} \end{cases} \tag{2.61}$$

$$\begin{pmatrix} \Delta \\ 0 \end{pmatrix}^T P x_a + x_a^T \begin{pmatrix} \sum_i \{w_i(\hat{z}) \cdot (A_i - D_d C)\} & -C_d \\ B_d C & A_d \end{pmatrix}^T P x_a +$$
$$+ x_a^T P \begin{pmatrix} \Delta \\ 0 \end{pmatrix} + x_a^T P \begin{pmatrix} \sum_i \{w_i(\hat{z}) \cdot (A_i - D_d C)\} & -C_d \\ B_d C & A_d \end{pmatrix} x_a < \tag{2.62}$$
$$< -x_a^T G x_a + \gamma^2 \begin{pmatrix} \Delta \\ 0 \end{pmatrix}^T \begin{pmatrix} \Delta \\ 0 \end{pmatrix}$$

As in the previous method, we use $\forall\ \lambda > 0, X, Y : X^T Y + Y^T X \leq \lambda X^T X + \lambda^{-1} Y^T Y$

Meaning: $\begin{pmatrix} \Delta \\ 0 \end{pmatrix}^T P x_a + x_a^T P \begin{pmatrix} \Delta \\ 0 \end{pmatrix} \leq \lambda \begin{pmatrix} \Delta \\ 0 \end{pmatrix}^T \begin{pmatrix} \Delta \\ 0 \end{pmatrix} + \lambda^{-1} x_a^T P P x_a$

Using this in the system inequality the unwanted terms will disappear:

$$x_a^T \left\{ \begin{pmatrix} \sum_i \{w_i(\hat{z})(A_i - D_d C)\} & -C_d \\ B_d C & A_d \end{pmatrix}^T P + P \begin{pmatrix} \sum_i \{w_i(\hat{z})(A_i - D_d C)\} & -C_d \\ B_d C & A_d \end{pmatrix} \right\} x_a +$$
$$+ \lambda \begin{pmatrix} \Delta \\ 0 \end{pmatrix}^T \begin{pmatrix} \Delta \\ 0 \end{pmatrix} + \lambda^{-1} x_a^T P P x_a < -x_a^T G x_a + \gamma^2 \begin{pmatrix} \Delta \\ 0 \end{pmatrix}^T \begin{pmatrix} \Delta \\ 0 \end{pmatrix} \tag{2.63}$$

An interesting observation is that, because λ >0 can be any coefficient, then it can be chosen as $\lambda = \xi^2$, which simplifies the relation; moreover, employing the convex sum property, we arrive at

$$x_a^T \left\{ \begin{pmatrix} \sum_i \{w_i(\hat{z}) \cdot (A_i - D_d C)\} & -C_d \\ B_d C & A_d \end{pmatrix}^T P + P \begin{pmatrix} \sum_i \{w_i(\hat{z}) \cdot (A_i - D_d C)\} & -C_d \\ B_d C & A_d \end{pmatrix} \right.$$
$$\left. + G + \gamma^2 P P \right\} x_a < 0 \tag{2.64}$$

In order to continue we use a few theorems used as well in Marquez et al. (2013). As mentioned in the stated article, we can make use of the logic: $If\, there (\exists)$ a small $\epsilon > 0$ so that $\left(\alpha \cdot R + R \cdot \alpha^T < 0\right)$ then $R \cdot \alpha^T +$

$\alpha \cdot R + \epsilon \cdot \alpha \cdot R \cdot \alpha^T < 0$

Indeed this is true, as R>0=> $\alpha \cdot R \cdot \alpha^T > 0$ so $\epsilon \cdot \alpha \cdot R \cdot \alpha^T > 0$

Therefore $R \cdot \alpha^T + \alpha \cdot R + \epsilon \cdot \alpha \cdot R \cdot \alpha^T < 0$ which can be written :

$$\underline{\epsilon R \alpha^T} + \underline{\underline{\epsilon \alpha R}} + \underline{\underline{\epsilon^2 \alpha R \alpha^T}} + \underline{R} - R < 0$$

Grouping the terms, the following logic is followed:

$$\begin{gathered} R\left(\epsilon\alpha^T + I\right) + \epsilon\alpha \cdot R\left(I + \epsilon\alpha^T\right) < R \\ (R + \epsilon\alpha \cdot R)\left(I + \epsilon\alpha^T\right) - R < 0 \\ -(I + \epsilon\alpha) \cdot R\left(I + \epsilon\alpha^T\right) + R > 0 \end{gathered}$$

By means of Schur format(as R>0) it results that:

$$\begin{pmatrix} R & I + \epsilon \cdot \alpha \\ I + \epsilon \cdot \alpha^T & R^{-1} \end{pmatrix} > 0 \tag{2.65}$$

We make use of the fact that

$$\begin{aligned} &(R^{-1} - I)^T \cdot R \cdot (R^{-1} - I) > 0 => \\ &(I - R) \cdot (R^{-1} - I) > 0 => \\ &R^{-1} - I - I + R > 0 => \\ &R^{-1} > 2I - R \end{aligned}$$

Theorem 1
$$\left\{ \begin{array}{l} \begin{pmatrix} a & b \\ b^T & d \end{pmatrix} > 0 \\ d > 0 \\ d < r \end{array} \right. => \begin{pmatrix} a & b \\ b^T & r \end{pmatrix} > 0, \tag{2.66}$$
where a, b, d are any appropriately dimensioned matrices.

This can be easily proven as follow. By means of the Schur complement (as $d > 0$), we can :

$$a - bd^{-1}b^T > 0 => a > bd^{-1}b^T \tag{2.67}$$

Yet $d < r$ implies that $d^{-1} > r^{-1}$. Therefore we multiply left and right by b and b transposed obtaining:

$$bd^{-1}b^T > br^{-1}b^T \tag{2.68}$$

From (2.67) and (2.68)=> $a > br^{-1}b^T$. Applying the Schur transform in the opposite direction, gives us the required proof. Thus applying this will imply the inequalities:

$$\begin{cases} \begin{pmatrix} R & I + \epsilon \cdot \alpha \\ I + \epsilon \cdot \alpha^T & 2I - R \end{pmatrix} > 0 \\ 2I - R < R^{-1} \end{cases} => \begin{pmatrix} R & I + \epsilon \cdot \alpha \\ I + \epsilon \cdot \alpha^T & R^{-1} \end{pmatrix} > 0 \tag{2.69}$$

So now we have arrived at this LMI:

$$\begin{pmatrix} R & I + \epsilon \cdot \alpha \\ I + \epsilon \cdot \alpha^T & 2I - R \end{pmatrix} > 0 \tag{2.70}$$

Returning to our system:

$$\begin{pmatrix} \sum_i \{w_i(\hat{z}) \cdot (A_i - D_d C)\} & -C_d \\ B_d C & A_d \end{pmatrix}^T P + P \begin{pmatrix} \sum_i \{w_i(\hat{z}) \cdot (A_i - D_d C)\} & -C_d \\ B_d C & A_d \end{pmatrix} + \\ + G + \gamma^2 PP < 0 \tag{2.71}$$

The $G + \gamma^2 PP$ term does not affect the previous theorem.

$$\begin{pmatrix} P & I+\epsilon\begin{pmatrix} \sum_i\{w_i(\hat{z})(A_i-D_dC)\} & -C_d \\ B_dC & A_d \end{pmatrix}^T \\ I+\epsilon\begin{pmatrix} \sum_i\{w_i(\hat{z})(A_i-D_dC)\} & -C_d \\ B_dC & A_d \end{pmatrix} & 2I-P \end{pmatrix} > 0 \tag{2.72}$$

Thus we have arrived at a system of LMI in 2.73, that once solved will gives us the observer:

$$\begin{pmatrix} P & I+\epsilon\begin{pmatrix} A_i-D_dC & -C_d \\ B_dC & A_d \end{pmatrix}^T \\ I+\epsilon\begin{pmatrix} A_i-D_dC & -C_d \\ B_dC & A_d \end{pmatrix} & 2I-P \end{pmatrix} > 0 \tag{2.73}$$

Here ϵ is chosen statically, so to avoid BMIs.

2.7 Conclusions

In this chapter, different nonlinear observers have been developed using the Takagi-Sugeno technique. The mentioned TS techniques show a high potential, as all the TS observers have the premise variables unmeasurable which is an even more challenging problem. The thesis' contributions in this chapter come from searching and testing different existing methods, techniques and tendencies, adapting them to a certain framework and adding some modifications in order to bring to the methods a higher numerical robustness.

We have also considered the Mean Value based method which is interesting as it can be seen as a different form of Takagi-Sugeno. The bounded stability TS observer brings an alternative to methods based on the Lipschitz approach. The observer developed using the Lipschitz constant proved hard to build and calibrate, as the correct Lipschitz values are hard to find. Also, lastly, the dynamic TS observer shows a new way to avoid the contact with Bilinear Matrix Inequalities.

This chapter was developed having as target the Fuel Cell application on which these methods were afterward applied. The FC due to its complexity and broad range of domains that interact, as well as the simulation software gave us the opportunity to verify these different nonlinear techniques, checking their viability and implementability.

Chapter 3

Fault Detection and Isolation

3.1 Introduction 45

3.2 Fault Detection and Estimation by Takagi-Sugeno PI observer 48

3.2.1 Observer development 50

3.3 Improved Takagi-Sugeno PI observer for Fault Detection and Estimation 56

3.3.1 Observer development 57

3.4 Conclusions 64

3.1 Introduction

Recently, the fuel cell research community has shown a considerable interest for Fault Detection and Diagnostic (FDD) in order to ensure safety, security, when faults occur. These faults must be detected on-line, with a fast response time in order for maintenance action to be taken in accordance. For active or passive Fault Tolerant Control problems, the fault estimation is required as well, in order to be used for accommodating in any command structure.

Different types of classifications for methods used for estimation or diagnosis exist. We distinguish two major classes:

- data driven methods (as signal based algorithms and knowledge based algorithms (State estimation via neural network Abdollahi et al. (2006))). These Data driven techniques are constructing having a large set of reference data within which the current data is fitted. For example, in the case of fault diagnostics, the current behavior is compared to a series of known healthy behaviors. If the data is not situated in the same functional interval, then a fault is signaled. Therefore this method follows a training step, that configures a classification algorithm. A review on data driven diagnostic for Fuel Cells is done in Li et al. (2014).
- model based methods. These approaches bring robustness in the sense of being more tolerant to uncertainties. Of course the main requirement for these methods is to determine all the system parameters (which may prove difficult).

A detailed review on different existing approaches correlated to Fuel Cells is done in the Fuel Cell Application chapter.

The general idea in Fault Diagnosis model based methods is to compare the available measurements of the monitored system with their corresponding predictions obtained using a system model, either analytical or qualitative. If they differ significantly, we can conclude that a fault has occurred. The well-known methods are:

1. Parity space approach Aitouche et al. (2011) which consists to generate relations linked to direct input-output model equations. Those relations are known also as analytical redundancy which serves for fault detection and isolation.
2. Observer based approach which aims at estimating the outputs of the system by using observers like the Luenberger observer in deterministic case and Kalman filters in stochastic case as the work of Bergsten and Palm (2000). The output estimation error is then used as residual in order to detect the faults. A special observer can be build to estimate the fault as well.

The set of residuals generated by the difference between the real system's output vector y and the estimated output vector $\hat{y}$ is defined as follow :

$$r = y - \hat{y} \tag{3.1}$$

The residual r is a function that can be used to detect a fault by means of a special logic block that analyzes this signal's evolution. It is clear from equation (3.1) that the output estimation error is affected by the faults. The system represented by this equation is asymptotically stable, since the stability conditions of the observers are fulfilled. In the ensuing development, we shall limit our attention only to sensor faults. Generally, fault detection is achieved by comparing the residuals (normalized by their variance) to a specified threshold. To be more precise, a bank of observers have to be designed to facilitate faults isolation. A well-known approach for sensor fault isolation is based on Dedicated Observers Scheme (DOS) (detailed in Chen and Patton (1999)) to increase robustness of such observer-based Diagnosis scheme. Each observer of the DOS is dedicated to each output of the multi-sensors to generate a set of residual signals which, are determined by the difference between the systems measurements and the estimated output of the observers. By the Decision mechanism of the residuals, the sensor faults can be detected and isolated as in figure 3.1. In this general schematic the Dedicated Observer Scheme is clearly determined by the stack of observers situated in parallel.

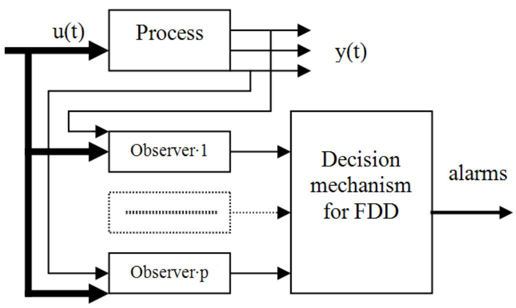

Figure 3.1: Fault in the sensor return pressure manifold and its reconstruction

The papers on diagnostics expand on a very large scale of approaches and processes, but we can mainly distinguish two categories of methods:

ones that manage the detection and isolation of faults (FDI) and others that manage also the fault estimation. The latter is a more difficult problem, as the complexity rises significantly. Solutions for state estimation exist, for example by means of sliding mode observers, or even proportional integral observers.

An interesting review on TS based fault detection is presented in Maquin (2009), the content expanding from nonlinear state estimation in general to the use of observer in fault detection by means of Unknown Input Observer(UIO) or Proportional Integral Observers (PIO). As an example we can cite the work of Ichalal et al. (2009), that manages sensor fault diagnosis considering uncertainties in the system matrices.

3.2 Fault Detection and Estimation by Takagi-Sugeno PI observer

The use of Unknown Input Observers (UIO) has been employed for a considerable time already in the construction of Fault Detection, Isolation and even Estimation as *e.g.*Martinez-Guerra and Diop (2004). These observers have been adapted also for TS representations, as the works of Chen and Saif (2007), Marx et al. (2007). Different processes have been tested by applying diagnostic techniques of this type, as in the work of Djemili et al. (2012), where the fault is an intake leakage estimation for a diesel engine, or the research of Ouyessaad et al. (2013) that considers a doubly fed induction generator in a wind turbine.

A similar approach to UIO is the so called Proportional Integral (PI) observer (Busawon and Kabore (2000)). The interest for such observers is that they can be used both for estimating states of the system and also for estimating the unknown inputs. In Takagi Sugeno representation, researches related to this type of observers are somewhat more recent, as Khedher et al. (2010), Aouaouda et al. (2013), Ichalal et al. (2010) in which unmeansurable premise variables are considered. An interesting recent work in this regard, is that of Youssef et al. (2014a) (Youssef et al. (2014b)), where sensor and actuator faults are considered; here, the unmeasurable premise variable is compensated by an added correction term in the observer.

In these approaches, generally it is considered that the fault is a polynomial of $k-1$ degree, that has its k^{th} derivative bounded. Regarding the embedded implementation of this algorithm, a too high value of k would imply numerical computations with high dimension matrices, thus posing memory and performance issues.

We will now develop a PI observer for sensor faults. Firstly, we start from a general TS model that is represented in equation (3.2).

$$\begin{cases} \dot{x} = \sum_{i=1}^{2^n} w_i(z(t))A_i x(t) + Bu(t) \\ y = Cx(t) + Ef_s(t) \end{cases} \tag{3.2}$$

We have considered the notations as in the previous TS models, where $x(t) \in \mathbb{R}^{n_x}$ is the time varying state vector, $u(t) \in \mathbb{R}^{n_u}$ is the system input vector, $y(t) \in \mathbb{R}^{n_y}$ is the output vector, $z(x) \in \mathbb{R}^n$ is the vector of n nonlinearities in the system, $f_s(t) \in \mathbb{R}^{n_{fs}}$ is the sensor fault vector, $w_i(z) : \mathbb{R}^n \to \mathbb{R}$ is the weighting function, and finally $A \in \mathbb{R}^{n_x \times n_x}$, $B \in \mathbb{R}^{n_x \times n_u}$, $C \in \mathbb{R}^{n_y \times n_x}$ and $E \in \mathbb{R}^{n_y \times n_{fs}}$ are the system matrices. It is assumed that the faults are of polynomial form having $k-1$ degree with bounded k$^{\text{th}}$ order derivative bounded, in other words, (3.3) is satisfied. Gao et al. (2007), Lendek et al. (2010) motivate the practicality of this assumption.

$$\begin{aligned} &\dot{f}_s(t) = f_{s1}(t) \\ &\dot{f}_{s1}(t) = f_{s2}(t) \\ &\dots \\ &\dot{f}_{s(k-1)}(t) = f_{sk}(t) \\ &f_{sk}(t) \leq f_{bound} \\ &f_{bound} > 0 \end{aligned} \tag{3.3}$$

3.2.1 Observer development

The associated TS observer that we will use is represented in equation (3.4).

$$\begin{cases} \dot{\hat{x}} = \sum_{i=1}^{2^n} \{w_i(\hat{z})[A_i\hat{x} + K_{Pi}(y-\hat{y})]\} + Bu \\ \hat{y} = C\hat{x} + E\hat{f}_s \\ \dot{\hat{f}}_s = \sum_{i=1}^{2^n} \{w_i(\hat{z})[K_{Ii}(y-\hat{y})]\} + \hat{f}_{s1} \\ \dot{\hat{f}}_{s1} = \sum_{i=1}^{2^n} \left\{w_i(\hat{z})\left[K_{Ii}^1(y-\hat{y})\right]\right\} + \hat{f}_{s2} \\ \ldots\ldots\ldots \\ \dot{\hat{f}}_{s(k-1)} = \sum_{i=1}^{2^n} \left\{w_i(\hat{z})\left[K_{Ii}^{k-1}(y-\hat{y})\right]\right\} + \hat{f}_{sk} \end{cases} \tag{3.4}$$

where $K_{Pi} \in \mathbb{R}^{n_x \times n_y}$, $K_{Ii} \in \mathbb{R}^{n_{fs} \times n_y}$, stand for the proportional gains and the integral gains, respectively. In order to achieve a more simpler expression of the TS system and the TS observer, a new extended system representation is considered as in (3.5), where the new system's states and matrices are defined as:

$$\bar{x} = \begin{pmatrix} x \\ f_s \\ f_{s1} \\ \ldots \\ f_{s(k-1)} \end{pmatrix} \bar{A}_i = \begin{pmatrix} A_i & 0 & 0 & \ldots & 0 \\ 0 & 0 & I & \ldots & \\ \ldots & \ldots & \ldots & \ldots & \ldots \\ 0 & 0 & 0 & \ldots & I \\ 0 & 0 & 0 & \ldots & 0 \end{pmatrix} \bar{B} = \begin{pmatrix} B \\ 0 \\ \ldots \\ 0 \end{pmatrix}$$

$$\bar{K}_i = \begin{pmatrix} K_{Pi} \\ K_{Ii} \\ K_{Ii}^1 \\ \ldots \\ K_{Ii}^{k-1} \end{pmatrix} G = \begin{pmatrix} 0 \\ 0 \\ \ldots \\ 0 \\ I \end{pmatrix} \bar{C} = \begin{pmatrix} C \\ E \\ 0 \\ \ldots \\ 0 \end{pmatrix}$$

where $\bar{x} \in \mathbb{R}^{n_x + k\times n_{fs}}$, $u \in \mathbb{R}^{n_u}$, $\bar{A}_i \in \mathbb{R}^{(n_x+k\times n_{fs})\times(n_x+k\times n_{fs})}$ and $\bar{B} \in$

$\mathbb{R}^{(n_x+k\times n_{fs})\times n_u}$, $\bar{K}_i \in \mathbb{R}^{(n_x+k\times n_{fs})\times n_y}$. Finally, $G \in \mathbb{R}^{(n_x+k\times n_{fs})\times n_{fs}}$ and $\bar{C} \in \mathbb{R}^{(n_y+(k\times n_{fs}))\times n_{fs}}$. Using such notations, one obtains the system expressed in (3.5), and the observer in (3.6).

$$\begin{cases} \dot{\bar{x}} = \sum_{i=1}^{2^n} \left\{ w_i(z)\bar{A}_i\bar{x} \right\} + \bar{B}u + Gf_{sk} \\ y = \bar{C}\bar{x} \end{cases} \tag{3.5}$$

$$\begin{cases} \dot{\hat{\bar{x}}} = \sum_{i=1}^{2^n} \left\{ w_i(\hat{z}) \left[\bar{A}_i\hat{\bar{x}} + \bar{K}_i(y-\hat{y}) \right] \right\} + \bar{B}u + G\hat{f}_{sk} \\ \hat{y} = \bar{C}\hat{\bar{x}} \end{cases} \tag{3.6}$$

In order to apply any stability solution using Lyapunov theory, one needs the expression of the state estimation error $e = \bar{x} - \hat{\bar{x}}$. The error between the real system and the observed system is presented in (3.7).

$$\begin{cases} \dot{\bar{x}} - \dot{\hat{\bar{x}}} = \sum_{i=1}^{2^n} \left\{ w_i(z)\bar{A}_i\bar{x} - w_i(\hat{z}) \left[\bar{A}_i\hat{\bar{x}} + \bar{K}_i(y-\hat{y}) \right] \right\} + G\left(f_{sk} - \hat{f}_{sk}\right) \\ y - \hat{y} = \bar{C}\left(\bar{x} - \hat{\bar{x}}\right) \end{cases} \tag{3.7}$$

By replacing the values of the output estimation error from (3.7), the state estimation error dynamics becomes (3.8). We take into account the convex sum property ($\sum w_i = 1$), thus we will introduce terms that are outside the sum inside it, so that we can group them conveniently.

$$\dot{e} = \sum_{i=1}^{2^n} \left\{ w_i(z)\bar{A}_i\bar{x} - w_i(\hat{z}) \left[\bar{A}_i\hat{\bar{x}} + \bar{K}_i(\bar{C}\left(\bar{x} - \hat{\bar{x}}\right)) \right] \right\} + G\left(f_{sk} - \hat{f}_{sk}\right) \tag{3.8}$$

We can see that we have weighting functions that depend on the estimated premise variables as well as weighting functions dependent on the measured premises. We will rewrite the expression (3.8) so that we can separate the values multiplied by the difference $(w_i(z) - w_i(\hat{z}))$ from the other terms:

$$\dot{e} = \sum_{i=1}^{2^n} \left\{ \begin{array}{l} w_i(z)\bar{A}_i\bar{x} + w_i(\hat{z})\bar{A}_i\bar{x} - w_i(\hat{z})\bar{A}_i\bar{x} - \\ -w_i(\hat{z})\bar{A}_i\hat{\bar{x}} - w_i(\hat{z})\bar{K}_i\bar{C}e \end{array} \right\} + G\left(f_{sk} - \hat{f}_{sk}\right) \tag{3.9}$$

Thus, finally we obtain the following equation:

$$\begin{cases} \dot{e} = \sum_{i=1}^{2^n} \left\{ w_i(\hat{z})\left[\bar{A}_i e - \bar{K}_i\left(\bar{C}e\right) + G\tilde{f}_{sk}\right]\right\} + \Delta \\ \tilde{f}_{sk} = \left(f_{sk} - \hat{f}_{sk}\right) \\ \Delta = \sum_{i=1}^{2^n} \left\{ (w_i(z) - w_i(\hat{z}))\bar{A}_i\bar{x} \right\} \end{cases} \tag{3.10}$$

It is obvious that if the estimation error converges to 0 then also Δ will converge to a null value. Also we observe that the extended states are bounded, as well as the Δ term (remembering that the membership functions are sub-unitary). The unknown inputs (sensor faults), having bounded derivative, it means that they are bounded themselves. Because of this, as stated by Youssef et al. (2014b), Ding (2013), or Ichalal et al. (2009), the optimization condition that is to be imposed on the observer is to have a minimal L_2 norm of the transfer from the pair ($\Delta(t)$; $\tilde{f}_{sk}(t)$) to $e(t)$. This implies the minimization of the ξ scalar in the inequality (3.11).

$$\|e\|_2 < \xi \left\| \begin{array}{cc} \tilde{f}_{sk}(t) & \Delta(t) \end{array} \right\| \tag{3.11}$$

We now apply Lyapunov stability to the estimation error e by taking into account the optimization problem (3.11). This is accomplished by imposing the following matrix inequality:

$$\dot{V} + e^T e - \xi^2 \Delta^T \Delta - \xi^2 \tilde{f}_{sk}^T \tilde{f}_{sk} < 0 \tag{3.12}$$

where we have chosen the Lyapunov function V as a quadratic one $e^T Pe$, having P appropriately dimensioned (square, symmetric and positive definite matrix). The term ξ, is a scalar to be minimized. Developing the derivative of the Lyapunov function one arrives at:

$$\dot{V} = \dot{e}^T P e + e^T P \dot{e}$$

The derivative is further developed using equation 3.10:

$$\begin{aligned} \dot{V} &= \sum_{i=1}^{2^n} \left\{ w_i(\hat{z}) \left[e^T \bar{A}_i^T - e^T \bar{C}^T \bar{K}_i^T + \tilde{f}_{sk}^T G^T \right] \right\} Pe + \\ &+ e^T P \sum_{i=1}^{2^n} \left\{ w_i(\hat{z}) \left[\bar{A}_i e - \bar{K}_i \bar{C} e + G \tilde{f}_{sk} \right] \right\} + \Delta^T P e + e^T P \Delta \end{aligned} \tag{3.13}$$

By replacing (3.13) in the inequality (3.12) and arranging the terms, we arrive at the new inequality (3.14) that guarantees the stability where ξ is to be minimized.

$$\begin{aligned} & e^T \sum_{i=1}^{2^n} \left\{ w_i(\hat{z}) \left[\bar{A}_i^T - \bar{C}^T \bar{K}_i^T \right] \right\} Pe + e^T P \sum_{i=1}^{2^n} \left\{ w_i(\hat{z}) \left[\bar{A}_i - \bar{K}_i \bar{C} \right] \right\} e + \\ & + \tilde{f}_{sk}^T G^T P e + e^T P G \tilde{f}_{sk} + \Delta^T P e + e^T P \Delta + e^T e - \xi^2 \Delta^T \Delta - \xi^2 \tilde{f}_{sk}^T \tilde{f}_{sk} < 0 \end{aligned} \tag{3.14}$$

We recall Theorem (1):

For any X, Y square matrices of equal dimensions, the inequality $X^T Y + Y^T X \leq \lambda X^T X + \lambda^{-1} Y^T Y$ is always satisfied for any positive scalar λ.

Using the theorem for any scalar λ:

$$\Delta^T P e + e^T P \Delta \leq \lambda \Delta^T \Delta + \lambda^{-1} e^T P P e$$

And the left side contains positive terms therefore we can replace it in the inequality (3.14). Also as λ can be any positive scalar then we can consider it equal to ξ^2. By doing this, we arrive at:

$$\begin{aligned} &e^T \sum_{i=1}^{2^n} \left\{ w_i(\hat{z}) \left[\bar{A}_i^T - \bar{C}^T \bar{K}_i^T \right] \right\} Pe + e^T P \sum_{i=1}^{2^n} \left\{ w_i(\hat{z}) \left[\bar{A}_i - \bar{K}_i \bar{C} \right] \right\} e + \\ &+ \tilde{f}_{sk}^T G^T Pe + e^T PG\tilde{f}_{sk} + \xi^{-2} e^T PPe + e^T e - \xi^2 \tilde{f}_{sk}^T \tilde{f}_{sk} < 0 \end{aligned} \tag{3.15}$$

Applying the same logic, for the other terms outside the sum, the equation becomes:

$$\tilde{f}_{sk}^T G^T Pe + e^T PG\tilde{f}_{sk} \leq \lambda \tilde{f}_{sk}^T \tilde{f}_{sk} + \lambda^{-1} e^T PGG^T Pe$$

So choosing λ as before we arrive at:

$$\begin{aligned} &e^T \sum_{i=1}^{2^n} \left\{ w_i(\hat{z}) \left[\bar{A}_i^T - \bar{C}^T \bar{K}_i^T \right] \right\} Pe + e^T P \sum_{i=1}^{2^n} \left\{ w_i(\hat{z}) \left[\bar{A}_i - \bar{K}_i \bar{C} \right] \right\} e + \\ &+ \xi^{-2} e^T PGG^T Pe + \xi^{-2} e^T PPe + e^T e < 0 \end{aligned} \tag{3.16}$$

The estimation error terms can now be separated:

$$\begin{aligned} &e^T \left\{ \sum_{i=1}^{2^n} \left[w_i(\hat{z}) \left(\bar{A}_i^T P - \bar{C}^T \bar{K}_i^T P + P\bar{A}_i - P\bar{K}_i \bar{C} \right) \right] + \right. \\ &\left. + \xi^{-2} PGG^T P + \xi^{-2} PP + I \right\} e < 0 \end{aligned} \tag{3.17}$$

It is known that for any negative definite matrix $R < 0$, and any vector s of appropriate dimension, the following inequality is satisfied:

$$s^T R s < 0$$

By applying this to the inequality (3.17), as well as the convex sum property of the weighting function, the final relation (3.18) is obtained.

$$\sum_{i=1}^{2^n} w_i(\hat{z}) \left[\bar{A}_i^T P - \bar{C}^T \bar{K}_i^T P + P\bar{A}_i - P\bar{K}_i \bar{C} + \xi^{-2} PGG^T P + \xi^{-2} PP + I \right] < 0 \tag{3.18}$$

The only impediment in obtaining an LMI form for inequality (3.18) is the multiplication with the weighting terms. In order to eliminate the terms, we apply the classic approach of considering each term in the sum negative definite. It is clear that this is always true, yet we have to be aware of the restriction that this supposition brings. Yet in many applications this supposition has proved to be realistic, even though it affects the overall performance of the result. Therefore the inequality becomes a set of inequalities defined in (3.19) for $i = 1..2^n$.

$$\bar{A}_i^T P - \bar{C}^T \bar{K}_i^T P + P\bar{A}_i - P\bar{K}_i\bar{C} + \xi^{-2} PGG^T P + \xi^{-2} PP + I < 0 \tag{3.19}$$

We see that the inequalities are not in an LMI form. In order to obtain such a form, we use the Schur complement.

Definition 1 *Suppose A, B, C are respectively $p \times p$, $p \times q$ and $q \times q$ matrices, and C is invertible. Let M be the matrix:*

$$M = \begin{bmatrix} A & B \\ B^T & C \end{bmatrix}$$

In this context, the following inequalities are equivalent:

$$M < 0$$
$$C < 0, A - BC^{-1}B^T < 0$$

By applying the Schur complement's property to (3.19), the set of LMIs in (3.20) is obtained, for all $i = 1..2^n$.

$$\begin{gathered} min \xi \\ \begin{pmatrix} \bar{A}_i^T P - \bar{C}^T Q_i^T + P\bar{A}_i - Q_i\bar{C} + I & P & PG \\ P & -\xi^2 I & 0 \\ G^T P & 0 & -\xi^2 I \end{pmatrix} < 0 \end{gathered} \tag{3.20}$$

where $Q_i = P\bar{K}_i$, I is an appropriately dimensioned Identity matrix, and the zeros are zero valued matrices. An improvement to the optimization procedure was suggested by Ichalal et al. (2009), by pole assignement of the matrices $(\bar{A}_i - \bar{K}_i C)$.

3.3 Improved Takagi-Sugeno PI observer for Fault Detection and Estimation

The previous PI observer poses an issue when considering the bounded stability that we have imposed, therefore in order to solve this problem and to improve the results, the observer is changed by adding a set of compensating terms.

Therefore the observer is still in a Proportional Integral (PI) observer form (citing the work of Youssef et al. (2014a), Youssef et al. (2014b)). The objective is the same, to estimate some states of the system as well as the fault itself. In this work, considering our interest, we will focus only on sensor faults.

Again, the fault is considered to be polynomial in nature, of $k-1$ degree, having the k^{th} derivative bounded. The fact that the last derivative is bounded and not zero gives a generality to the considered case; it can also be interpreted as an additive and bounded perturbation.

The added terms act as sliding terms. In this context other work has been done in order to achieve fault and state estimation using sliding mode observers directly. Recent interesting works are Poschke et al. (2014) and Alwi and Edwards (2013). These approaches differ, mainly by the fact that the sliding term is essential in the working of the observer and the unmeasured premise variables are treated by means of Lipschitz constants. In this work, the sliding term is only a correcting term, thus the chattering effect is less of a problem.

Further, the development of the observer is treated in detail. Firstly, we start from a general TS model that is represented in equation (3.21).

$$\begin{cases} \dot{x} = \sum_{i=1}^{2^n} w_i(z(t))A_i x(t) + Bu(t) \\ y = Cx(t) + Ef_s(t) \end{cases} \tag{3.21}$$

As before, the notations signify: $x(t) \in \mathbb{R}^{n_x}$ is the time varying state vector, $u(t) \in \mathbb{R}^{n_u}$ is the system input vector, $y(t) \in \mathbb{R}^{n_y}$ is the output vector, $z(x) \in \mathbb{R}^n$ is the vector of n nonlinearities in the system, $f_s(t) \in \mathbb{R}^{n_{fs}}$ is the sensor fault vector, $w_i(z) : \mathbb{R}^n \to \mathbb{R}$ is the weighting function, and finally $A \in \mathbb{R}^{n_x \times n_x}$, $B \in \mathbb{R}^{n_x \times n_u}$, $C \in \mathbb{R}^{n_y \times n_x}$ and $E \in \mathbb{R}^{n_y \times n_{fs}}$ are the system matrices. As the faults can be represented in polynomial form of $k-1$ degree with bounded k$^{\text{th}}$ order derivative, (3.22) needs to be satisfied.

$$\begin{array}{l} \dot{f}_s(t) = f_{s1}(t) \\ \dot{f}_{s1}(t) = f_{s2}(t) \\ \ldots \\ \dot{f}_{s(k-1)}(t) = f_{sk}(t) \\ f_{sk}(t) \leq f_{bound} \\ f_{bound} > 0 \end{array} \tag{3.22}$$

3.3.1 Observer development

The associated TS observer will now be represented as in equation (3.23).

$$\begin{cases} \dot{\hat{x}} = \sum_{i=1}^{2^n} \{w_i(\hat{z})[A_i\hat{x} + K_{Pi}(y - \hat{y})]\} + Bu + v_x \\ \hat{y} = C\hat{x} + E\hat{f}_s \\ \dot{\hat{f}}_s = \sum_{i=1}^{2^n} \{w_i(\hat{z})[K_{Ii}(y - \hat{y})]\} + \hat{f}_{s1} + v_f \\ \dot{\hat{f}}_{s1} = \sum_{i=1}^{2^n} \left\{w_i(\hat{z})\left[K_{Ii}^1(y - \hat{y})\right]\right\} + \hat{f}_{s2} + v_{f1} \\ \ldots\ldots\ldots \\ \dot{\hat{f}}_{s(k-1)} = \sum_{i=1}^{2^n} \left\{w_i(\hat{z})\left[K_{Ii}^{k-1}(y - \hat{y})\right]\right\} + v_{f(k-1)} \end{cases} \tag{3.23}$$

where $K_{Pi} \in \mathbb{R}^{n_x \times n_y}$, $K_{Ii} \in \mathbb{R}^{n_{fs} \times n_y}$, for all k the integral gains, $K_{Ii}^j \in \mathbb{R}^{n_{fs} \times n_y}$. The $v_x(t)$, $v_f(t)$ and $v_{fi}(t)$(for $i = 1..k-1$) are switching functions used to compensate terms that bring an error in the estimation (their form will be determined when building the stabilization algorithm). In order to achieve a more simpler expression of the TS system and the TS observer, a new extended system representation is considered as in (3.24), where the new system's states and matrices are defined as:

$$\bar{x} = \begin{pmatrix} x \\ f_s \\ f_{s1} \\ \dots \\ f_{s(k-1)} \end{pmatrix} v = \begin{pmatrix} v_x \\ v_f \\ v_{f1} \\ \dots \\ v_{f(k-1)} \end{pmatrix} \bar{A}_i = \begin{pmatrix} A_i & 0 & 0 & \dots & 0 \\ 0 & 0 & I & \dots & 0 \\ \dots & \dots & \dots & \dots & \dots \\ 0 & 0 & 0 & \dots & I \\ 0 & 0 & 0 & \dots & 0 \end{pmatrix}$$

$$\bar{B} = \begin{pmatrix} B \\ 0 \\ \dots \\ 0 \end{pmatrix} \bar{K}_i = \begin{pmatrix} K_{Pi} \\ K_{Ii} \\ K_{Ii}^1 \\ \dots \\ K_{Ii}^{k-1} \end{pmatrix} G = \begin{pmatrix} 0 \\ 0 \\ \dots \\ 0 \\ I \end{pmatrix} \bar{C} = \begin{pmatrix} C & E & 0 & \dots & 0 \end{pmatrix}$$

where $\bar{x} \in \mathbb{R}^{n_x+k\times n_{fs}}$, $u \in \mathbb{R}^{n_u}$, $\bar{A}_i \in \mathbb{R}^{(n_x+k\times n_{fs})\times(n_x+k\times n_{fs})}$ and $\bar{B} \in \mathbb{R}^{(n_x+k\times n_{fs})\times n_u}$, $\bar{K}_i \in \mathbb{R}^{(n_x+k\times n_{fs})\times n_y}$. Finally, $G \in \mathbb{R}^{(n_x+k\times n_{fs})\times n_{fs}}$ and $\bar{C} \in \mathbb{R}^{n_y\times(n_x+(k\times n_{fs}))}$. Using such notations, one obtains the system expressed in (3.24), and the observer in (3.25).

$$\begin{cases} \dot{\bar{x}} = \sum_{i=1}^{2^n} \left\{ w_i(z)\bar{A}_i\bar{x} \right\} + \bar{B}u + Gf_{sk} \\ y = \bar{C}\bar{x} \end{cases} \tag{3.24}$$

$$\begin{cases} \dot{\hat{\bar{x}}} = \sum_{i=1}^{2^n} \left\{ w_i(\hat{z})\left[\bar{A}_i\hat{\bar{x}} + \bar{K}_i(y-\hat{y})\right] \right\} + \bar{B}u + v \\ \hat{y} = \bar{C}\hat{\bar{x}} \end{cases} \tag{3.25}$$

In order to apply any stability solution using Lyapunov theory, one needs the expression of the state estimation error dynamics $e = \bar{x} - \hat{\bar{x}}$. The error between the real system and the observed system is presented in (3.26).

$$\begin{cases} \dot{e} = \dot{\bar{x}} - \dot{\hat{\bar{x}}} = \sum_{i=1}^{2^n} \left\{ w_i(z)\bar{A}_i\bar{x} - w_i(\hat{z})\left[\bar{A}_i\hat{\bar{x}} + \bar{K}_i(y-\hat{y})\right]\right\} + Gf_{sk} - v \\ y - \hat{y} = \bar{C}\left(\bar{x} - \hat{\bar{x}}\right) \end{cases} \tag{3.26}$$

By replacing the values of the output estimation error from (3.26), the state estimation error dynamics becomes (3.27). We take into account the convex sum property ($\sum w_i = 1$), thus we will introduce terms that are outside the sum inside it, so that we can group them conveniently.

$$\dot{e} = \sum_{i=1}^{2^n} \left\{ w_i(z)\bar{A}_i\bar{x} - w_i(\hat{z})\left[\bar{A}_i\hat{\bar{x}} + \bar{K}_i(\bar{C}\left(\bar{x} - \hat{\bar{x}}\right))\right]\right\} + Gf_{sk} - v \tag{3.27}$$

We can see that we have weighting functions that depend on the estimated premise variables as well as weighting functions dependent on the measured premises. We will rewrite the expression (3.27) so that we can separate the values multiplied by the difference $(w_i(z) - w_i(\hat{z}))$ from the other terms:

$$\dot{e} = \sum_{i=1}^{2^n} \left\{ \begin{array}{l} w_i(z)\bar{A}_i\bar{x} + w_i(\hat{z})\bar{A}_i\bar{x} - w_i(\hat{z})\bar{A}_i\bar{x} - \\ -w_i(\hat{z})\bar{A}_i\hat{\bar{x}} - w_i(\hat{z})\bar{K}_i\bar{C}e \end{array} \right\} + Gf_{sk} - v \tag{3.28}$$

Thus, finally we obtain the following equation:

$$\begin{cases} \dot{e} = \sum_{i=1}^{2^n} \left\{ w_i(\hat{z})\left[\bar{A}_i e - \bar{K}_i\left(\bar{C}e\right) + Gf_{sk}\right]\right\} + \Delta - v \\ \Delta = \sum_{i=1}^{2^n} \left\{ (w_i(z) - w_i(\hat{z}))\bar{A}_i\bar{x} \right\} \end{cases} \tag{3.29}$$

It is obvious that if the estimation error converges to 0 then also Δ will converge to a null value. Also we observe that the extended states are bounded, as well as the Δ term (remembering that the membership functions are sub-unitary). The unknown inputs (sensor faults), having bounded derivative, it means that they are bounded themselves. Because of this, as stated by Youssef et al. (2014b), Ding (2013), or Ichalal et al. (2009), the optimization condition that is to be imposed on the observer is to have a minimal L_2 norm of the transfer from the pair ($\Delta(t)$; $f_{sk}(t)$) to $e(t)$. This implies the minimization of the ξ scalar in the inequality (3.30).

$$\|e\| < \xi \left\| \begin{matrix} f_{sk}(t) & \Delta(t) \end{matrix} \right\| \tag{3.30}$$

We now apply Lyapunov stability to the estimation error e by taking into account the optimization problem (3.30). We have added also the demand for exponential behavior for the stability in order to control the performance of the response by choosing a good α positive scalar. This is accomplished by imposing the following matrix inequality:

$$\dot{V} + e^T e - \xi^2 \Delta^T \Delta - \xi^2 f_{sk}^T f_{sk} + \alpha V < 0 \tag{3.31}$$

where we have chosen the Lyapunov function V as a quadratic one $e^T Pe$, having P appropriately dimensioned square, symmetric and positive definite matrix. The term ξ, is a scalar to be minimized. Developing the derivative of the Lyapunov function one arrives at:

$$\dot{V} = \dot{e}^T Pe + e^T P\dot{e}$$

The derivative is developed using equation 3.29:

$$\begin{gathered} \dot{V} = \sum_{i=1}^{2^n} \left\{ w_i(\hat{z}) \left[e^T \bar{A}_i^T - e^T \bar{C}^T \bar{K}_i^T + f_{sk}^T G^T \right] \right\} Pe + \Delta^T Pe + e^T P\Delta + \\ + e^T P \sum_{i=1}^{2^n} \left\{ w_i(\hat{z}) \left[\bar{A}_i e - \bar{K}_i \bar{C} e + G f_{sk} \right] \right\} - v^T Pe - e^T P v \end{gathered} \tag{3.32}$$

By replacing (3.32) in the inequality (3.31) and arranging the terms, we arrive at the new inequality (3.33) that guarantees the stability where ξ is to be minimized.

$$e^T \sum_{i=1}^{2^n} \left\{ w_i(\hat{z}) \left[\bar{A}_i^T - \bar{C}^T \bar{K}_i^T \right] \right\} Pe + e^T P \sum_{i=1}^{2^n} \left\{ w_i(\hat{z}) \left[\bar{A}_i - \bar{K}_i \bar{C} \right] \right\} e + \Delta^T Pe +$$
$$+ e^T P \Delta + f_{sk}^T G^T Pe + e^T PG f_{sk} - 2e^T Pv + e^T e - \xi^2 \Delta^T \Delta - \xi^2 f_{sk}^T f_{sk} + e^T Pe < 0 \tag{3.33}$$

Using the same matrix Theorem, as in the previous PI observer:

For any X, Y square matrices of equal dimensions, the inequality $X^T Y + Y^T X \leq \lambda X^T X + \lambda^{-1} Y^T Y$ is always satisfied for any positive scalar λ. ,

by taking any scalar λ, the following is true:

$$\Delta^T Pe + e^T P \Delta \leq \lambda \Delta^T \Delta + \lambda^{-1} e^T PPe$$

And the left side contains positive terms therefore we can replace it in the inequality (3.33). Also as λ can be any positive scalar then we can consider it ξ^2. By doing this, we arrive at:

$$e^T \sum_{i=1}^{2^n} \left\{ w_i(\hat{z}) \left[\bar{A}_i^T - \bar{C}^T \bar{K}_i^T \right] \right\} Pe + e^T P \sum_{i=1}^{2^n} \left\{ w_i(\hat{z}) \left[\bar{A}_i - \bar{K}_i \bar{C} \right] \right\} e +$$
$$+ f_{sk}^T G^T Pe + e^T PG f_{sk} + \xi^{-2} e^T PPe + e^T e - \xi^2 f_{sk}^T f_{sk} - 2e^T Pv + e^T Pe < 0 \tag{3.34}$$

Applying the same logic, for the other terms outside the sum, the equation becomes:

$$f_{sk}^T G^T Pe + e^T PG f_{sk} \leq \lambda f_{sk}^T f_{sk} + \lambda^{-1} e^T PGG^T Pe$$

The inequality (3.34) gets simplified, arriving at the form (3.35).

$$e^T \sum_{i=1}^{2^n} \left\{ w_i(\hat{z}) \left[\bar{A}_i^T - \bar{C}^T \bar{K}_i^T \right] \right\} Pe + e^T P \sum_{i=1}^{2^n} \left\{ w_i(\hat{z}) \left[\bar{A}_i - \bar{K}_i \bar{C} \right] \right\} e +$$
$$+ \left(\lambda - \xi^2 \right) f_{bound}^T f_{bound} + \lambda^{-1} e^T PGG^T Pe + \xi^{-2} e^T PPe + e^T e - 2e^T Pv + e^T Pe < 0 \tag{3.35}$$

By considering the λ as we did, a constraint is added to the stability. Thus we see the use of the sliding term that will help to compensate this error that will arise. Also we notice that only the sliding term is not bounded left and right by respectively e^T and e. In consequence the term v can be developed as:

$$\begin{cases} v = 0 \qquad if\ e_y^T e_y < \varepsilon \\ v = \delta \frac{P^{-1}\bar{C}^T \sqrt{e_y^T e_y} e_y}{2e_y^T e_y} + \left(\lambda - \xi^2\right) f_{bound}^T f_{bound} \frac{P^{-1}\bar{C}^T e_y}{2e_y^T e_y} \qquad if\ e_y^T e_y \geq \varepsilon \end{cases} \tag{3.36}$$

where $e_y = y - \hat{y} = \bar{C}e$, ε is a certain small scalar, that prevents chattering when the norm of the output estimation error is close to 0. This parameter is chosen as small as possible, but big enough to eliminate chattering. The term δ is also a scalar chosen as it will be shown. By rewriting the value of v into (3.35), $2e^T P v$ becomes $\delta\sqrt{e_y^T e_y} I + \left(\lambda - \xi^2\right) f_{bound}^T f_{bound}$. By replacing this parameter and by arranging the estimation error terms, the stability condition is rewritten as:

$$\begin{aligned} e^T \Big\{ \sum_{i=1}^{2^n} \left[w_i(\hat{z}) \left(\bar{A}_i^T P - \bar{C}^T \bar{K}_i^T P + P\bar{A}_i - P\bar{K}_i\bar{C} \right) \right] + \\ + \lambda^{-1} PGG^T P + \xi^{-2} PP + I + P \Big\} e - \sqrt{e_y^T e_y}\, \delta \cdot I < 0 \end{aligned} \tag{3.37}$$

By accepting some constraint in resolving the inequalities, (3.37) can be expressed as:

$$\begin{gathered} e^T \left\{ \sum_{i=1}^{2^n} \left[w_i(\hat{z}) \begin{pmatrix} \bar{A}_i^T P - \bar{C}^T \bar{K}_i^T P + P\bar{A}_i - P\bar{K}_i\bar{C} + I + \\ + P + \lambda^{-1} PGG^T P + \xi^{-2} PP \end{pmatrix} \right] \right\} e < e^T R e \\ e^T R e - \sqrt{e_y^T e_y}\, \delta \cdot I < 0 \end{gathered} \tag{3.38}$$

for a certain R matrix. As it is known that for any negative definite matrix $M < 0$, and any vector s of appropriate dimension, the following inequality is satisfied:

$$s^T M s < 0$$

.

Using this property, the system of inequalities becomes:

$$\begin{array}{c} \sum_{i=1}^{2^n}\left[w_i(\hat{z})\left(\begin{array}{c} \bar{A}_i^T P - \bar{C}^T \bar{K}_i^T P + P\bar{A}_i - P\bar{K}_i\bar{C} + I + \\ +P + \lambda^{-1}PGG^T P + \xi^{-2}PP - R \end{array} \right)\right] < 0 \\ \frac{\|e\|^2 \cdot max(eigenval(R))}{\sqrt{e_y^T e_y}} < \delta \end{array} \tag{3.39}$$

The $\|e_y\|^2$ represents the square of the l^2 norm, value that we can deduce offline, therefore the computation of δ can be done outside the LMI.

In order to get an LMI form for inequality (3.39), we apply the classic approach of considering each term in the sum as negative definite. It is clear that it is always true, yet, as always, we have to be aware of the restriction that this supposition brings. On the other hand, in many applications this supposition has proved to be realistic, even though it affects the overall performance of the result. Also using the Schur transform presented in definition (1), the system of inequalities becomes (3.40) for $i = 1..2^n$.

$$\begin{array}{c} min \xi, \delta \\ \begin{pmatrix} \bar{A}_i^T P - \bar{C}^T Q_i^T + P\bar{A}_i - Q_i\bar{C} + I + P - R & P & PG \\ P & -\xi^2 I & 0 \\ G^T P & 0 & -\lambda I \end{pmatrix} < 0 \\ \frac{\|e\|^2 \cdot max(eigenval(R))}{\sqrt{e_y^T e_y}} < \delta \end{array} \tag{3.40}$$

where Q_i are used just as temporary variables being equal to $P\bar{K}_i$, and I is an appropriately dimensioned Identity matrix, and the zeros are zero valued matrices.

3.4 Conclusions

In this chapter we have developed an algorithm for sensor fault estimation that can also estimate system states. Sensor faults were chosen as the focus of the thesis was on building virtual sensors and not on control. The solution is presented as a set of LMIs, that can be solved with specialized optimization software like Yalmip or the Matlab internal solver. The algorithm is based on a PI type observer, where the faults are considered to have a special form. In order to arrive to the LMI form, some suppositions were made like the quadratic Lyapunov function and the Parallel Distributed method for the TS system. The PI TS observer proves to be very interesting as it manages to estimate the value of the fault, thus being able to be integrated in fault tolerant control algorithms. The auxiliary sliding terms add precision at the expense of more time in configuring the observer parameters and in a slightly faster sampling time when implemented.

Chapter 4

On nonlinear embedded system development

4.1 Introduction 66

4.2 On Embedded Devices 68

4.3 Integrating Nonlinear Algorithms 71

4.4 Parallel Computing 75

4.4.1 Context 75

4.4.2 Motivation 76

4.4.2.1 *USART and SPI* 77

4.4.2.2 *Simulation testing* 79

4.5 Testing and validating using AMESim 83

4.6 Application example: Three water tank system 87

4.6.1 Takagi-Sugeno Observer 88

4.6.2 The Embedded system and HIL validation platform 89

4.6.2.1 *System description and modeling* 91

4.6.2.2 *Takagi-Sugeno transformation* 93

4.6.2.3 *The AMESim System* 94

4.6.2.4 *The real time simulation* 95

4.6.2.5 *Validation on a real system* 97

4.7 Conclusions 100

4.1 Introduction

Embedded systems play a crucial role in real time process automation, their computational power representing an important constraint to the performance of the whole system. Such systems are dedicated to the process at hand and to a certain functionality, yet the degree of specialization may differ; thus we find:

- complex embedded systems based on real-time operating systems as Windows CE, QNX, LynxOS, just to name a few (as an example for such a solution in a stationary context, there is the SIMATIC PC-based Controllers based on real-time compatible WindowsCE).
- on the other hand there exists fully dedicated systems as the FPGAs (field programmable gate arrays) or ASICs (application specific integrated circuit) or microcontroller based ones.

The attractiveness of the former embedded system approaches, is that the programming complexity reduces, having the capability to write code in grafcet language or even the SysML language Schutz et al. (2014). On the other hand this generality can reasonably be expected to incur in a reduced overall processing power and even a reduced compatibility with unknown external devices.

Furthermore the latter category, of small scaled embedded systems, as they become more powerful and financially attractive, has seen a continuous increase in usage in the last decade. In applications of control, diagnostics and signal processing, more complex and efficient strategies, as nonlinear or intelligent algorithms, start to be implemented on this type of systems, as for example in mechanical processes (having a slower response demand) Kendoul et al. (2007) or Pearce et al. (2014). Also, as the requirement for more complex methodologies increases, a more in-depth study of the possibilities and the feasibility of implementing complex algorithms on these types of platforms becomes increasingly useful.

Throughout the thesis, for the embedded part, an Atmel microcontroller solution is employed, supported by its versatility and its size per price ratio. In order to ease further the development effort, an Arduino platform is used. A parallel architecture is developed to increase the total system capability by means of distributed resources.

Another objective of the current work is to analyze the implementability of the Takagi-Sugeno approach, presented in previous chapters, on embedded systems. The choice for this nonlinear approach is motivated by the fact that it has a simple implementation form (being a blend of linear systems expressed numerically as a set of matrix operations) as well as having a structured design procedure (being easily obtained by means of a sector nonlinearity transformation Enrique et al. (2008)).

Concerning the implementation on a physical system, it is advisable to test an embedded system prior to deploying it on the real process, in order to avoid a potential instability or lack of robustness regarding uncertainties of the model or communication Zander et al. (2011). Therefore it is generally adopted the use of a validated and high reliability simulation software to replace the real system in the first hardware in the loop testing stage (HIL). As such, a professional software dedicated to model validation has been chosen, more precisely LMS AMESim Bourdon et al. (2007), to reproduce the process behavior. In order to create an interface between the simulated process and the embedded platform, Simulink is used on a Windows operating system. The choice for Windows was done as it is the most commonly used operating system, despite its lack of real time behavior. The acceptance of this drawback adds to the accessibility and the generality of this validation procedure, being able to adapt it to other simulators as well.

In conclusion the chapter's goals are firstly to synthesize the use of small scaled embedded systems in complex model based techniques, secondly to illustrate the feasibility of implementing a Takagi Sugeno model on an embedded microcontroller based platform and thirdly to present the procedure for validating a physical embedded system using a Hardware In The Loop architecture, where a simulation software replaces the process. As an application example, a three water tank system was chosen.

4.2 On Embedded Devices

An embedded device is an electronic numerical system, with dedicated role as part of a larger hardware system that respects real-time constraints.

When talking about embedded devices which are small scaled and with high level of specialization, we generally refer to embedded systems that are based on microcontrollers, but there are also dedicated boards with separated microprocessor, memory unit and peripheral units (microcontrollers having the processing, peripheral and memory units already incorporated).

We can distinguish three classes of embedded devices:

- *Microcontroller based boards* as Arduino boards;
- *FPGA* which are good for parallel computing;
- *Processor based boards:* as Raspberry PI, Beagle board, that act like small computers.

Each of them has certain advantages and disadvantages. In this thesis, the use of Arduino boards has been chosen, seeking the minimal performance type of processors that can cope with the requirements.

An FPGA, is an electronic gate array that can be dynamically arranged in a wanted configuration by means of software. They are commonly seen in signal processing applications, having the ability of parallel computations, thus escaping the sequential logic of microcontrollers. On the downside, they function at a digital gate level therefore programming a complex logic becomes a real challenge despite specific high level programming languages, because one has to take into account the limited number of available gates of each FPGA. Of course new FPGA models become increasingly powerful, integrating both floating point units and even microcontrollers in the same SoC (System on Chip). For example ALTERA Stratix 10 has an up to 10 Tflops of IEEE 754 compliant single precision floating point as well as an integrated quad-core 64 bit ARM® Cortex®-A53 hard processor with 1.5 GHz. As an example for using FPGA for model based techniques we can cite the work of Bonato et al. (2007) who has developed an extended Kalman Filter based on an FPGA.

For either microcontroller based or processor based embedded systems, the dominant architecture currently is RISC (Reduced Instruction Set Computing) giving the advantage of fewer processing cycles per instruction (thus heat, power and cost reduction), although some CISC (Complex Instruction Set Computing) devices can also be mentioned, although generally only low performance ones (8/16 bits for microcontrollers, yet really powerful and reliable systems of this architecture for microprocessor based boards). The used word size ranges from 8bit to 32bit and even sometimes 64bit (ARMv8), whereas the clock frequency ranges from 16Mhz for basic devices to 400Mhz for microcontrollers (less than 100Mhz for accessible microcontroller boards) and 1Ghz for some microprocessor based systems.

As a dominant example for RISC architecture, the family of ARM processors is the most spread. And in this family the ARMv6 core architecture is a renowned 32 bit example, as well as the newer ARMv7 that presents a hardware floating point unit (with ARMv6-M, ARMv7-M, ARMv7-R versions being respectively, the microcontroller and real time versions of the architecture). When talking about ARM cores, there are the ARMv1,v5,v6,v7,v8,etc. that represent architectural standards, that are incorporated in IPs (Intelectual Property) like ARM11 or ARM Cortex-M3, that become silicon circuits in different companies not necessarily the “ARM holdings“ company. As an example, the Arduino DUE board has a physical SAM3X8E processor, that is an ARM Cortex-M3 core respecting the ARMv7-M core architecture.

Considering the different types of Arduino boards approached in this thesis, a comparative study is presented in the table 4.1.

Table 4.1: Microcontroller boards

Arduino UNO	**Arduino MEGA 2560**	**Arduino DUE**
Atmel AVR Atmega328, 8 bit RISC microcontroller	Atmel AVR Atmega2560, 8 bit RISC microcontroller	Atmel 32 bit SMART SAM3X ARM Cortex-M3 microcontroller
• attractive for its low price and its compactness. • in its basic form, the microcontroller is encapsulated as DIP (dual in-line package), therefore once programmed the microcontroller can be directly extracted from the board and used in another dedicated circuit. • it only has 32kBytes of flash memory (to store the code). • it has 2kBytes of RAM memory (to store variables). • it works on a 16MHz clock frequency, that is sufficient only for small systems.	• it is a slightly more financially demanding. • yet it has a lot more input/outputs. • it presents several more serial channels. • it has a larger memory (256kBytes flash, 8kBytes RAM). • the clock is 16MHz, as in the UNO.	• it has the same price as an Arduino MEGA. • it has the same number of inputs/outputs. • its memory is higher: 512kBytes of flash memory and 96kBytes of RAM. • the processor architecture is different being an ARM11 with 32 bit architecture. • it can store far more complex system models with numerous large matrices. • it also can reach up to 84MHz clock frequency, which can be used to consequently reduce the calculation time on these complex systems.

The interest for embedded boards like the Arduino, Raspberry Pi or Beagle Boards is that they integrate different additional hardware both for performance enhancement (external clocks), safety and also for facilitating the connectivity with other boards. In the case of processor based boards, integration of memory and peripheral units is fundamental for their functionality and not just an addition. From a software point of view, the existence of pre-defined packages and higher level languages for the boards, speeds up the programming phase; yet for processor based boards, for real time, high performance applications, the processor needs to be programmed directly (so called "Bare Metal Programming") which is quite a cumbersome effort. For BeagleBone Black this is done by means of Texas Instruments "StarterWare", whereas for Raspeberry Pie, the more general open source software is the Pre-built GNU toolchain for ARM Cortex-M & Cortex-R processors.

The coding that is done in the Arduino IDE is embedded C language which is better for code re-usage and visibility, mixed with assembly language in order to optimize the computational speed. A variable discretization is used for the observer, meaning it is recalculated each sampling time inside each microcontroller, this helping in tackling the problem of lost samples.

Finally, the last characteristic to mention for small scale embedded devices, is that the whole system should be seen as a collaborative entity between different specialized modules. More precisely, if we want to add an LCD display, we may allocate one small microcontroller for receiving and sending data, as well as to manage the display driver itself, so there are other independent embedded devices that take care of the system model for example. The display in figure 4.1 that we used is a 16x4 LCD.

4.3 Integrating Nonlinear Algorithms

Generally speaking, the integration of model based techniques into embedded systems presents its own challenges, both in terms of processing speed and memory issues. This becomes even more complex with the addition of non linearities in the equations.

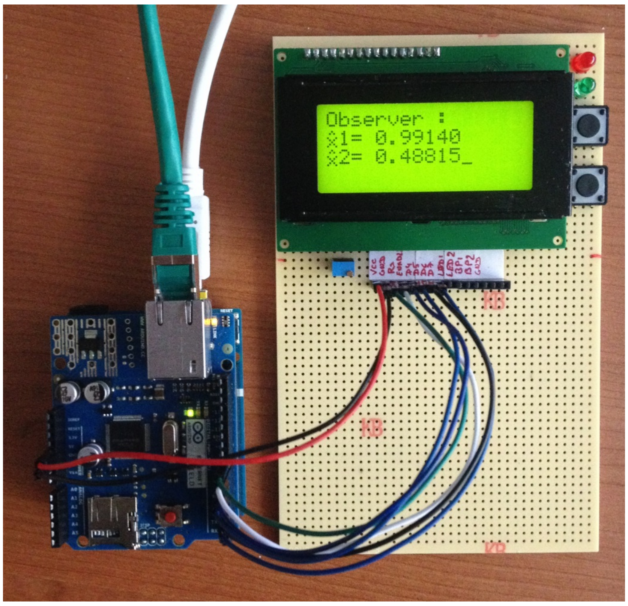

Figure 4.1: Entire Arduino system with Ethernet shield and LCD

When working with dynamical model based techniques, the numerical implementation most likely demands a set of characteristics that should be taken into account:

- matrix operations are fundamental.
- mathematical operands are in floating point format.
- there are sampling time constraints.

First aspect to be considered is the fact that small scaled embedded systems lack a hardware floating point unit. This can be solved by software reproduction of the floating point, adding constraints on the floating point precision, or by working with integer values (having multiplied beforehand the whole equality by multiples of 2, and dividing them afterward).

On the other hand, the Arduino DUE's processor has a hardware floating point unit. In general, a compromise has to be done in order to balance the size of the floating point type (therefore the computational speed) and the precision of results. This is because a negative effect is when the floating point size is reduced too much, mathematical operations between small scaled values and high valued numbers generate big errors (this is due to the way the floating point is represented). For example a good floating point representation is the IEEE 754 half-precision or single precision floating point representations Goldberg (1991):

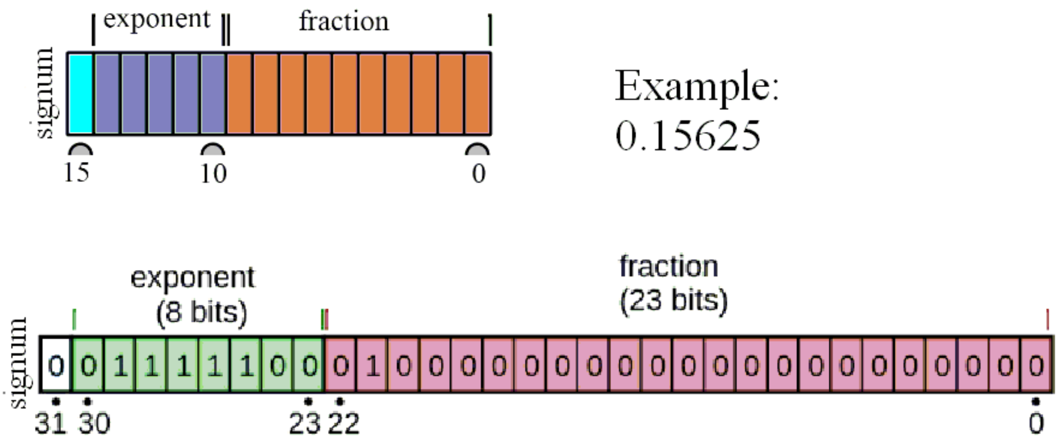

Figure 4.2: IEEE754 floating point format in 16 and 32 bit configuration

An example regarding the precision loss:

*single fs=101325.6*100.0; //100 bars (or just a potential multiplication by 100)*
fs+0.5 generates 10132562.0 //the 0.5 is completely ignored
*double fd=101325.6*100.0;*
fd+0.5 generates 10132561.5 //having a 64 bit representation resolves this lack of precision
So even at 100 bar, or just by multiplication we can arrive at such a faulty case.

Secondly, a common occurring problem is that the matrices are likely to contain a considerable amount of zeros (even if it is a sparse matrix or not). This problem implies a larger memory space occupied which is scarce in a microcontroller. Therefore, in order to keep at a minimum the memory space, the matrices should be saved in vector form, ignoring the zero terms when implementing the equations.

But the most important issue is the sampling time. In case it is chosen to work in a fixed sampling time, losses in communication would affect the result because some samples may be lost when faults occur, therefore stability itself can be lost. There are different solutions possible:

If a buffer is added to the transducer so that the sample is repeated until it has been received (let us say t_{k+d}), then the coefficients for the observers would not be the correct ones $d \cdot T_e \neq t_{k+d}$ (problem that can be corrected by considering the sampling time as a delay to the system), yet there will be a continuously increasing delay, which is problematic. Another solution is presented in Omran et al. (2013), Fiter et al. (2012) where $t_{k+1} = t_k + \tau(x(t_k))$, meaning a state dependent sampling time τ.

On the other hand, if no buffer is considered, meaning that once a data is not sent correctly, the transducer will pass to the new sample. Still, we have to take into account the sampling time lost in transmission. A simple solution would be to calculate gains in a continuous manner an to do a re-discretization (Euler method for example) at each program loop. The problem here is the reduced robustness when number of losses is to big.

When choosing the Takagi Sugeno method in this thesis, we have also considered the numerical advantages and inconvenient brought by the methodology. The general TS representation represented as a blended sum of linear systems is reminded in equation (4.1).

$$\begin{cases} \dot{x} = \sum_{i=1}^{n} w_i(z)\left(A_i x + B_i u\right) \\ y = \sum_{i=1}^{n} w_i(z)\left(C_i x\right) \end{cases} \tag{4.1}$$

As before, in the equation, we consider i as the number of a fuzzy rule, x the system states vector, y the system outputs vector, z the vector of nonlinear terms and u the system inputs vector and the matrices A_i, B_i, C_i representing constant system matrices. So the nonlinearities occurring inside the system matrices transfer inside the weighting functions w_i, therefore becoming a simple scalar that multiplies with the linear system representations, simplifying the computations as inter-matrices operations are cumbersome. Also seeing the sum representation, it comes to mind immediately the possibility of parallel calculus to improve the computational time. This aspect is treated in a further subchapter.

What needs also to be considered is the fact that the weighting functions respect a convex sum property ($\sum_i w_i(z) = 1$), thus having subunitary values. This is important, because numerically one has to deal with multiplications of subunitary scalars with high floating point values.

In literature, in the observer construction (either for state estimation or diagnosis) the Luenberger type observer is usually employed. The general form for Luenberger TS observer is recalled in equation (4.2). So as the LMI is created offline, the numerical implementation remains similar to that of the TS model itself having another constant matrix multiplied with the error vector.

$$\begin{cases} \dot{\hat{x}} = \sum_i^n w_i(\hat{z})(A_i\hat{x} + B_i u + L_i(\hat{y} - y)) \\ \hat{y} = \sum_i^n w_i(\hat{z}) C_i \hat{x} \end{cases} \tag{4.2}$$

4.4 Parallel Computing

4.4.1 Context

In the last decade, the evolution in processing power has steadily decreased in acceleration, as the processor speed approaches a maximum level. This level is determined by the transistor technology that barely manages to reach a 7nm scale and can reduce to somewhere around 4nm at most. Thus in order to improve system performance, the most common practice is to adapt a parallel computing approach.

The 8 bit microcontrollers were chosen in this study considering their accessibility, simple design compared to ARM processor based ones and robustness in IN/OUT ports. In consequence, the Arduino Mega 2560 was chosen.

This board is based on the ATmega2560 microcontroller, adding to the board some other components to enhance its functionality, components as DC to DC regulators for exterior power supply (giving both 5V

Table 4.2: Atmega2560 characteristics

Microcontroller	ATmega2560
Operating Voltage	5V
Input Voltage (recommended)	54 (of which 15 provide PWM output)
Digital I/O Pins	7-12 V
Analog Input Pins	16
DC Current per I/O Pin	40 mA
DC Current for 3.3V Pin	50mA
Flash Memory	256 KB of which 8 KB used by bootloader
SRAM	8KB
EEPROM	4KB
Clock Speed	16Mhz

and 3.3V), and a USB port that can be used in a serial communication by means of an ATmega16U2 microcontroller that acts as a serial-to-USB converter. The characteristics of this particular processor are enumerated briefly in tabel 4.2.

4.4.2 Motivation

When working with fast processes, also in a nonlinear model based context, strict requirements appear for processing power and memory management. Therefore, the solution adopted was to include parallel computations by connecting two processors in a distributed collaborative regime.

A fast solution of communication between the two has to be chosen. The communication capabilities of the ATmega2560 microcontroller are based on different types of serial protocols:

1. *Four Programmable Serial USART*
2. *Master/Slave SPI Serial Interface*
3. *Byte Oriented 2-wire Serial Interface*

4.4.2.1 *USART and SPI*

There exist the possibility to attach an Ethernet module to the employed Arduino platform. This would give the system a higher robustness in communication and also the advantage of multipoint connections (for adding also process transducers for example). An Ethernet module can reach a theoretical transfer rate of 100 Mbit/second, yet in practice, the Ethernet module, being connected to the Arduino board, reaches a lower transfer rate. This is due to the fact that this module is in fact physically connected to the microcontroller by an SPI link (Serial Peripheral Interface).

On the other hand, the four hardware serial UARTs (*Universal Asynchronous Receiver/Transmitter* transmit one bit at a time at a specified data rate (i.e. 9600bps, 115200bps, etc.)) for TTL (transistor-transistor logic) serial communication at 5V. The TTL supposes a logic high ('1') that is represented by Vcc and a logic low ('0') which is 0V.

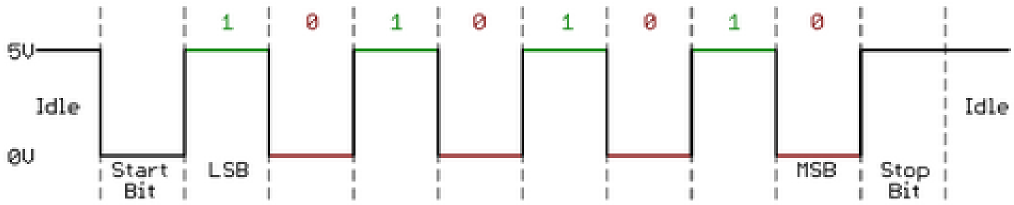

Figure 4.3: An example of 0b01010101 signal TTL and RS-232

It is of interest for us to show the difference between Synchronous/ asynchronous serial communication in order to motivate the choices that were taken.

The Serial Peripheral Interface (SPI) represents a synchronous serial communication bus interface very common for embedded systems, sensors, displays etc. The protocol was created by Motorola becoming afterward a *de facto standard* (meaning a standard appeared from practice and not official standardization), therefore small variations do exist.

For the 16 MHz Arduino board, the SPI speed can reach a maximum of 16 MHz divided by 2, therefore 8 MHz , plus the startup / close connection. As such, because of the SPI, in order to send one byte over a serial connection 10 bits are required (startbit - data - stopbit), so the best case scenario would reach a transfer speed of 100kbit/s. Some rudimentary tests have indicated ***10Kbit/s***.

Therefore we make use of the parallel communication as IO-pins are not required. Sensors being smart (transducers), an Ethernet/Serial protocol is used.

The SPI communication works in a full duplex regime, making use of the master-slave architecture. The selection between different slave devices is done by means of individual slave select (SS) lines. The principle is presented in figure 4.4, where the SPI connections are shown, both in a one-to-one communication and in a one-to-many connection.The physical implementation of the SPI protocol is based here on a 4 wire serial bus, presenting itself as a synchronous serial interface.

The communication timing for the serial protocol is defined in Annex figure C.1.

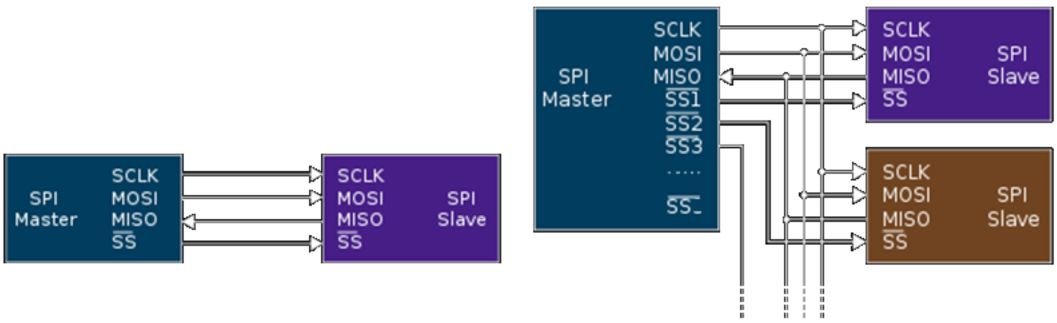

Figure 4.4: a) One on One connection b) One master, multiple slaves connection

The SPI bus specifies four logic signals:

- SCLK: Serial Clock (output from master).
- MOSI: Master Output, Slave Input (output from master).
- MISO: Master Input, Slave Output (output from slave).
- SS: Slave Select (active low, output from master).

We will not enter into detail about the significance of each port. The objective for mentioning them is to see the general functionality, on the one hand for helping with the software development part, and on the other to see the physical constraints that may appear.

4.4.2.2 *Simulation testing*

As a proof of concept, we show the basis of a simple 4 bit parallel computation distributed between 2 embedded systems.

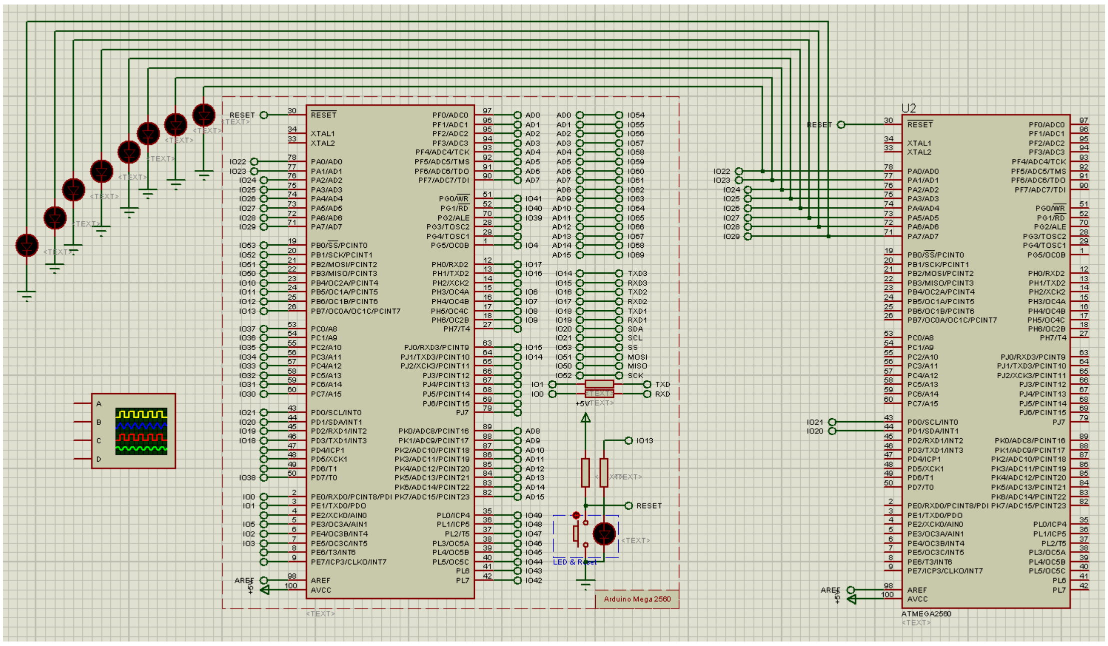

Figure 4.5: Proteus simulation showing 8 bit communication

LEDs are used as intermediary to better see the results. Also the communication has some delays so that the effect is visible. The master sends a value to the slave. The slave increments the value and sends it back. Therefore we will see an incremented value on the LEDs.

The physical connection is presented in figure 4.5 implemented in a electronic simulator Labcenter Electronics Isis Proteus, that can simulate microcontrollers as well.

As we can see in figure 4.6, the master is powered from the usb port and it shares Ground and Vcc to the slave (ground is important to be shared). The 2 yellow wires connect bit 0 and bit 1 of PortD.

They represent synchronization bits between the 2. The violet wires represent the 8 data wires connected to PortA. (they change direction, from reading to writing).

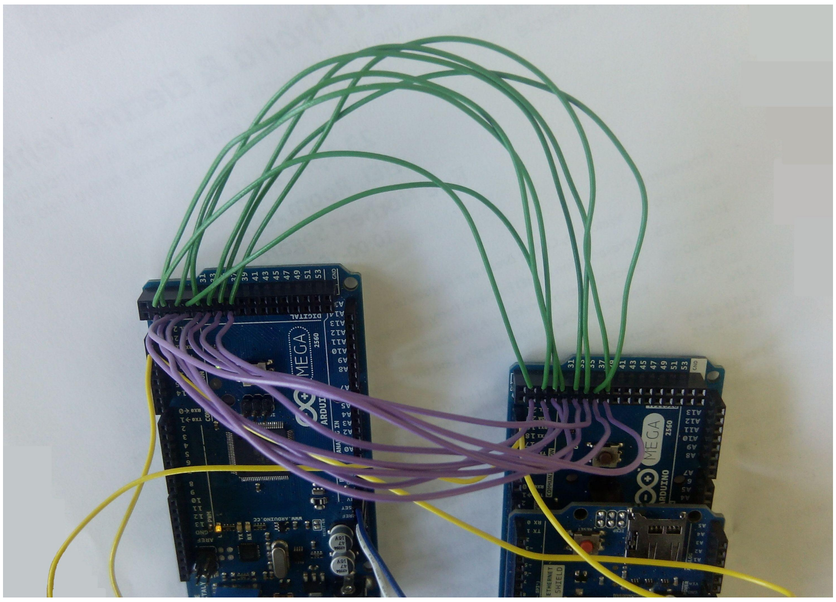

Figure 4.6: Physical implementation of the parallel configuration

The code for both master and slave is presented in the following table. Also it is important to note that the pull-up registers have to be activated for reading.

Master code	**Slave code**

// the setup runs once reset is pressed:
void setup(){ //initialize digital pin as output
//pinMode(led, OUTPUT);
asm("ldi R16,0b00000001");
// D0=output...D1=input
asm("out 0x0A,R16");
//(out DDRD,R16)direction register of portD
asm("ldi R22,0b10111001"); //a random number
//asm("sbi 0x0B,0");
	// the setup runs once reset is pressed:
	void setup(){ //initialize digital pin as output
	//pinMode(led, OUTPUT);
	asm("ldi R16,0b00000010");
	// D0=input...D1=output
	asm("out 0x0A,R16");
	//(out DDRD,R16)direction register of portD
	}

//first bit set in PORTD	
}	
// the loop routine runs over and	// the loop routine runs over and
over again forever:	over again forever:
void loop() {	void loop() {
//Reads from ethernet new state	//Prepare PortA to read
values	
asm("push R22");	asm("ldi R16,0x00");
delay(3000);	//PortA input(0)
// wait for 3 seconds	asm("out 0x01,R16");
asm("pop R22");	//(out DDRA,R16)direction register
	for port A
//Prepare PortA data to be sent	asm("ldi R16,0xFF");
asm("ldi R16,0xFF");	asm("out 0x02,R16");
//PortA output(1)	//(out PORTA,R16) Pull-up
	registers become active for PortA
asm("out 0x01,R16");	//enter loop to wait for uC 1 to write
	the data
//(out DDRA,R16)direction register	asm("label1:");
for port A	
asm("out 0x02,R22");	asm("sbis 0x09,0");
//move data to be sent in PORTA	//skip if bit in io register becomes 1
asm("push R22");	asm("rjmp label1");
delay(1000);	//read Data fro PortA
// wait for 3 seconds	asm("in R22,0x00");
asm("pop R22");	//PinA is 0x00
//Tell 2nd uC data ready	//Do own computations
asm("sbi 0x0B,0");	asm("inc R22");
//first bit set in PORTD	//just for test we increment the
	value read
//make own computations	//Prepare PortA to write
//enter loop while uC2 reads and	asm("ldi R16,0xFF");
calculates	
asm("label1:");	//PortA output(1)
asm("sbis 0x09,1");	asm("out 0x01,R16");

//skip if second bit in io register D becomes 1
asm("rjmp label1");
//read data from PinA
asm("ldi R16,0x00");
//PortA input(0)
asm("out 0x01,R16");
//(out DDRA,R16)direction register for port A
asm("ldi R16,0xFF");
asm("out 0x02,R16");
//(out PORTA,R16) Activate Pull Up registers for PortA
asm("in R22,0x00");
//PinA is 0x00
//do something with the data
asm("inc R22");
asm("push R22");
delay(1000);
// wait for 3 seconds
asm("pop R22");
//Confirm to uC2 that the data was read and to be prepared
asm("cbi 0x0B,0");
//first bit cleared in PORTD
//wait that uC2 cleares its PortD bit
asm("label2:");
asm("sbic 0x09,1");
//skip if bit in io register is cleared
asm("rjmp label2");
//0x00 PinA
//0x09 PinD
}
	//(out DDRA,R16)direction register for port A
	asm("out 0x02,R22");
	//move data to be sent in PORTA
	//Signal PortD1=1
	asm("sbi 0x0B,1");
	//second bit set in PORTD
	//wait that uC1 cleares its PortD bit 0
	asm("label2:");
	asm("sbic 0x09,0");
	//skip if bit in io register is cleared
	
	asm("rjmp label2");
	//set also the second bit in PortD
	asm("cbi 0x0B,1");
	//second bit set in PORTD
	//0x00 PinA
	//0x09 PinD
	}

Table 4.3: Distributed computation code

What we observe immediately in the code is the usage of embedded assembly language inside the natural Arduino C language. Thus the processor clock is used in an optimal manner. Of course, communication with exterior by Ethernet and other complex tasks remain in C, as it would become a difficult task to program.

The logic behind everything is presented in the schematics 4.7.

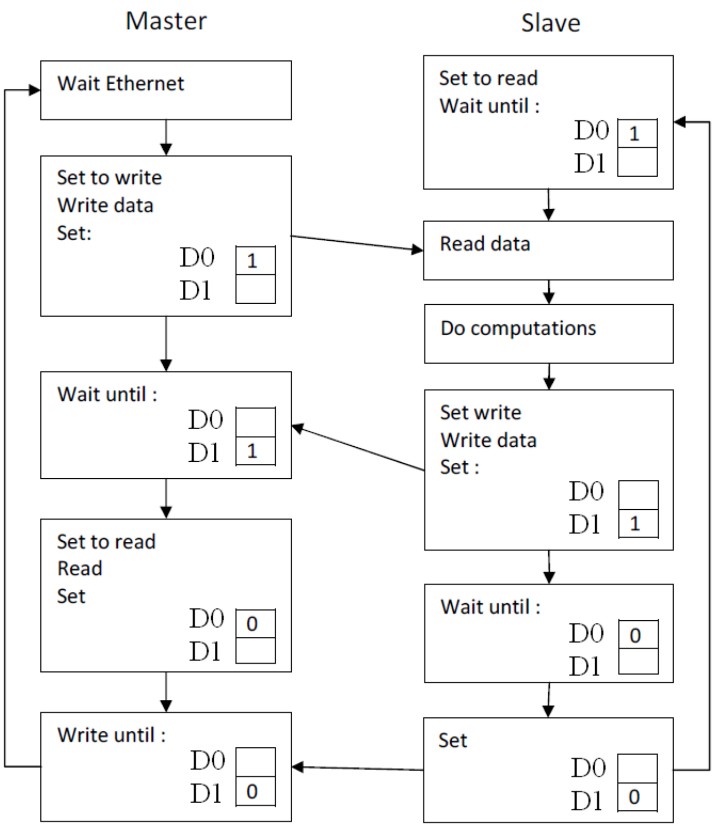

Figure 4.7: Schematic of parallel computation

4.5 Testing and validating using AMESim

Once the implementation phase has been realized for the embedded system, a real time simulation comes naturally next. Therefore, as previously mentioned, a Hardware in the Loop testing is employed by replacing the real physical system with a virtual process simulated by AMESim Bourdon et al. (2007).

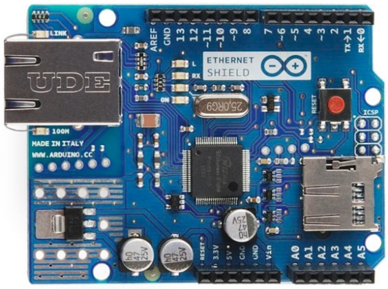

Figure 4.8: Arduino Ethernet shield

The basic functional schematic at the base of the implementation of the embedded HIL validation structure is shown in figure 4.9. Although the operating system is Windows, which by default does not satisfy real time constraints, by using the Matlab Real Time Kernel, only the processing threads of interest to the task at hand are kept at a top priority level being over-passed just by core root threads like system inputs and operating system messaging interrupts.

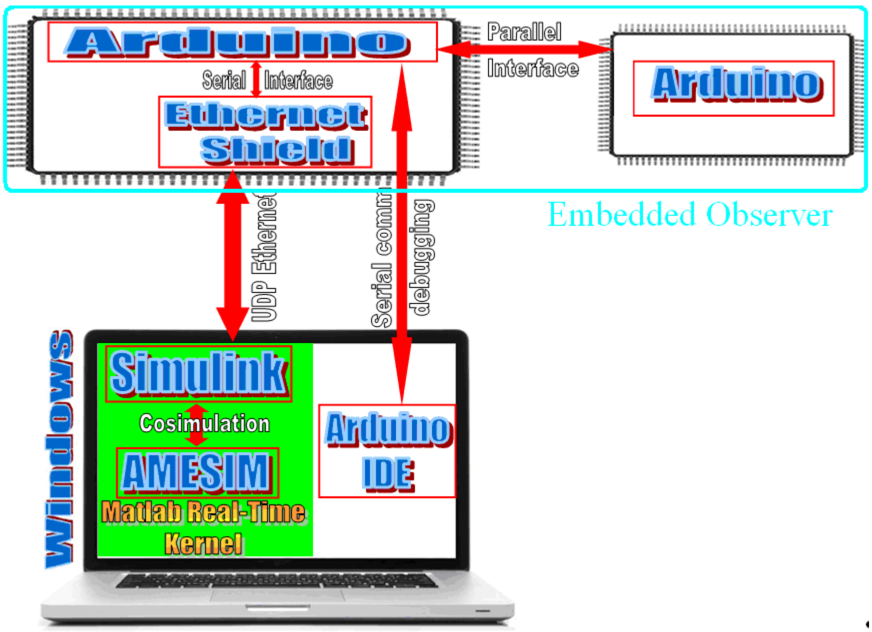

Figure 4.9: HIL connection diagram for testing

As AMESim needs Simulink for operating a real time data exchange, the creation of a co-simulation AMESim/Simulink is required. As the co-simulation is built, the Real Time Windows Target toolbox in Simulink manages the compilation of the program that will be executed in the

Real Time Windows Kernel of Matlab.

We will test two communication protocols with a computer : serial and Ethernet in UDP. Serial is the classical protocol used with Arduino, it is used to upload programs and to monitor data. There is an Ethernet library in Arduino, though we need an Arduino shield to add the Ethernet port.

The interactions schematic behind the implementation of the embedded validation structure is shown as functional blocks in 4.10.

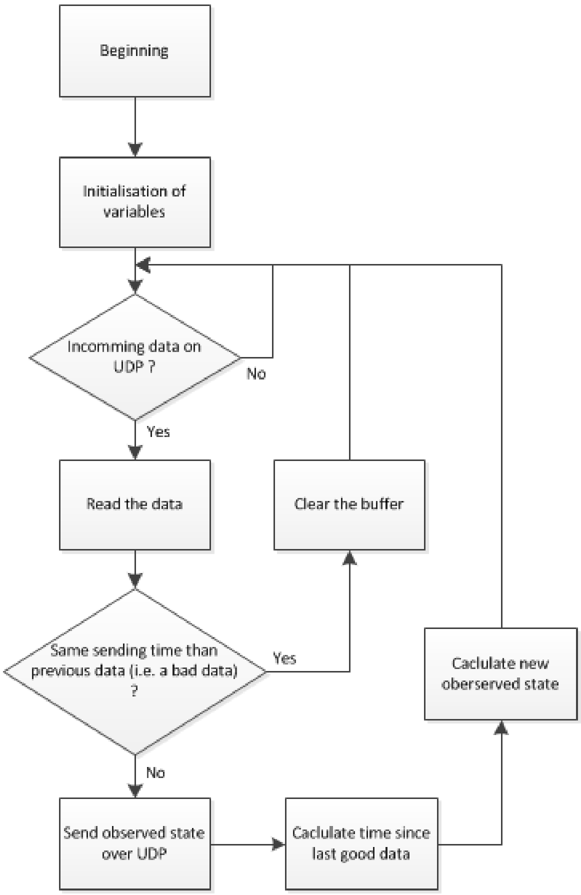

Figure 4.10: Logical diagram of the Arduino pseudo-code

As using an UDP protocol allows us to do easy debugging on the serial interface and because this protocol is able to have both incoming and outgoing data at the same time, we will prefer to use UDP (we emphasize the necessity for UDP and not TCP whose secure protocol would slow further the communication). Also as we want the communication between the computer that hosts the simulation software and the physical device to be as general as possible so that it's easily adapted to any potential microcontroller, this furthers our choice of an Ethernet UDP connection. This choice implies that we need to supply such an Ethernet module for every Arduino or device that needs to be connected to the system. This of course is not a big impediment, as by means of an Ethernet switch it will become easier to add other components to our system. What each such intelligent (adapted to Ethernet) device needs, is an IP and a Mac address and of course a secure connection to the switch. The maximum accepted length for Ethernet cable is long enough, although having the drawback of high power consumption to achieve such distances. Last aspect for this connection is the robustness to electromagnetic perturbations. The 6e category has shielded twisted pairs of wires, even more densely twisted than other categories, making it capable of 250 Mhz communication in perturbed magnetic field.

As we already mentioned, the block "To Simulink" used in AMESim can act in real-time regime using the kernel of Matlab. Then, all we need, is to make a real-time communication between the Arduino and Simulink. This can be done using the blocks of the Real-Time Windows Target toolbox. In our case, the blocks that we will use are Stream Input and Stream Output. Using those blocks, we can choose the type of board and/or communication that we want and decide of the formatting of the messages sent and received. It is noteworthy that the most appropriate version of Matlab is R2012a and that it is necessary to do the following steps in Simulink to have a simulation run in real-time with AMESim (minimum R12 version):

- In the "Control Panel" go to "Code Generation"
- In "Target Selection" click on "Browse" at the end of the line "System target file"
- Choose "rtwin.tlc"
- Go to "Solver" and in "Solver options" choose "Fixed-step" as "Type" and enter your sample time
- In the Stream Input and Output blocks enter the exact same sample time
- In the AMESim block go to "Run parameters" and enter your sample

time in “Print interval”, “Sample time”, and “Step”

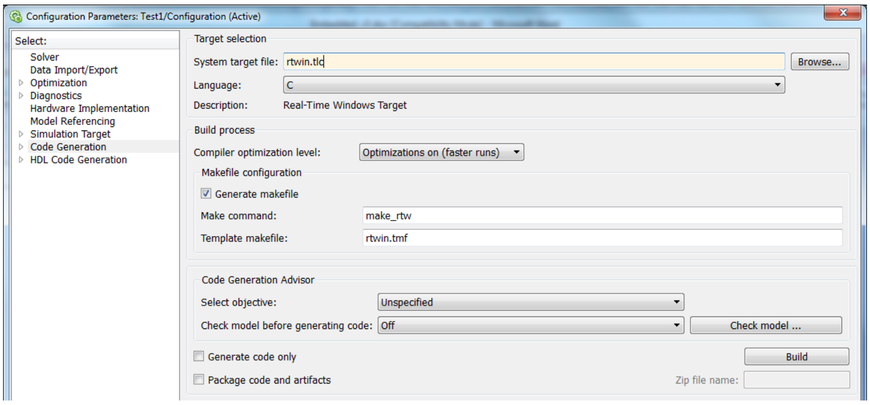

Figure 4.11: Simulation Configuration Parameters

It is also required to establish the formatting of the data we send and receive, especially for the floating point values. What is important to note here is that Simulink comes into play, therefore the data has to be correctly formatted in Simulink as well.

For the communication with the external device, there are two possibilities: using Stream Input/Output as in figure 4.12 or Packet Input/Output as in Annex figure C.2. Stream input treats numeric data as a string of characters. Thus for example in floating point case, the sign (“-“ or nothing) counts as one character and the point also counts as one character. Then, for example, the number “-1.3829” is written on 7 characters. Whereas for Packet data, we only need to worry on the bit order and data size.

4.6 Application example: Three water tank system

As an application example, a nonlinear analysis of a three tank water system has been selected as it represents a basic example that brings some interesting complexity when looked upon from a nonlinear perspective, and also brings us closer to the main application, the Fuel Cell. After the construction of the state space model, the T-S transformation is applied, and for the newly built representation, the observer is constructed. A similar approach, also with unmeasurable premise variables can be seen

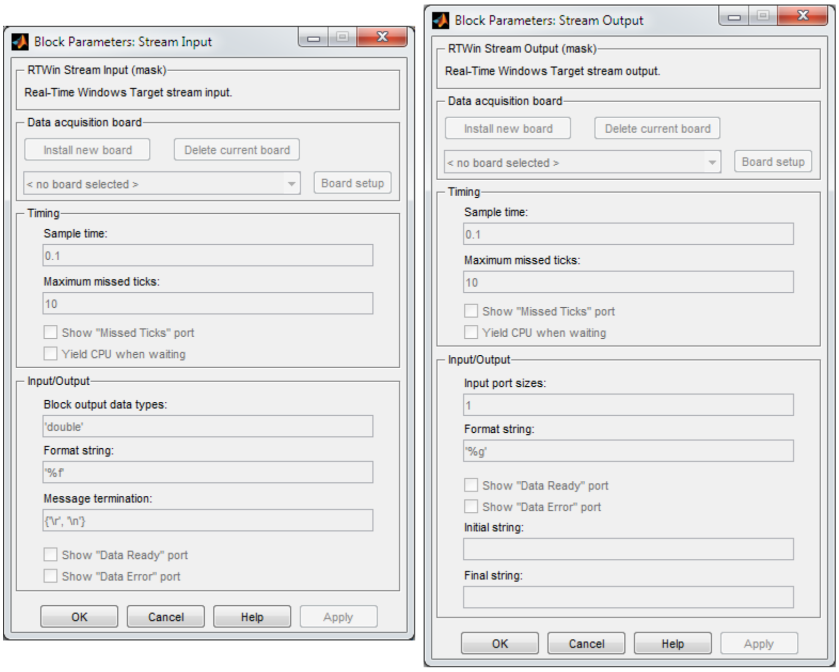

Figure 4.12: Interface for the Stream Input block || Interface for the Stream Output block

in Ghorbel et al. (2014). Others have used the application in nonlinear studies, even fault diagnosis like in Rincon-Pasaye et al. (2008).

4.6.1 Takagi-Sugeno Observer

Using the T-S representation, by sector non-linearity technique Lendek et al. (2011) the observer itself can be constructed.

In order to construct the observer presented in previous chapter of the form of equation 4.2, we need to calculate the observer gains. This will be done by employing Matlab's implicit LMI solver or YALMIP toolbox to resolve the LMIs presented in equation 4.3.

$$\begin{gathered} \text{For}\, i = 1:8 \\ \begin{pmatrix} A_i^T P - C^T Q_i + P A_i - Q_i C + I + 2\alpha P & P \\ P & -\lambda \end{pmatrix} < 0 \end{gathered} \tag{4.3}$$

So building the observer implies resolving a system of 8 LMIs (number of 8 because there are 3 nonlinearities as we will see further on), where $P \in \mathbb{R}^{3\times 3}$ a symmetrical positive definite matrix, so that size(P)=size(A), $C \in \mathbb{R}^{2\times 3}$, $\alpha > 0$ is a scalar, I is an appropriate identity matrix, and Q_i a set of temporary matrices, so that $Q_i = P \cdot L_i$ and $size(Q_i) = size(A_i C)$.

4.6.2 The Embedded system and HIL validation platform

The embedded platform is based on two Arduino Mega 2560, as the number of input/outputs of the ATMEGA 2560 is bigger than the standard UNO version. The two microcontrollers are connected in between themselves as in 4.13. The connection can be done both by serial transfer or parallel one (by digital pins). In the application chosen in the current thesis both configurations are possible, yet it has to be taken into account that floating point data is transferred (stored on 16 bits), so the serial communication has a slower transfer time thus a reduced performance, so a preference for a parallel connection is emphasized.

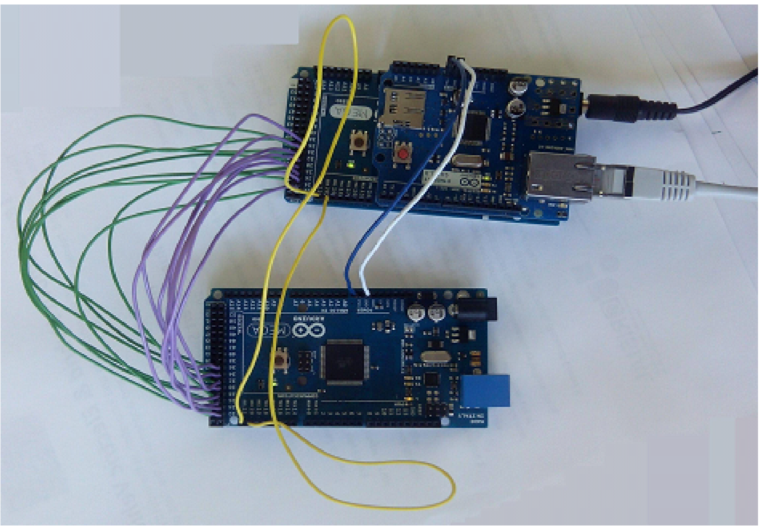

Figure 4.13: Hardware implementation

As we may lose some information with the connection to Simulink, it is necessary to have an algorithm that will check the received data before using it for calculations. Furthermore, we don't know the duration of the lost data, it may be 1 sample time or up to 20 times the sample time (as more than this becomes unacceptable). So we will use a variable sample time in our algorithm and so it is required to receive the simulation time from AMESim. We will now identify this lost data as 'bad data' because they don't give us the expected value. For the implementation of the hardware in the loop (HIL) architecture, the microcontroller based platforms are connected through the master one to a computer that hosts the simulation software. The communication protocol between the computer hosting the software and the embedded system communication has been chosen as described before, an Ethernet UDP connection, as it fits the requirement. For this, a 5 ms sampling time can be reached at the 16Mhz of the microcontroller. Also a serial connection was tested and proven to be working as required, with a minimal sampling time of 5ms. The Arduino code has been written directly in the Arduino's associated editor/compiler. When the observer has been programmed, a variable discretization was employed; therefore lost samples do not affect the overall performance.

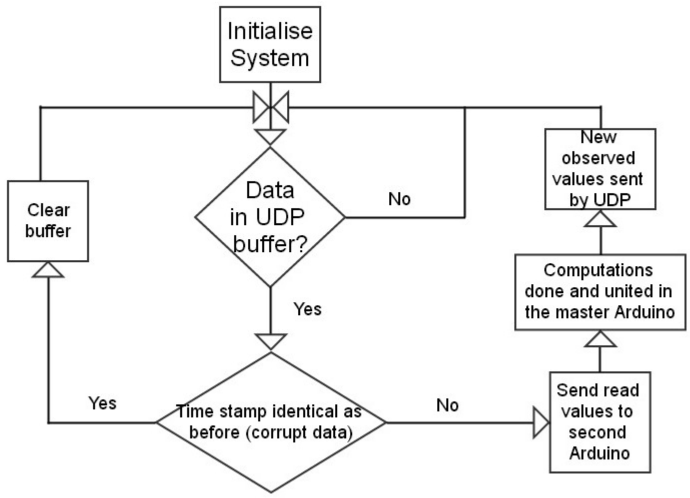

Figure 4.14: Logical diagram of Arduino code

The time lost because of the computations done in floating point (which is done at software level) and also due to the fact that TS model is represented as a sum, gave us the possibility to implement a distributed solution, where 2 processors divides the workload at each sampling time. A simplified logical diagram is presented in figure 4.14.

4.6.2.1 *System description and modeling*

The system is analyzed from a nonlinear perspective to show the potential of using T-S techniques on an embedded platform. As it can be seen in figure 4.15, the height of the first tank and the third tank has been considered measurable while the second tank's height is the estimated parameter.

In this system, we have an input pump supplying the first tank Q_{p_1} as well as another pump for the third tank Q_{p_2}. The last tank presents a valve evacuating water outwards, where atmospheric pressure P_{atm} is encountered. Also, a valve between it and the middle tank is present. The second tank has only the two interconnection valves while the first tank presents only one valve supplying the second tank. A supposition is made, that the flow of the third tank pump is smaller than the first one, thus the levels in tanks will always remain in a descending step, the first the highest level, then the second and the smallest water level in the third at all times.

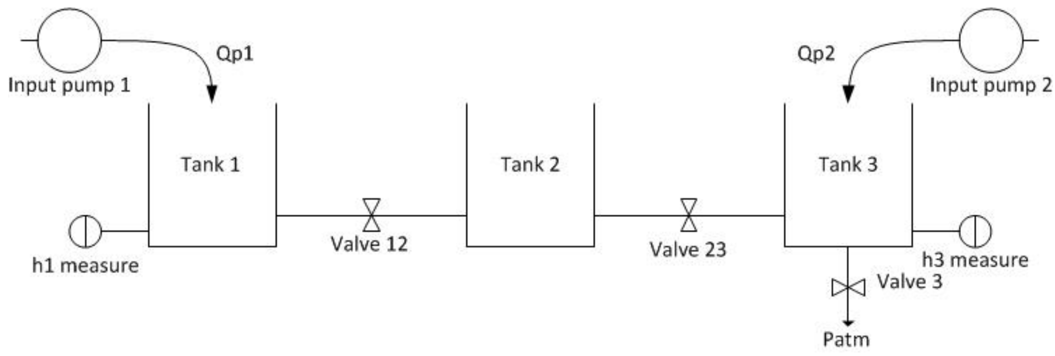

Figure 4.15: Three tanks system representation

We will use the notations h_i for the heights of liquid in each tank, V_i for the volumes of the three tanks, C_{P_3}, $C_{P_{12}}$, $C_{P_{23}}$ the flow coefficients of each valve, all valves being considered identical. Also Q_{P_1} and Q_{P_2} are the water flows of the two pumps, Q_{12}, Q_{23} are the water flows in between the tanks and Q_3 is the evacuation flow. Finally the auxiliary terms that appear in the equations are P_1, P_2, P_3 the pressures respectively of the first valve, second valve and the evacuation valve, S_i the surfaces of the tanks and ρ the density. Their values are found in the Annex in C.1. By neglecting the atmospheric pressure, equations 4.4 are found.

$$\begin{aligned}
&\frac{d(V_1)}{dt} = Q_{P_1} - Q_{12}\\
&\frac{d(V_2)}{dt} = Q_{12} - Q_{23}\\
&\frac{d(V_3)}{dt} = Q_{P_2} + Q_{23} - Q_3\\
&V_1 = S_1 h_1\,;\; V_2 = S_2 h_2\,;\; V_3 = S_3 h_3\\
&Q_3 = C_{P_3}\sqrt{P_3}\\
&Q_{12} = C_{P_{12}} sgn(P_1 - P_2)\sqrt{|P_1 - P_2|}\\
&Q_{23} = C_{P_{23}} sgn(P_2 - P_3)\sqrt{|P_2 - P_3|}\\
&P_1 = \rho g h_1\,;\; P_2 = \rho g h_2\,;\; P_3 = \rho g h_3
\end{aligned} \tag{4.4}$$

Developing further, the system equations become 4.5.

$$\begin{aligned}
\frac{dh_1}{dt} &= \frac{1}{S_1}\left(Q_{P_1} - C_{P_{12}} sgn(h_1 - h_2)\sqrt{\rho g}\sqrt{|h_1 - h_2|}\right)\\
\frac{dh_2}{dt} &= \frac{1}{S_2}\left(C_{P_{12}} sgn(h_1 - h_2)\sqrt{\rho g}\sqrt{|h_1 - h_2|} - C_{P_{23}} sgn(h_2 - h_3)\sqrt{\rho g}\sqrt{|h_2 - h_3|}\right)\\
\frac{dh_3}{dt} &= \frac{1}{S_3}\left(Q_{P_2} + C_{P_{23}} sgn(h_2 - h_3)\sqrt{\rho g}\sqrt{|h_2 - h_3|} - C_{P_3}\sqrt{\rho g}\sqrt{h_3}\right)
\end{aligned} \tag{4.5}$$

Now, the equivalent state-space form can be built, considering $S_1 = S_2 = S_3$ and $C_{P_{12}} = C_{P_{23}} = C_{P_3}$. As it can be seen, the inputs are the pump flows, and the states are the three heights and finally the output is the first and last tanks' height:

$$\begin{aligned}
u &= \begin{bmatrix} Q_{P_1} \\ Q_{P_2} \end{bmatrix}\\
x &= \begin{bmatrix} h_1 \\ h_2 \\ h_3 \end{bmatrix}\\
y &= \begin{bmatrix} h_1 \\ h_3 \end{bmatrix} = \begin{bmatrix} x_1 \\ x_3 \end{bmatrix} = h(x)
\end{aligned} \tag{4.6}$$

We consider therefore u, x and y as the input vector, state vector and output vector respectively.

$$\begin{cases} \dot{x} = -\frac{C_P\sqrt{\rho g}}{S}\begin{bmatrix} sgn(h_1-h_2)\sqrt{|h_1-h_2|} \\ -sgn(h_1-h_2)\sqrt{|h_1-h_2|}+sgn(h_2-h_3)\sqrt{|h_2-h_3|} \\ -sgn(h_2-h_3)\sqrt{|h_2-h_3|}+\sqrt{h_3} \end{bmatrix}+ \\ +\begin{bmatrix} \frac{1}{S} & 0 \\ 0 & 0 \\ 0 & \frac{1}{S} \end{bmatrix}u \\ y=\begin{bmatrix} x_1 \\ x_3 \end{bmatrix}=\begin{bmatrix} 1 & 0 & 0 \\ 0 & 0 & 1 \end{bmatrix}x = Cx \end{cases} \tag{4.7}$$

As it can be seen, the nonlinearities are present as square roots, that have no differentiability in 0, yet for the regime in which we work, we will not reach this point.

4.6.2.2 *Takagi-Sugeno transformation*

In order to obtain the state observer, it is first needed to modify the state space form, so that it can be used to write the Takagi-Sugeno (TS) representation. So equation 4.7 is written as equation 4.8:

$$\begin{cases} \dot{x} = -\frac{C_P\sqrt{\rho g}}{S}\begin{bmatrix} z_1 & -z_1 & 0 \\ -z_1 & z_1+z_2 & -z_2 \\ 0 & -z_2 & z_2+z_3 \end{bmatrix}x+\frac{1}{S}\begin{bmatrix} 1 & 0 \\ 0 & 0 \\ 0 & 1 \end{bmatrix}u \\ y=x_1=\begin{bmatrix} 1 & 0 & 0 \\ 0 & 0 & 1 \end{bmatrix}x \end{cases} \tag{4.8}$$

Where we have separated the nonlinearities in the variables z, that have the values as follows:

$$z=\begin{bmatrix} z_1 \\ z_2 \\ z_3 \end{bmatrix}=\begin{bmatrix} sgn(x_1-x_2)\frac{1}{\sqrt{|x_1-x_2|}} \\ sgn(x_2-x_3)\frac{1}{\sqrt{|x_2-x_3|}} \\ \frac{1}{\sqrt{x_3}} \end{bmatrix} \tag{4.9}$$

For the sector nonlinearity transformation we have to establish the conditions for the heights, where some additional constraints are added so that singular values are eliminated:

$$\begin{aligned} 0,05 \leq h_1 \leq 0,6m \\ 0,05 \leq h_2 \leq 0,6m \\ 0,05 \leq h_3 \leq 0,6m \end{aligned} \tag{4.10}$$

The three valves have similar characteristics, and the flow on the left pump is bigger, therefore the only possibility for the water levels to be equal would be when the pump starts or when the tanks are empty, in which case the observer is not useful. Therefore, it is impossible that the difference between levels of the 3 tanks will change their sign. Even if this had happened, one could resolve this problem, by separating the system into multiple systems that switch according to the value of the difference between heights. Once all the observers are built, the one that will be active is chosen in a switching manner. Of course the main regime is the case when all the square roots are different from 0. The parameters for the system are found in Annex equations C.2, C.3, C.4, C.5.

4.6.2.3 *The AMESim System*

For the validation part, one has to first construct the AMESim model, by adding all the elements, configuring their parameters, and then the co-simulation block with Simulink needs to be added in Amesim as well as in figure 4.16. For the Simulink part (figure 4.16), Matlab 2012a have been used. The Amesim version is R12.

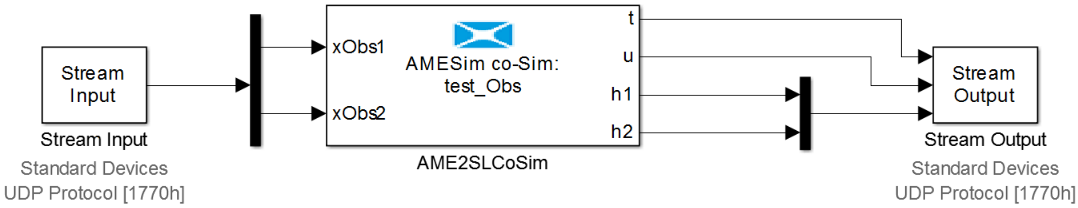

Figure 4.16: Simulink diagram including co-simulation block

As the connection between Amesim and Simulink is done, by using Matlab real time workshop we add the input/output blocks that will connect via Ethernet to the microcontroller. The real time compilation is then done, and the whole system is run from Simulink.

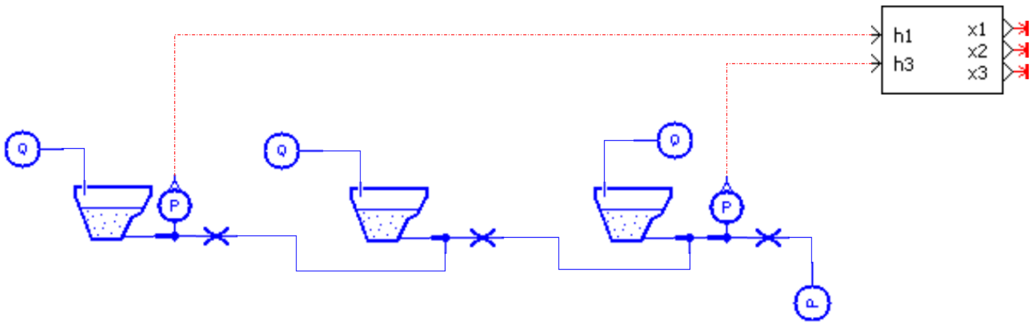

Figure 4.17: AMESim implementation of the three tank system

4.6.2.4 *The real time simulation*

By means of the experimental setup described previously, a performance analysis is done in real time, and the parameters are configured for optimal results.

As it can be observed in figures 4.18 and 4.19, the estimation of the water level in the second tank stabilizes in about 10 seconds, which is an adequate time response. Also the overshoot of the estimation is in an acceptable interval.

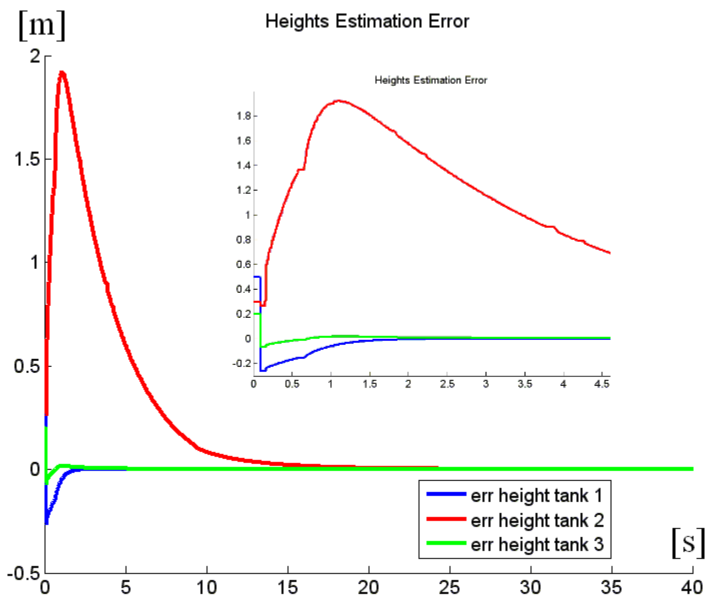

Figure 4.18: Estimation error dynamics of the 3 heights (tank 1, 2 and 3)

It is important to notice that perturbation added to the communication in a forcefully manner, can be seen to affect the system like in figure 4.19 at second 0.7 (in the zoomed pane), but performance remains good overall, thus proving its robustness to data loss.

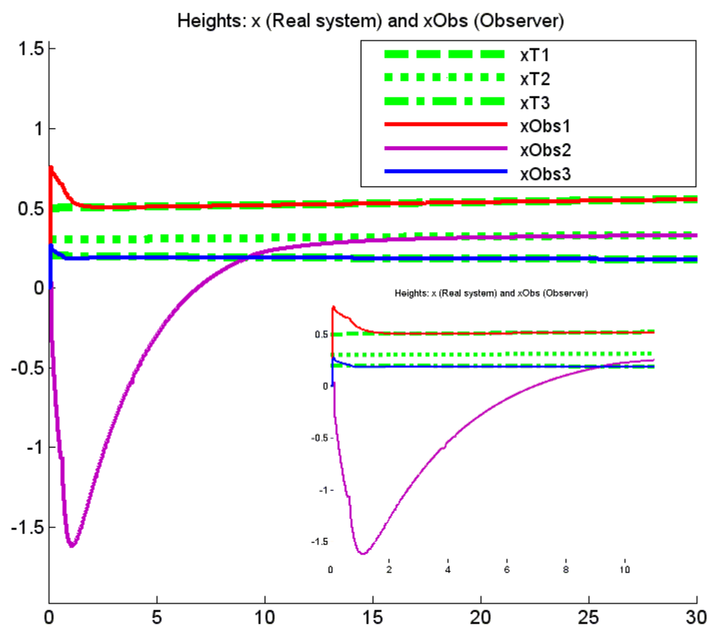

Figure 4.19: Real/Estimated water levels evolution

We can see in figure 4.20 that even adding a lot of missed ticks and loss of information doesn't perturb our algorithm and the plot of the observed stated is nearly identical to the case where we have no missed ticks.

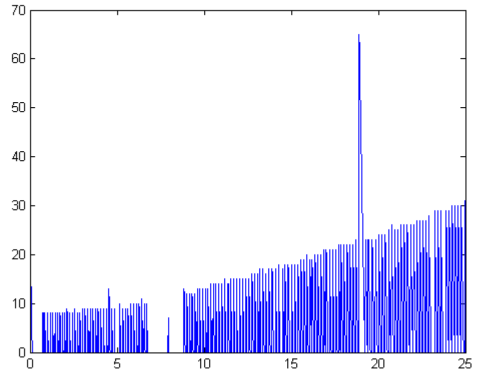

Figure 4.20: Missed ticks for the measured premise variables observer calculated by Arduino in real-time

4.6.2.5 *Validation on a real system*

Once the tests had been finished the embedded observer has been installed on a real 3 tank platform AMIRA DTS200 (figure 4.21).

Figure 4.21: AMIRA DTS 200 system

The system communicates with Simulink over a data acquisition board, the National Instrument PCI 6024 E (as in figure 4.24).

Simulink has digital and analogic input/output blocks in the Real-Time Windows Target Toolbox for this particular board, which is perfect to work with the Arduino. In this 3 tank system, the two pumps are driven by the computer through digital to analog converter of the board and sensors measure the 3 heights and are read by the computer through analog to digital converter. We then use 2 analog output blocks and 3 analog input blocks.

The computer on which the board is installed is protected and we connect access to the Ethernet UDP connection with the Arduino so we will use Serial connection.

After the implementation, also adding some filters on the inputs and outputs, the estimation error stabilizes in 8 seconds as can be seen in the figure 4.22. By introducing short perturbations, into the system, by means of purge valves openings, the observer still manages to regain stability (as in figure 4.23).

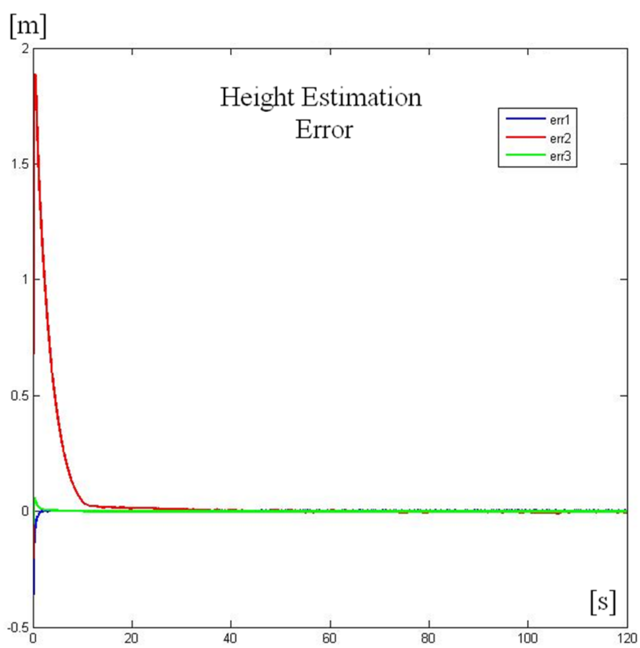

Figure 4.22: AMIRA DTS 200 estimation error dynamics in time

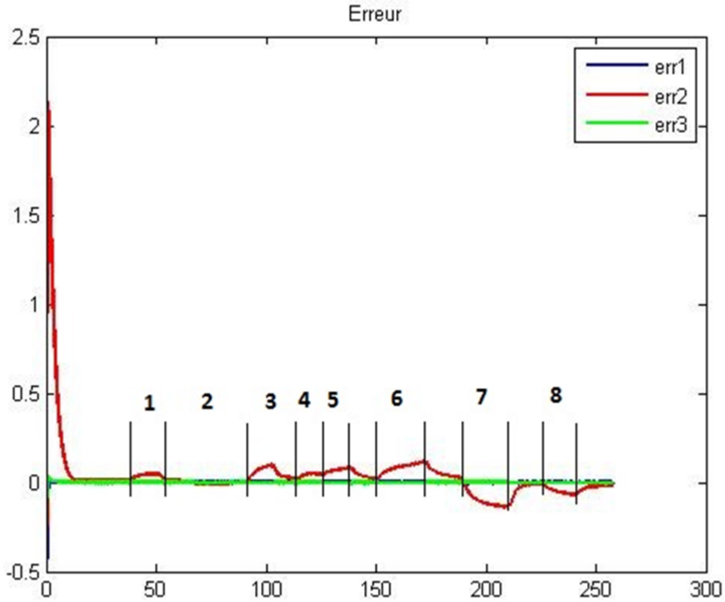

Figure 4.23: AMIRA DTS 200 with faults injected in time

where the numbered sections in the figure represent:

1. Leakage in tank 1 (fault 1)
2. Leakage in tank 2 (fault 2)
3. Leakage in tank 3 (fault 3)
4. Pump of tank 1 does not work (no input flow) (fault 4)
5. Pump of tank 3 does not work (no input flow) (fault 5)
6. Valve between tank 2 and tank 3 is blocked (fault 6)
7. Valve between tank 3 and atmosphere is blocked (fault 7)
8. Valve between tank 1 and tank 2 is blocked (fault 8).

We can see that the observer detects the faults, mainly on the observer error on the height of the second tank, but the leakage in the tank 2 is nearly undetectable. Experimentally, a threshold of 1mm gives good fault detection performance and can detect all of these defaults. Though, this observer was only done to show the working principle, so it doesn't allow to isolate and identify faults easily, yet it can be easily adapted for such tasks.

Figure 4.24: PCI 6024 E acquisition board

4.7 Conclusions

A Harware In the Loop (HIL) methodology to test in real time an embedded nonlinear observer was developed and applied to a three tank system. An important aspect of the work is that the validation method can be applied to many processes, ranging from mechanical to chemical or electrical, as the simulation platform and the communication protocol, both support it. The hardware in the loop testing permits a robust validation of an observer/controller or even a diagnostic system, testing also unpredictable communication and time response errors, as well as other physical constraints that may appear, as insufficient memory or processing power.

An embedded nonlinear observer was developed using the Takagi Sugeno approach and applied to a real three tank system after the prior real time HIL validation. As previously seen, the observer's performances on the HIL testing bench reproduce the behavior of the real system thus reducing implementation time and also avoiding potential dangerous faults on the real system. The testing also takes into consideration communication losses and memory and computation timing errors. Another important objective addressed here was to show the capability of a T-S system to be represented on small scaled microcontroller platforms. Finally, by doing the parallel calculus in between two microcontrollers, the performance of the whole system has increased.

As a perspective work that can be built upon what was presented, we would consider the implementation on FPGA or microprocessor based systems, and also the analysis of more complex dynamic sampling time procedures.

Chapter 5

Application: Fuel Cell System

5.1 Fuel Cell preliminaries 105

5.2 Fuel Cell Modeling and TS representation 109

5.2.1 Fuel Cell gaseous model 109

5.2.1.1 *TS representation for gaseous Model* 112

5.2.1.2 *Tranformation of the simplified model into a Mean value form* 114

5.2.2 Fuel Cell gaseous model with temperature measurement 117

5.2.3 Fuel Cell Model with water vapor 118

5.3 Observer implementation 122

5.3.1 Observer results of Lipschitz approach for FC model with vapor 122

5.3.2 Observer results of bounded stability approach for vapor gaseous FC model 124

5.3.3 Mean value based Observer, for the gaseous model 126

5.3.3.1 *Observability* 126

5.3.3.2 *Building a Symmetric System* 127

5.3.3.3 *Applying robustness to the observer* 130

5.3.3.4 *Numerical Results* 131

5.3.4 The embedded solution 133

5.4 Fuel Cell diagnosis 136

5.4.1 Fault trees analysis of FCS 136

5.4.2 Knowledge based approaches for FCS 137

5.4.2.1 *Diagnostic by Signal Processing Approach* 137

5.4.2.2 *Diagnostic by Artificial Intelligence Approach* 138

5.4.2.3 *Diagnostic by Experimental Approach* . . . 138

5.4.3 Model based approaches for FCS 141

5.4.3.1 *Diagnostic by ARRs* 141

5.4.3.2 *Diagnostic by Parameter identification* . . 142

5.4.3.3 *Diagnostic by Stochastic Approach* 143

5.4.3.4 *Structural analysis for Fuel Cells* 143

5.4.3.5 *Diagnostic by Observers* 144

5.4.4 Takagi-Sugeno PI observer for the FCS 144

5.4.5 Advanced Takagi-Sugeno PI observer applied to FCS 146

5.5 Conclusions 151

5.1 Fuel Cell preliminaries

The Hydrogen Fuel Cell systems have seen a spur in interest in the last decade, both in research and industrial areas, despite the still high production cost, because of their elevated efficiency, reduced pollution level and the potential independence from fossil fuels. Fuel Cells (FCs), act as efficient electrochemical power sources, and can behave as an electrolyser or inverse electrolyser thus converting chemical energy into electrical power (figure 5.1) or the opposite. These two functionalities complement each other especially in stationary applications (eg: renewable energy management). Throughout the thesis we have taken into account only the production of electricity from Hydrogen. FC science and technology cuts across multiple disciplines, including materials science, fluid and temperature dynamics, electrics, electrochemistry, and catalysis. It is always a major challenge to fully understand all the processes within a FC. These are the reasons for that the energy generation systems based on FCs are so complex to model.

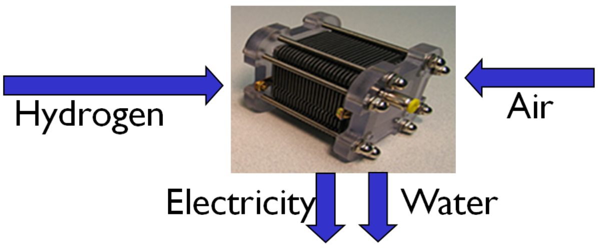

Figure 5.1: Functional behavior of a hydrogen Fuel Cell

At their core, two elements contribute at their functionality: firstly the catalysts that break the molecule bonds (that generally consists in a thin layer of platinum placed on a porous medium for the anode, and nickel for the cathode side) and secondly, an electrolyte that permits the passage of only the positive ions and not the electrons obtained from the dissociation of the molecules (usually a solid polymer membrane or a non-porous ceramic compound).

Amongst different types of Fuel Cells (FC) like solid oxide or alkaline ones Kirubakaran et al. (2009), the proton exchange membrane (P.E.M.) type Barbir (2012) stands out, because of its low working temperature, and proves to be best suited for vehicle applications. In electrical vehicles, the energy storage plays one of the most important roles Lukic et al. (2008), so the research on Fuel Cells will boost the acceptance of electrical vehicles as well. They are practical for this particular application not only because of the functional temperature but also the PEM Fuel Cell's low weight and physical robustness. Except their still high cost, existing models of FC based cars show good performances like: Michelin that has constructed a vehicle that reaches 450Km attainable range running with 140km/h; General Motors 320Km running with 160km/h; Hyundai ix35 FCEV, 594 Km (5.6 Kg of hydrogen); or the new Toyota Mirai, that should be commercialized in 2015, arriving presumably at 650Km.

Therefore it directly competes with batteries which have been developing continuously for many years, yet prove inferior in some aspects to hydrogen technology as shown in Thomas (2009), both as weight per storage capacity and energy density; these represent two important factors, that add to the slow recharge rate of a battery. They present: lower/zero emission, silent functioning, high efficiency and fast refill time in comparison to the batteries.

The Fuel Cells are small scaled devices therefore the development of virtual sensors would reduce the price. Also, a state observer may be used for diagnostics Zhang et al. (2013). The majority of the papers that take into account the dynamics and not only the static models of FCs, focus only upon the electrical part of the fuel cell ignoring the auxiliary components Kim et al. (2013) or treating just the compressor separately Matraji et al. (2011). Nevertheless papers such as Pukrushpan et al. (2004), have to be mentioned as a thorough review upon all the components used so far. Indeed, for the more general case of system diagnosis, we find also alternative approaches to model based techniques (for which a good review is Petrone et al. (2013)) as experimental ones (ex: impedance spectroscopy as in Steiner et al. (2011) or the newer work of Debenjak et al. (2013) that detect flooding and drying phenomena, neuro-fuzzy techniques). As there is still no standardization in different existing types of FCs, a functional model would be easier to adapt to any particular case instead of experimental approaches that require extensive training data. Two types of models are known: steady state FCS models and dynamic FCS models. The former ones serve as a mean to design FC components and to choose the operating points. On another hand, even if they are not suitable for control and diagnosis studies, they are handy in establishing the effects of different parameters as pressure, temperature or the fuel cell voltage. Turner et al Turner et al. (1999) included the transient effect of fuel cell stack temperature in his dynamic model. Pukrushpan et al Pukrushpan et al. (2004) presented a nonlinear fuel cell system dynamic model suitable for control study. Also model based approaches Hosseini et al. (2012), Aitouche et al. (2011) have the potential to give fast response to time variations, therefore being very efficient for online diagnosis Hafaifa et al. (2010) as well as control Pisano et al. (2013). Also, a modeling based on bond graph is done in Rallières (2011). Of course one has to mention the greatest inconvenient of model based techniques that is the difficulty in parameter estimation. The state observer acts as a virtual sensors and it is designed to estimate cathode and anode pressures and mass flows of oxygen and hydrogen which are generally not measured. The mass flow rates of reactant gases play a pivotal role in the reliable and efficient operation of FCS.

The developed model is for a Polymer Electrolyte Membrane Fuel Cell Stack that uses a Nafion 117 membrane, integrating auxiliary components as in figure 5.2.

The model focuses on components with medium time dynamics from a vehicle like configuration, meaning the focus is on the gaseous part. In vehicle applications, the auxiliary components play an important role, as the piping occupies significant volume. In short, the Fuel Cell comprises of an anode (the hydrogen part), a cathode (the oxygen part), an air compressor Zhao (2013) to augment the air pressure, a hydrogen tank adapted with a valve, the diffusion layer and the membrane and all the nozzles and pipes. Also there are other adjacent parts but their role in modeling is not fundamental, like the humidifier unit (being a device that increases the moisture in the compressed air), cooling unit (cooling can be done by a water distribution system, cooled by a ventilator or directly applying the cool air to the hot areas of the FC).

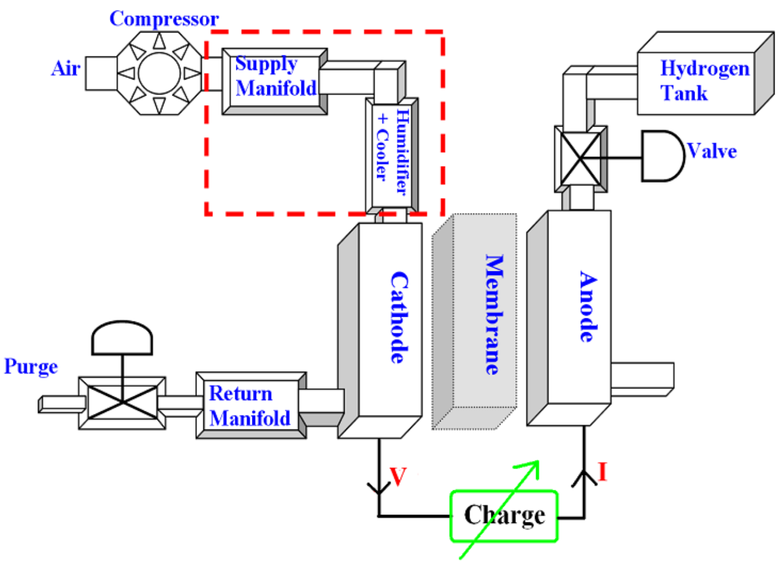

Figure 5.2: Block view of fuel cell stack with auxiliary elements

For integrating the FC stack inside an electrical system, as a vehicle, a DC to DC converter is required as well as a DC to AC inverter. Also, electrical storage devices are used to prevent any stiff electrical dynamics on the FC stack and to enable braking energy recovery in case of use in transportation. The storage devices may be batteries or super capacitors as in Amin et al. (2014).

The current work considers the case of pure Oxygen as input on the cathode side and takes the humidifying and cooling units as ideal elements. Concerning the pressure difference between the anode and cathode, it is kept null by means of a pressure regulator. A constant pressure difference has been seen to offer good performances in many cases.

The temperature inside the fuel cell is considered homogenous, so spatial variations in general are ignored, yet the temperature is not constant, compared to Olteanu et al. (2014). Only by measuring parameters outside the fuel cell with the aid of the observer, will allow us to deduce what happens inside the anode and cathode respectively. Moreover the gases will be considered ideal. The flow characteristics, the manifold dynamics, and consequently, the reactant partial pressures were included in the transient phenomena captured in the proposed model.

5.2 Fuel Cell Modeling and TS representation

5.2.1 Fuel Cell gaseous model

The mathematical model of the FC is brought in a state space form considering the compressor's flow and electrical current as inputs to the system. Therefore the accumulated mass of oxygen and hydrogen reacts or passes freely towards the return manifold that consists of pipes and valves. The valve models for gaseous mediums have a nonlinear behavior with two distinct patterns depending on the pressure difference that arises: choked or unchoked regime. Therefore as the pressure difference may overpass 2 bar both situations have to be taken into account. The TS representation will help with this, so that a switching between the two may not be required. The equations for a volume chamber and a valve are given by equation 5.1. One thing to be noted is that throughout the thesis, we will concentrate on the Oxygen side to avoid having cumbersome matrices. This is done as the auxiliary components which dominate are similar in functionality and the pressure difference between Anode and cathode is correlated by a regulator.

$$\begin{aligned}
&\frac{dm}{dt} = W_{in} - W_{out}\\
&\frac{dp_{in}}{dt} = \frac{\gamma R_a}{V}\left(T_{in}W_{in} - T_{out}W_{out}\right)\\
&W_{out} = \frac{C_D A_T p_{out}}{\sqrt{R_a T_{in}}} \times \begin{cases} \left(\frac{p_{out}}{p_{in}}\right)^{\frac{1}{\gamma}} \sqrt{\frac{2\gamma}{\gamma-1}\left(1-\left(\frac{p_{out}}{p_{in}}\right)^{\frac{\gamma-1}{\gamma}}\right)} & if\ \frac{p_{out}}{p_{in}} > P_{crit} \\ \sqrt{\gamma}\left(\frac{2}{\gamma+1}\right)^{\frac{2\gamma}{2(\gamma-1)}} & if\ \frac{p_{out}}{p_{in}} \leq P_{crit} \end{cases}\\
&P_{crit} = \left(\frac{2}{\gamma+1}\right)^{\frac{\gamma}{\gamma-1}}
\end{aligned} \tag{5.1}$$

Here m is the mass inside the chamber, p_{in}, T_{in} and W_{in} the input pressure, temperature and flow, p_{out}, T_{out} and W_{out} the output pressure, temperature and flow, V the volume of the chamber, γ the adiabatic coefficient of air, R_a the specific perfect gas constant of air (Oxygen for the current case), C_D the flow coefficient of the valve and A_T the cross section of the valve. The input flow of the supply manifold (W_{in}) will be considered as an input to the system with known temperature and pressure and the return manifold flow (W_{in}) will exit toward the exterior. The critical pressure is is presented in equation 5.1. The system parameters are presented in the Annex in figures A.1, A.2 and A.3.

Regarding the whole FC model, we will suppose that we measure the pressures and mass at the supply and return manifold, as indeed the measurement of the pressure and mass inside the cathode is expensive and impractical. Of course, in order to avoid measuring mass, one can have a pressure and temperature sensor in order to deduce the mass by means of the perfect gas law $PV = mR_aT$.

One can represent the equations for the cathode side of the Fuel cell as in equation 5.2 (the hydrogen side is identical), defining the dynamics for the mass flows of the Supply Manifold-Cathode-Return manifold, as well as the dynamics of the pressures of the same three elements:

$$\begin{cases} \frac{dm_{sm}}{dt} = W_{in} - W_{outsm} \\ \frac{dm_{cs}}{dt} = W_{outsm} - W_{outcs} - W_{O_2react} \\ \frac{dm_{rm}}{dt} = W_{outcs} - W_{O_2react} - W_{outrm} \\ \frac{dp_{sm}}{dt} = \frac{\gamma R_a}{V_{sm}} (T_{smin} W_{in} - T_{sm} W_{outsm}) \\ \frac{dp_{cs}}{dt} = \frac{\gamma R_a}{V_{cs}} \left(T_{csin} W_{outsm} - T_{cs} W_{outcs} - T_{cs} W_{O_2react}\right) \\ \frac{dp_{rm}}{dt} = \frac{\gamma R_a}{V_{rm}} \left(T_{rmin} W_{outcs} - T_{r\,\min} W_{O_2react} - T_{rm} W_{outrm}\right) \end{cases}, \tag{5.2}$$

where the mass flow terms in (5.2) that represent the mass flow output of the Supply manifold (W_{outsm}), Return manifold (W_{outrm}), Cathode (W_{outcs}) and the Mass flow that reacts in the cell (W_{O_2react}) are shown in (5.3). We can see the influence of the electrical current I, on the reacted mass flow depending on the number of cells (N), Oxygen molar mass (M_{O_2}) and Faraday number (F). Finally $\frac{dm_{sm}}{dt}$, $\frac{dm_{cs}}{dt}$, $\frac{dm_{rm}}{dt}$, $\frac{dp_{sm}}{dt}$, $\frac{dp_{cs}}{dt}$ and $\frac{dp_{rm}}{dt}$ represent respectively , the time derivatives of the masses of the supply manifold chamber, cathode chamber, return manifold chamber and the time derivatives of the pressures of the supply manifold chamber, cathode chamber and the return manifold chamber.

$$
\begin{aligned}
&P_{crit} = \left(\frac{2}{\gamma+1}\right)^{\frac{\gamma}{\gamma-1}} \\
&W_{outsm} = \frac{C_{Dsm}A_{Tsm}p_{sm}}{\sqrt{R_a T_{sm}}} \times \begin{cases} \left(\frac{p_{cs}}{p_{sm}}\right)^{\frac{1}{\gamma}} \sqrt{\frac{2\gamma}{\gamma-1}\left(1-\left(\frac{p_{cs}}{p_{sm}}\right)^{\frac{\gamma-1}{\gamma}}\right)}\ if\ \frac{p_{cs}}{p_{sm}} > P_{crit} \\ \sqrt{\gamma}\left(\frac{2}{\gamma+1}\right)^{\frac{2\gamma}{2(\gamma-1)}}\ if\ \frac{p_{cs}}{p_{sm}} \leq P_{crit} \end{cases} \\
&W_{outcs} = \frac{C_{Dcs}A_{Tcs}p_{cs}}{\sqrt{R_a T_{cs}}} \times \begin{cases} \left(\frac{p_{rm}}{p_{cs}}\right)^{\frac{1}{\gamma}} \sqrt{\frac{2\gamma}{\gamma-1}\left(1-\left(\frac{p_{rm}}{p_{cs}}\right)^{\frac{\gamma-1}{\gamma}}\right)}\ if\ \frac{p_{rm}}{p_{cs}} > P_{crit} \\ \sqrt{\gamma}\left(\frac{2}{\gamma+1}\right)^{\frac{2\gamma}{2(\gamma-1)}}\ if\ \frac{p_{rm}}{p_{cs}} \leq P_{crit} \end{cases} \\
&W_{outrm} = \frac{C_{Drm}A_{Trm}p_{rm}}{\sqrt{R_a T_{rm}}} \times \begin{cases} \left(\frac{p_{atm}}{p_{rm}}\right)^{\frac{1}{\gamma}} \sqrt{\frac{2\gamma}{\gamma-1}\left(1-\left(\frac{p_{atm}}{p_{rm}}\right)^{\frac{\gamma-1}{\gamma}}\right)}\ if\ \frac{p_{atm}}{p_{rm}} > P_{crit} \\ \sqrt{\gamma}\left(\frac{2}{\gamma+1}\right)^{\frac{2\gamma}{2(\gamma-1)}}\ if\ \frac{p_{atm}}{p_{rm}} \leq P_{crit} \end{cases} \\
&W_{O_2 react} = \frac{NIM_{O_2}}{2F}
\end{aligned}
\tag{5.3}
$$

$$
\begin{bmatrix} T_{sm} & T_{cs} & T_{rm} \end{bmatrix} = \begin{bmatrix} \frac{p_{sm}V_{sm}}{R_a m_{sm}} & \frac{p_{cs}V_{cs}}{R_a m_{cs}} & \frac{p_{rm}V_{rm}}{R_a m_{rm}} \end{bmatrix} \tag{5.4}
$$

Therefore by doing a set of transformations and by considering as the system's inputs: the electrical current and the mass flow of the compressor, we arrive at its state space equivalent in (5.5).

$$
\begin{cases}
u = \begin{bmatrix} W_{in} & I \end{bmatrix}^T \\
x = \begin{bmatrix} m_{sm} & m_{cs} & m_{rm} & p_{sm} & p_{cs} & p_{rm} \end{bmatrix}^T \\
\dot{x} = A(x) + Bu \\
y = \begin{bmatrix} m_{sm} \\ m_{rm} \\ p_{sm} \\ p_{rm} \end{bmatrix} = Cx = \begin{bmatrix} 1 & 0 & 0 & 0 & 0 & 0 \\ 0 & 0 & 1 & 0 & 0 & 0 \\ 0 & 0 & 0 & 1 & 0 & 0 \\ 0 & 0 & 0 & 0 & 0 & 1 \end{bmatrix} x
\end{cases}, \tag{5.5}
$$

$$
B = \begin{bmatrix} 0 & \frac{-nM_{O_2}}{2F} & \frac{-nM_{O_2}}{2F} & 0 & \frac{-nM_{O_2}}{2F}\frac{\gamma R_a T_{cs}}{V_{cs}} & \frac{-nM_{O_2}}{2F}\frac{\gamma R_a T_{r\min}}{V_{rm}} \\ 1 & 0 & 0 & \frac{\gamma R_a T_{smin}}{V_{sm}} & 0 & 0 \end{bmatrix}^T, \tag{5.6}
$$

where the matrix A is presented in equation (5.7) representing the system state matrix, and it is the carrier of the nonlinear terms and B is the system input matrix.

$$A(x)=\begin{bmatrix} -\frac{C_{Dsm}A_{Tsm}}{\sqrt{V_{sm}}}\sqrt{\frac{p_{sm}}{m_{sm}}}\alpha & 0 & 0 & 0 & 0 & 0 \\ \frac{C_{Dsm}A_{Tsm}}{\sqrt{V_{sm}}}\sqrt{\frac{p_{sm}}{m_{sm}}}\alpha & -\frac{C_{Dcs}A_{Tcs}}{\sqrt{V_{cs}}}\sqrt{\frac{p_c}{m_c}}\beta & 0 & 0 & 0 & 0 \\ 0 & \frac{C_{Dcs}A_{Tcs}}{\sqrt{V_{cs}}}\sqrt{\frac{p_c}{m_c}}\beta & \frac{C_{Drm}A_{Trm}}{\sqrt{V_{rm}}}\sqrt{\frac{p_{rm}}{m_{rm}}}\delta & 0 & 0 & 0 \\ 0 & 0 & 0 & -\frac{\gamma}{V_{sm}}C_{Dsm}A_{Tsm}\sqrt{V_{sm}}\sqrt{\frac{p_{sm}}{m_{sm}}}\alpha & 0 & 0 \\ 0 & 0 & 0 & \frac{\gamma}{V_{cs}}C_{Dsm}A_{Tsm}\sqrt{V_{sm}}\sqrt{\frac{p_{sm}}{m_{sm}}}\alpha & -\frac{\gamma}{V_{cs}}C_{Dcs}A_{Tcs}\sqrt{V_{cs}}\sqrt{\frac{p_c}{m_c}}\beta & 0 \\ 0 & 0 & 0 & 0 & \frac{\gamma}{V_{rm}}C_{Dcs}A_{Tcs}\sqrt{V_{cs}}\sqrt{\frac{p_c}{m_c}}\beta & -C_{Drm}A_{Drm}\sqrt{V_{sm}}\sqrt{\frac{p_{rm}}{m_{rm}}}\delta \end{bmatrix}x$$

$$\alpha=\begin{cases}\sqrt{\frac{2\gamma}{\gamma-1}\left(\left(\frac{p_{cs}}{p_{sm}}\right)^{\frac{2}{\gamma}}-\left(\frac{p_{cs}}{p_{sm}}\right)^{\frac{\gamma+1}{\gamma}}\right)}\ if\ \frac{p_{cs}}{p_{sm}}>P_{crit}\\ \sqrt{\gamma}\left(\frac{2}{\gamma+1}\right)^{\frac{2\gamma}{2(\gamma-1)}}\ if\ \frac{p_{cs}}{p_{sm}}\le P_{crit}\end{cases}$$
$$\beta=\begin{cases}\sqrt{\frac{2\gamma}{\gamma-1}\left(\left(\frac{p_{rm}}{p_{cs}}\right)^{\frac{2}{\gamma}}-\left(\frac{p_{rm}}{p_{cs}}\right)^{\frac{\gamma+1}{\gamma}}\right)}\ if\ \frac{p_{rm}}{p_{cs}}>P_{crit}\\ \sqrt{\gamma}\left(\frac{2}{\gamma+1}\right)^{\frac{2\gamma}{2(\gamma-1)}}\ if\ \frac{p_{rm}}{p_{cs}}\le P_{crit}\end{cases}$$
$$\delta=\begin{cases}\sqrt{\frac{2\gamma}{\gamma-1}\left(\left(\frac{P_{atm}}{p_{rm}}\right)^{\frac{2}{\gamma}}-\left(\frac{P_{atm}}{p_{rm}}\right)^{\frac{\gamma+1}{\gamma}}\right)}\ if\ \frac{P_{atm}}{p_{rm}}>P_{crit}\\ \sqrt{\gamma}\left(\frac{2}{\gamma+1}\right)^{\frac{2\gamma}{2(\gamma-1)}}\ if\ \frac{P_{atm}}{p_{rm}}\le P_{crit}\end{cases} \tag{5.7}$$

For the parameter values, please refer to the Annex A.

5.2.1.1 *TS representation for gaseous Model*

By considering a general TS model which is presented as a sum of linear systems (as described in the estimation chapter), we can transform the nonlinear FC model into this special format that is easier to manipulate. This is done with the aid of weighting functions w_i that eliminate the nonlinearities in the system matrices as presented in equation (5.8).

$$\begin{cases} \dot{x} = \sum_{i=1}^{8} w_i(z) A_i x + Bu \\ y = Cx \end{cases} \tag{5.8}$$

Here, as usual, the states vector is represented with the notation x, u the input vector and y the output vector. Also it is considered that B and C system matrices do not depend on the states and the notation A_i is used for all the 2^n linear fuzzy systems; also z represents the vector of nonlinear terms, defined as premise variables (nonlinear terms).

In order to obtain the state observer, it is first required to modify the state space form in (5.5), so that it reaches a Takagi-Sugeno (TS) representation. So from equation (5.5), in order to get to the form (5.8) we separate in the matrix A all the z nonlinearities, arriving eventualy at (5.9). The vectorial notation for the states x is used considering the states presented in (5.5).

$$z = \begin{bmatrix} z_1 \\ z_2 \\ z_3 \end{bmatrix} = \begin{bmatrix} \sqrt{\frac{p_{sm}}{m_{sm}}}\alpha \\ \sqrt{\frac{p_{cs}}{m_{cs}}}\beta \\ \sqrt{\frac{p_{rm}}{m_{rms}}}\delta \end{bmatrix} = \begin{bmatrix} \sqrt{\frac{x(4)}{x(1)}}\alpha \\ \sqrt{\frac{x(5)}{x(2)}}\beta \\ \sqrt{\frac{x(6)}{x(3)}}\delta \end{bmatrix} \tag{5.9}$$

The nonlinear information for the system contained in the premise variables can now be analyzed, so by means of the sector nonlinearity method, the minimum and maximum of each of the three premise variables z_1, z_2, z_3 can be determined and finally the membership functions can be built. The values determined experimentally for the system at hand is in table (5.1).

Table 5.1: Premise variables's min/max values

Symbol	**Quantity**
$z_{1_{\min}} = 1$	$z_{1_{\max}} = 1500$
$z_{2_{\min}} = 3$	$z_{2_{\max}} = 7000$
$z_{3_{\min}} = 3$	$z_{3_{\max}} = 1500$

From different types of possible membership functions, triangular membership function were chosen as in (5.10); where $MF_{min}(z_i)$, $MF_{Max}(z_i)$ are the minimum / maximum membership functions associated to the

i^{th} premise variable z_i. With these values, one is able to construct the normalized weighting functions w_i as in (5.11) where $i = 1..8$ for all the possible combinations.

$$MF_{min}(z_i) = \frac{z_{i,Max} - z_i}{z_{i,Max} - z_{i,\min}}; MF_{Max}(z_i) = \frac{z_i - z_{i,\min}}{z_{i,Max} - z_{i,\min}} \tag{5.10}$$

$$\begin{array}{l} h_1 = MF_{min}(z_1)MF_{min}(z_2)MF_{min}(z_3) \\ h_2 = MF_{min}(z_1)MF_{min}(z_2)MF_{Max}(z_3) \\ -------------------------- \\ h_8 = MF_{Max}(z_1)MF_{Max}(z_2)MF_{Max}(z_3) \\ w_i = \frac{h_i}{\sum\limits_{i=1}^{2^3} h_i}; \end{array} \tag{5.11}$$

5.2.1.2 *Tranformation of the simplified model into a Mean value form*

It is interesting to see the difference in form between the TS and the mean value based approach. Here we will emphasize something else, which is that in methods like Takagi-Sugeno or Mean Value based methods, the way the nonlinear terms are chosen is crucial. Therefore we will change the form of the system as in the author's paper Olteanu et al. (2012). By applying the theory to our system we change the system format so that we have the general form required.

$$\left\{ \begin{array}{l} \dot{x} = Ax + \Phi(x) + g(y,u) \\ y = Cx \end{array} \right. \tag{5.12}$$

$$x = \begin{pmatrix} m_{O_2} \\ m_{H_2} \\ m_{sm} \\ p_{sm} \\ p_{rm} \end{pmatrix} \quad u = \begin{pmatrix} I_{st} \\ A_{T,rm} \end{pmatrix} \quad y = \begin{pmatrix} p_{sm} \\ p_{rm} \end{pmatrix} \tag{5.13}$$

$$A = \begin{pmatrix} -f_{cst2} & 0 & 0 & k_{sm,out} & k_{ca,out} \\ 0 & -f_{cst5} & 0 & f_{cst3} & 0 \\ k_{sm,out}f_{cst1} & 0 & 13.3 & -k_{sm,out} & 0 \\ 0 & 3.21 \cdot 10^8 & 5.4321 \cdot 10^7 & 69 & 0 \\ (f_{cst6}f_{cst1}) & 0 & 0 & 0 & -f_{cst6} \end{pmatrix} \quad (5.14)$$

$$\Phi(z) = \begin{pmatrix} 0 \\ 0 \\ -13.3m_{sm} \\ z_1 f_{cst9} m_{O_2} - 3.21 \cdot 10^8 m_{H_2} - 5.4321 \cdot 10^7 m_{sm} + (f_{cst11}z_2 - f_{cst8}z_1 - 69)\, p_{sm} \\ 0 \end{pmatrix} \quad (5.15)$$

$$C = \begin{pmatrix} 0 & 0 & 0 & 1 & 0 \\ 0 & 0 & 0 & 0 & 1 \end{pmatrix} \quad (5.16)$$

The parameters in the equation can be found in the Annex A.2. The general observer schema will be in consequence:

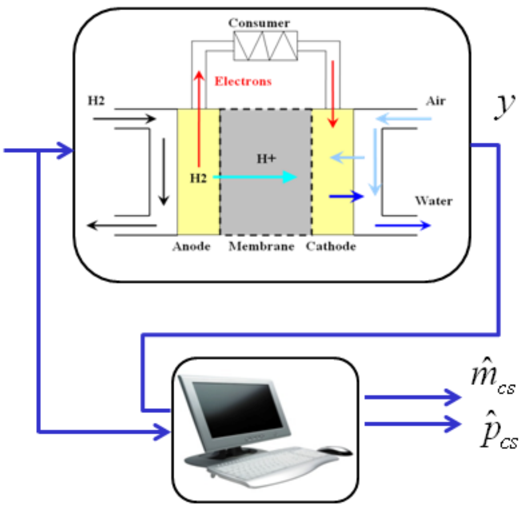

Figure 5.3: General Observer Schema adapted to our FC System

Determining the bounds of the Jacobian Matrix

Now we calculate the Jacobian, and so we reach the following matrix:

$$J\Phi(x) = \begin{pmatrix} 0 & 0 & 0 & 0 & 0 \\ 0 & 0 & 0 & 0 & 0 \\ 0 & 0 & -13.3 & 0 & 0 \\ z_1 f_{cst9} & -3.2110^8 & (-5.432110^7 - f_{cst9} z_{11} z_1 + f_{cst8} z_1^2) & \left(-69 + f_{cst9} z_{11} + f_{cst11}(\frac{-1+\gamma}{\gamma}) z_2 - 2 f_{cst8} z_1\right) & 0 \\ 0 & 0 & 0 & 0 & 0 \end{pmatrix} \tag{5.17}$$

We now find the minimum and maximum of each term. This has been done by means of simulating at different initial conditions. The following possibilities were tested:

$$\begin{cases} x_1 = (0.005 \vee 0.06) \\ x_2 = (10^-4 \vee 2 * 10^-3) \\ x_3 = (0.01 \vee 0.12) \\ x_4 = \left(5 * 10^4 \vee 6 * 10^5\right) \\ x_5 = \left(5 * 10^4 \vee 5 * 10^5\right) \end{cases} \tag{5.18}$$

$$\begin{cases} h_{4,1} \in (1.9422\mathbf{e} + \mathbf{007}; 2.7968e + \mathbf{009}) \\ h_{4,2} = -3.2110^8 \\ h_{4,3} \in (-1.3257\mathbf{e} + \mathbf{00}9; 1.6837\mathbf{e} + \mathbf{0}10) \\ h_{4,4} \in (-655.3592; 159.9110) \\ h_{3,3}\text{=-13.3} \end{cases}, \tag{5.19}$$

where the term $Z_H = 5 * 5 - n_0 = 25 - 20 = 5$, having n_0 as the number of terms equal to zero.

$$H^{\max} = 5\begin{pmatrix} 0 & 0 & 0 & 0 & 0 \\ 0 & 0 & 0 & 0 & 0 \\ 0 & 0 & -13.3 & 0 & 0 \\ 2.7968\mathbf{e}+\mathbf{009} & -3.2110^{8} & 1.6837\mathbf{e}+010 & 159.9110 & 0 \\ 0 & 0 & 0 & 0 & 0 \end{pmatrix} \tag{5.20}$$

$$H^{\min} = 5\begin{pmatrix} 0 & 0 & 0 & 0 & 0 \\ 0 & 0 & 0 & 0 & 0 \\ 0 & 0 & -13.3 & 0 & 0 \\ 1.9422\mathbf{e}+\mathbf{00}7 & -3.2110^{8} & -1.3257\mathbf{e}+\mathbf{00}9 & -655.3592 & 0 \\ 0 & 0 & 0 & 0 & 0 \end{pmatrix} \tag{5.21}$$

5.2.2 Fuel Cell gaseous model with temperature measurement

We can also suppose that we measure the temperatures in the supply and return manifold instead of the masses of gas, which is more applicable considering that many temperature sensors exist but it is much more expensive to measure mass. Using the perfect gas law one obtains:

$$u = W_{in} \quad x = \begin{bmatrix} m_{sm} \\ m_{cs} \\ m_{rm} \\ p_{sm} \\ p_{cs} \\ p_{rm} \end{bmatrix} \quad y = \begin{bmatrix} T_{sm} \\ T_{rm} \\ p_{sm} \\ p_{rm} \end{bmatrix} = \begin{bmatrix} \frac{p_{sm}V_{sm}}{Rm_{sm}^2} & 0 & 0 & 0 & 0 & 0 \\ 0 & 0 & \frac{p_{rm}V_{rm}}{Rm_{rm}^2} & 0 & 0 & 0 \\ 0 & 0 & 0 & 1 & 0 & 0 \\ 0 & 0 & 0 & 0 & 0 & 1 \end{bmatrix} x$$

We will jump the trnasformation to TS form step as it is obvious. Thus the system is expressed as:

$$B = \begin{bmatrix} 1 \\ 0 \\ 0 \\ \frac{\gamma R_a T_{smin}}{V_{sm}} \\ 0 \\ 0 \end{bmatrix}$$

$$A(x) = \begin{bmatrix} -\frac{C_{Dsm}A_{Tsm}}{\sqrt{V_{sm}}}z_1 & 0 & 0 & 0 \\ \frac{C_{Dsm}A_{Tsm}}{\sqrt{V_{sm}}}z_1 & -\frac{C_{Dcs}A_{Tcs}}{\sqrt{V_{cs}}}z_2 & 0 & 0 \\ 0 & \frac{C_{Dcs}A_{Tcs}}{\sqrt{V_{cs}}}z_2 & \frac{C_{Drm}A_{Trm}}{\sqrt{V_{rm}}}z_3 & 0 \\ 0 & 0 & 0 & -\frac{\gamma}{V_{sm}}C_{Dsm}A_{Tsm}\sqrt{V_{sm}}z_1 \\ 0 & 0 & 0 & \frac{\gamma}{V_{cs}}C_{Dsm}A_{Tsm}\sqrt{V_{sm}}z_1 \\ 0 & 0 & 0 & 0 \end{bmatrix}$$
$$\begin{bmatrix} 0 & 0 \\ 0 & 0 \\ 0 & 0 \\ 0 & 0 \\ -\frac{\gamma}{V_{cs}}C_{Dcs}A_{Tcs}\sqrt{V_{cs}}z_2 & 0 \\ \frac{\gamma}{V_{rm}}C_{Dcs}A_{Tcs}\sqrt{V_{cs}}z_2 & -C_{Drm}A_{Drm}\sqrt{V_{sm}}z_3 \end{bmatrix} x$$

Finally the nonlinear terms (premise variables) are consequently:

$$z = \begin{bmatrix} \sqrt{\frac{p_{sm}}{m_{sm}}}\alpha \\ \sqrt{\frac{p_{cs}}{m_{cs}}}\beta \\ \sqrt{\frac{p_{rm}}{m_{rms}}}\delta \\ \frac{p_{sm}}{m_{sm}^2} \\ \frac{p_{rm}}{m_{rm}^2} \end{bmatrix} = \begin{bmatrix} \sqrt{\frac{x(4)}{x(1)}}\alpha \\ \sqrt{\frac{x(5)}{x(2)}}\beta \\ \sqrt{\frac{x(6)}{x(3)}}\delta \\ \frac{x(4)}{(x(1))^2} \\ \frac{x(6)}{(x(3))^2} \end{bmatrix}$$

5.2.3 Fuel Cell Model with water vapor

State space representation

For ideal gases, the mass conservation law is applied resulting (5.22). The compressor's mass flow is considered as input to the system, the possibility to add a controller so that it follows a desired flow exists. The mass that accumulates in the cathode, depending on the quantity of oxygen that enters, will either be ejected or will react with the hydrogen ions. Furthermore, inside the cathode, vapor is generated, where some of it is ejected towards the return manifold (consisting of pipes and valves), while another part adds inside the cathode, increasing the general pressure. The work is done under the hypothesis that there is no humidification neither of the oxygen nor of the hydrogen, and the FC is self humidifying [12]. Concerning the valve mathematical model, a linear model has been chosen for the cases when we have small pressure differences, whereas a chocked regime equation was demanded for the cathode purge valves and anode. This is because of the big pressure difference created with the atmosphere. As the return manifold pressures overpass 2 bar, ignoring the unchoked regime brings no limitations.

$$\begin{cases} \frac{dp_{sm}}{dt} = \frac{R_{O_2}.T_{st}}{V_{sm}}(W_{cp} - W_{sm,out}) \\ \frac{dp_{rm}}{dt} = \frac{R_a T_{rm}}{V_{rm}}\left(W_{ca,out} - W_{rm,out}\right) \\ \frac{dp_{O_2,ca}}{dt} = \frac{R_{O_2} T_{st}}{V_{ca}}\left(W_{O_2,ca,in} - W_{O_2,ca,out} - W_{O_2,reacted}\right) \\ \frac{dp_{v,ca}}{dt} = \frac{R_v T_{st}}{V_{ca}}\left(-W_{v,ca,out} + W_{v,ca,gen}\right) \\ \frac{dp_{H_2,an}}{dt} = \frac{R_{H_2} T_{st}}{V_{an}}\left(W_{H_2,an,in} - W_{H_2,an,out} - W_{H_2,reacted}\right) \end{cases} \tag{5.22}$$

The electrical current present as input, represents the demanded current by the consumer system attached to the fuel cell. Finally, the system is described by (5.23).

$$\begin{cases} \frac{dp_v}{dt} = \frac{R_v T_{st}}{V_{ca}} \left[\left(k_{ca} \left(p_{ca,O_2} + p_v - p_{rm} \right) \left(-1 + \frac{M_{O_2} p_{ca,O_2}}{M_{O_2} p_{ca,O_2} + M_v p_v} \right) \right) + \left(\frac{n M_v}{2 \cdot F} \right) I_{st} \right] \\ \frac{dp_{ca,O_2}}{dt} = \frac{R_{O_2} T_{st}}{V_{ca}} \left[\begin{array}{l} k_{sm} \left(p_{sm} - p_{ca,O_2} - p_v \right) - k_{ca} \left(p_{ca,O_2} - (p_{rm} - p_v) \right) - \\ - \left(\frac{n M_{O_2}}{4F} \right) I_{st} \end{array} \right] \\ \frac{dp_{rm}}{dt} = \frac{R_a T_{st}}{V_{rm}} \left[\begin{array}{l} k_{ca} \cdot \left(p_{ca,O_2} + p_v - p_{rm} \right) - \\ - \frac{A_{T,rm} C_{d,rm} p_{rm}}{\sqrt{\bar{R} T_{atm}}} \sqrt{\gamma} \left(\frac{2}{\gamma+1} \right)^{\frac{\gamma+1}{2(\gamma-1)}} \end{array} \right] \\ \frac{dp_{sm}}{dt} = \frac{R_a T_{st}}{V_{rm}} \left[W_{cp} - k_{sm} \left(p_{sm} - p_{ca,O_2} - p_v \right) \right] \\ \frac{dp_{an,H_2}}{dt} = \frac{R_{H2} T_{st}}{V_{an}} \left[\begin{array}{l} K K_1 \left(p_{sm} - p_{an,H_2} \right) - \\ - A_{an} p_{an,H_2} \frac{C_{d,an} \sqrt{\gamma} \left(\frac{2}{\gamma+1} \right)^{\frac{\gamma+1}{2(\gamma-1)}}}{\sqrt{\bar{R} T_{atm}}} - M_{H_2} \frac{n I_{st}}{2F} \end{array} \right] \end{cases} \tag{5.23}$$

Takagi Sugeno Representation

The choice of nonlinear terms is important, the objective being to keep their number to a minimum, while maintaining the observability of each new linear system that will be built.

For developing the TS system, it is needed to rewrite the initial state space model so that the nonlinear terms can be separated. A separation of the nonlinear terms into the 2 matrices is seen in (5.25): $A_x(x)$ and $B_x(x)$. The chosen PEMFC system has 5 states (Pressures of Vapor; Oxygen in Cathode; Return manifold; Supply Manifold; Hydrogen in the Anode), with two of them, the Return Manifold and the Supply Manifold Pressures, being measured (5.24).

$$x = \begin{pmatrix} p_v \\ p_{ca,O_2} \\ p_{rm} \\ p_{sm} \\ p_{an,H_2} \end{pmatrix}; u = \begin{pmatrix} I_{st} \\ A_{T,rm} \\ W_{in} \end{pmatrix}; y = \begin{pmatrix} p_{rm} \\ p_{sm} \end{pmatrix} \tag{5.24}$$

Concerning the observability property, the condition that each linear system is observable depends on the minimum and maximum values chosen in the nonlinearity sector stage and also on the selection of the premise variables.

$$A_x(x) = \begin{pmatrix} -k_{ca}cst1 & cst1\left[-k_{ca}+k_{ca}Z_1+k_{ca}Z_2)\right] & cst1\left[k_{ca}-k_{ca}Z_1\right] & 0 & 0 \\ cst2\left[-k_{sm}-k_{ca}\right] & cst2\left[-k_{sm}-k_{ca}\right] & cst2k_{ca} & 0 & 0 \\ cst3k_{ca} & cst3k_{ca} & -cst3k_{ca} & 0 & 0 \\ cst3k_{sm} & cst3k_{sm} & -cst3k_{sm} & 0 & \\ 0 & 0 & 0 & cst5 & -cst6-cst5 \end{pmatrix},$$

$$B_x(x) = \begin{pmatrix} cst1\left[\frac{nM_v}{2F}\right] & 0 & 0 \\ cst2\left[-\frac{nM_{O_2}}{4F}\right] & 0 & 0 \\ 0 & -\frac{R_aT_{st}}{V_{rm}}\frac{C_{d,rm}\sqrt{\gamma}\left(\frac{2}{\gamma+1}\right)^{\frac{\gamma+1}{2(\gamma-1)}}}{\sqrt{\bar{R}T_{atm}}}(p_{rm}) & 0 \\ 0 & 0 & \frac{R_aT_{st}}{V_{rm}} \\ -\frac{R_{H2}T_{st}}{V_{an}}M_{H_2}\frac{n}{2F} & 0 & 0 \end{pmatrix} \tag{5.25}$$

where the parameters are presented in Annex, as well as the constants in A and A.1. In conclusion there are three premise variables:

$$\begin{aligned} Z_1(p_v, p_{ca,O_2}) &= \frac{M_{O_2}p_{ca,O_2}}{M_{O_2}p_{ca,O_2}+M_vp_v} \\ Z_2(p_v, p_{ca,O_2}) &= \frac{M_{O_2}p_v}{M_{O_2}p_{ca,O_2}+M_vp_v} \\ Z_3(p_{rm}) &= p_{rm} \end{aligned} \tag{5.26}$$

Therefore by choosing triangular membership function they are written as (5.27), where *MF* represents the membership function associated to the i-th premise variable z_i. We are being thus able to write the normalized membership functions w_i as showed in (5.28).

$$\begin{cases} MF_{min}(z_i) = \frac{z_i - z_{i,Max}}{z_{i,Max}-z_{i,min}} \\ MF_{Max}(z_i) = \frac{z_i - z_{i,min}}{z_{i,Max}-z_{i,min}} \end{cases} \tag{5.27}$$

$$\begin{cases} h_1 = MF_{Max}(z_1)MF_{Max}(z_2)MF_{Max}(z_3) \\ h_2 = MF_{Max}(z_1)MF_{Max}(z_2)MF_{min}(z_3) \\ \ldots\ldots \\ h_8 = MF_{min}(z_1)MF_{min}(z_2)MF_{\min}(z_3) \\ --------------------- \\ w_1 = \frac{h_1}{\sum\limits_{i=1}^{8} h_i}; \ldots; w_8 = \frac{h_8}{\sum\limits_{i=1}^{8} h_i} \end{cases} \tag{5.28}$$

5.3 Observer implementation

5.3.1 Observer results of Lipschitz approach for FC model with vapor

By implementing the presented techniques, we obtained the following results.

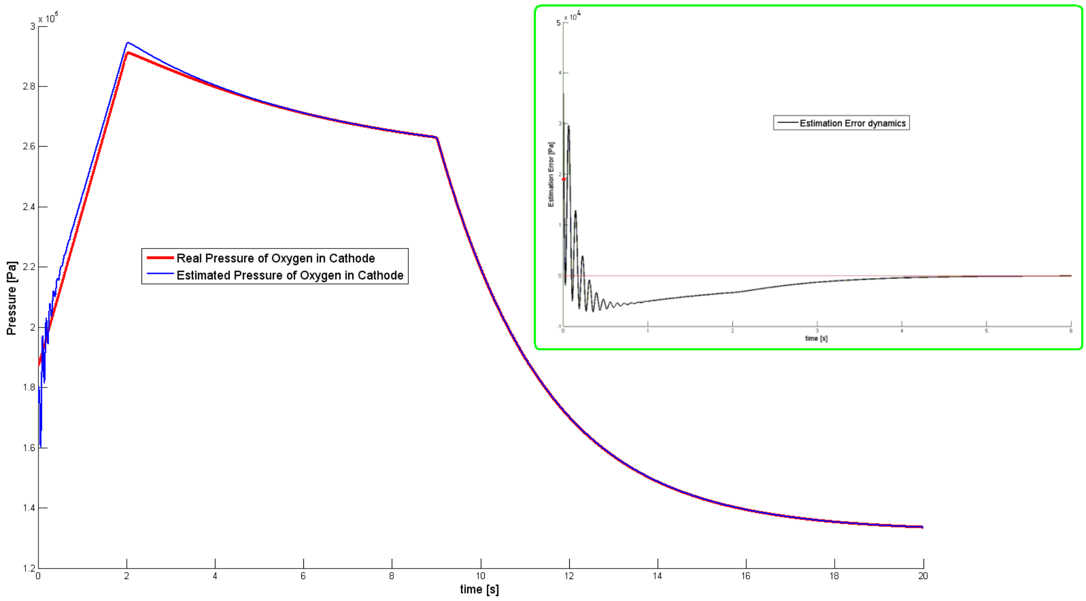

Figure 5.4: The evolution of the real and estimated values of the Oxygen Pressure in the cathode

In figure 5.4 we have tested the performance of the Observer on the Oxygen Pressure inside the cathode with a different initial state than the system. We can see that the estimation error reaches stability with no static error. The stabilization requires a certain time because of the high sloped evolution (better seen in figure 5.4). The difference in initial values between the system and the observer is somewhere around $2 \cdot 10^4$ Pa, shown by the red dot in the zoomed image. In figure 5.6 we wanted

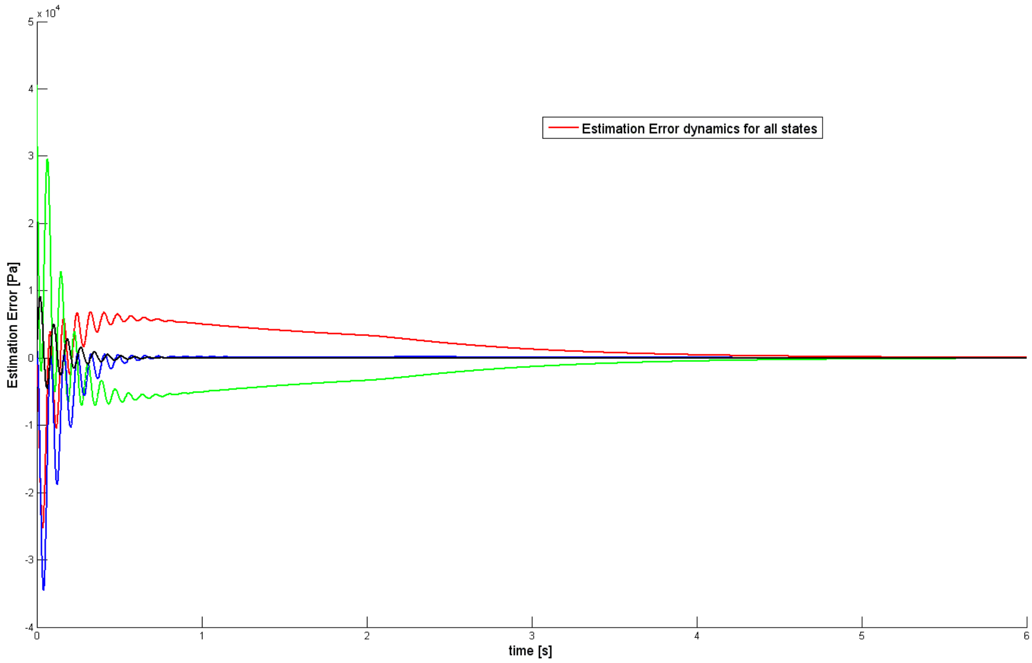

Figure 5.5: The evolution of the estimation error for all the states (Lipschitz method)

to show the general transitional evolution of the estimation error. Here we can see the powerful oscillatory behavior in the beginning of the simulation. This is caused by the existence of non-minimum phase zeros in the $(A_0 - L_i \cdot C)$ that force an undershoot and some consequent oscillations. Also regarding the time required for stabilization, this is due to the eigenvalues of the $(A_0 - L_i \cdot C)$. When the eigenvalues are chosen too close to -1, the LMI resolution will not find any solutions. This could be caused by the restrictions generated in the construction of the LMIs or/and the minimum and maximum values chosen for the Jacobian.

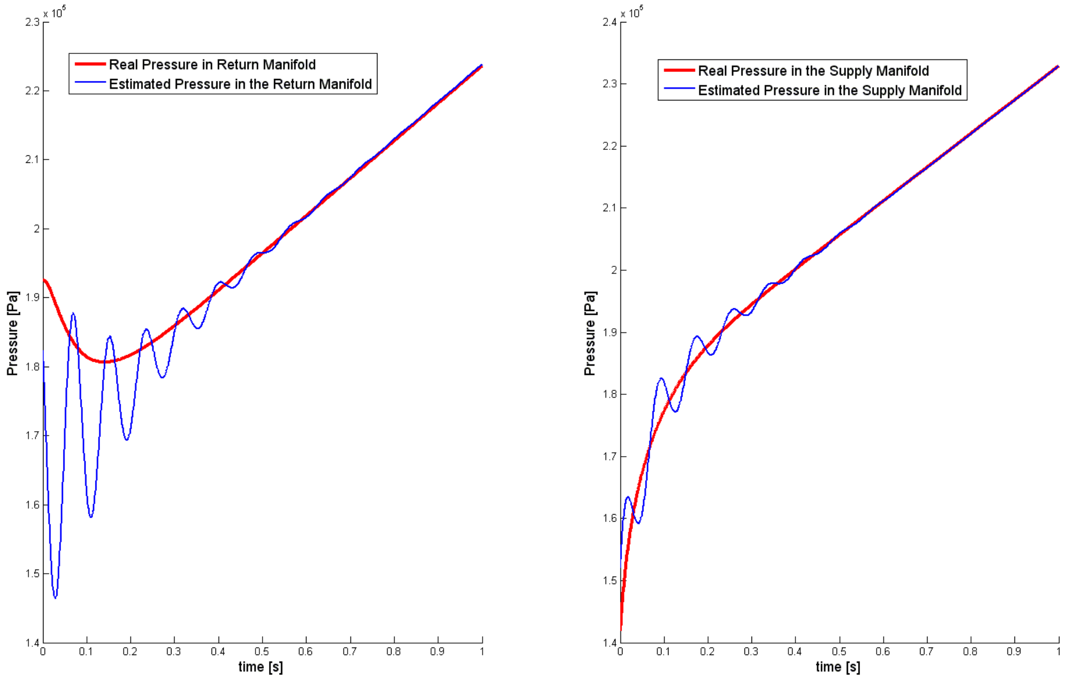

Figure 5.6: Stabilization of the estimation error, for Return Manifold/Supply Manifold Pressures(Lipschitz method)

5.3.2 Observer results of bounded stability approach for vapor gaseous FC model

In the case of included water vapor, the AMESim validation shows a small difference between the employed model and the reference one in figure 5.7.

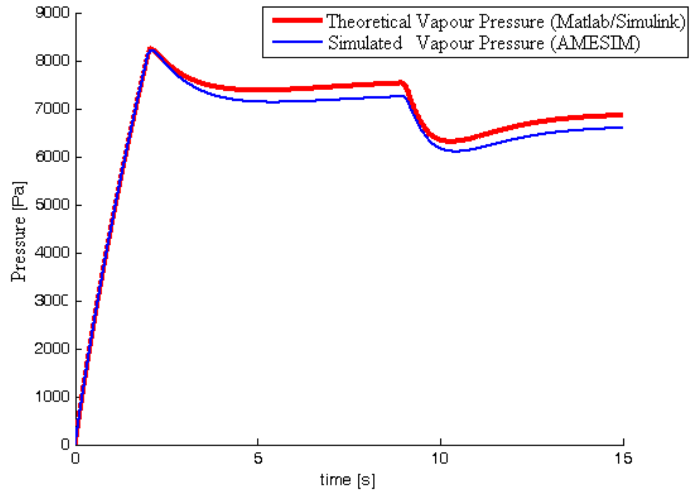

Figure 5.7: The vapor Pressure present inside the cathode volume

By applying the proposed observer using the stated LMI's, the observer gains are found. For these values we simulate and obtain at a varying input the following: One can see the good convergence of the estimation error 5.8. Here the red lines is the estimation error of the vapor pressure. As the pressure is almost null in the beginning the error starts at 0 but it accelerates rapidly as the FC starts. This is compensated by the observer. Another estimation is done for the oxygen pressure in the cathode presented next.

Also here, we observer a characteristic of this observer type, that it does not present oscillations in the beginning anymore, yet it cannot force the convergence at around 0.4 seconds. The reduced convergence speed is also due to the fact that at around 0.4s the system response is very nonlinear, thus the weighting functions of the TS representation would also have nonlinear values. Figure 5.9 presents the estimation of Oxygen pressure with a different initial state from the process.

The powerful influence in three stages of the control of the Return Manifold valve can be easily seen on all the states. Only the generation of vapor being mainly affected by electrical current increases in figure 5.7. A small difference can indeed be seen, being generated by the used equations, but it is in acceptable limits.

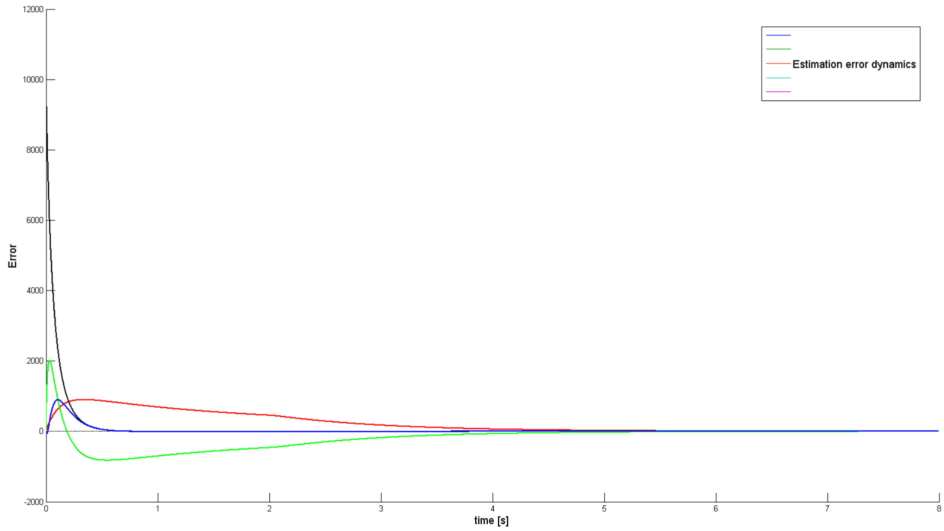

Figure 5.8: The estimation error dynamics of the states (bounded observer)

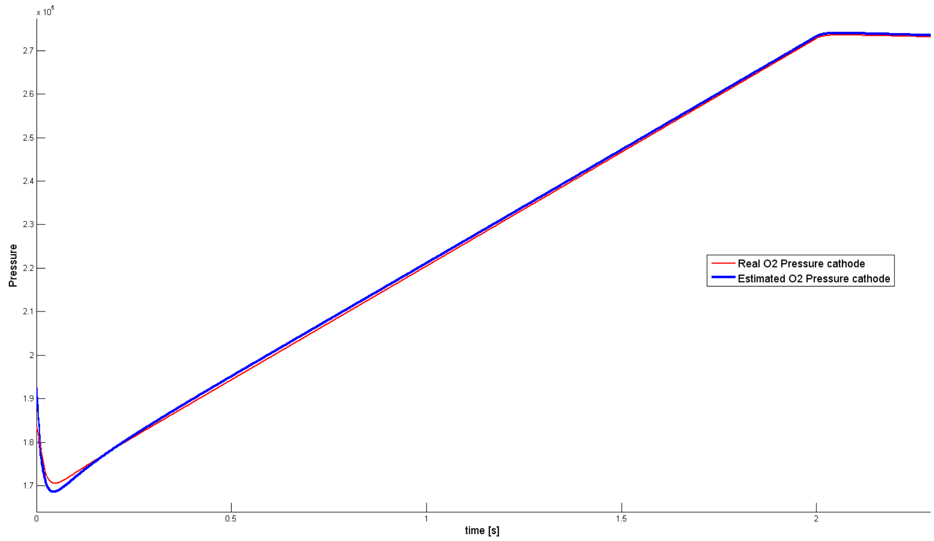

Figure 5.9: The estimation in parallel with the real value for Pressure O2

5.3.3 Mean value based Observer, for the gaseous model

5.3.3.1 *Observability*

We will now apply the observer based on the Mean value principle, as presented in the chapter describing estimation techniques. The condition of observability is satisfied by the nonlinear system viewed as a whole. Although not sufficient, the observability has to be applicable for each virtual linear system determined by A and C and all $[A+H_{i,j}^{max,min}, C]$. One important aspect is for the system to be numerically stable, and to have the numerical values which are not scattered at different scales (for our system, the values are not well scaled). For this we add some terms to the matrix A and then subtract the same terms from matrix $\Phi(x)$. Also the values chosen are carefully picked so that we can do a numerical modification to the LMIs in order for the computations not to have ill posed matrices. These added values are: $A(4,2) = 3.21 * 10^8$, $A(4,3) = 5.4321 * 10^7$, $A(3,3) = 13.3$, $A(4,3) = 69$.

5.3.3.2 *Building a Symmetric System*

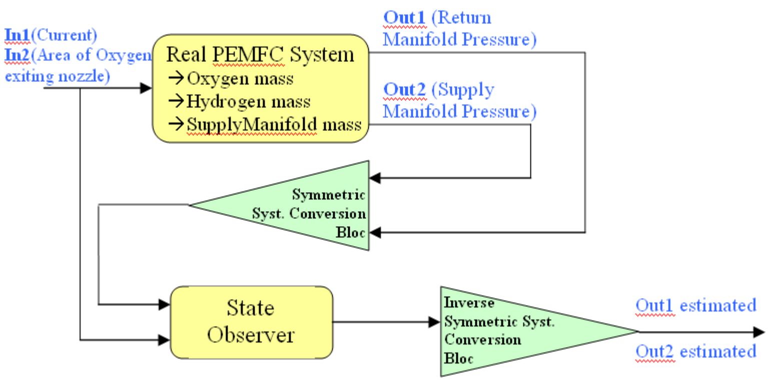

Figure 5.10: General Observer logic adapted to our FC system

For the Luenberger Observer's Gains, we need to perform the resolution of a system of 8 inequalities. As mentioned, our system's matrices are numerically ill posed (amplitudes of largely different scales). To enter into more detail, the procedure for solving this issue starts by multiplying the inequality left and right with a matrix on each side. The matrices will be diagonal, and the values of each of them have to be chosen, following all the possibilities of $A + H_i^{min}$ respectively $A + H_i^{max}$. In the end we choose (by means of experiment):

$$P = \begin{pmatrix} 10^{-7} & 0 & 0 & 0 & 0 \\ 0 & 10^{-7} & 0 & 0 & 0 \\ 0 & 0 & 10^{-7} & 0 & 0 \\ 0 & 0 & 0 & 10 & 0 \\ 0 & 0 & 0 & 0 & 1 \end{pmatrix} P^{-1} = \begin{pmatrix} 10^{7} & 0 & 0 & 0 & 0 \\ 0 & 10^{7} & 0 & 0 & 0 \\ 0 & 0 & 10^{7} & 0 & 0 \\ 0 & 0 & 0 & 10^{-1} & 0 \\ 0 & 0 & 0 & 0 & 1 \end{pmatrix} \tag{5.29}$$

The symmetry is to be taken into consideration $P = P^T$. We apply the similarity transformation, which implies that if we consider a new state as being $\bar{x} = P^{-1}x$, then the system passes from equation (5.30) to (5.31).

$$\begin{cases} P^{-1}\dot{x} = P^{-1}APP^{-1}xP + P^{-1}\Phi(x) + P^{-1}g(y,u) + P^{-1}Fc; \\ y = CPP^{-1}x \end{cases} \tag{5.30}$$

$$\begin{cases} \dot{\bar{x}} = \bar{A}\bar{x} + P^{-1}\Phi(x) + \bar{g}(y,u) + \bar{F}_c \\ \bar{y} = \bar{C}\bar{x} \end{cases}, \tag{5.31}$$

by making the notations:

$$\begin{aligned} &\bar{x} = P^{-1}x \\ &\bar{y} = y \\ &\bar{C} = CP \\ &\bar{g} = P^{-1}g \\ &\bar{A} = P^{-1}(A)P \\ &\bar{F}_c = P^{-1}F_c \end{aligned} \tag{5.32}$$

Important to note the behavior of $\Phi(x)$, dependent on x, and not the new state $\bar{x}$, because the transformation of x is not possible being situated in nonlinear equations. The new observer becomes:

$$\begin{cases} \dot{\hat{\bar{x}}} = \bar{A}\hat{\bar{x}} + P^{-1}\Phi(\hat{x}) + \bar{g}(y,u) + L(\bar{y} - \hat{\bar{y}}) + \bar{F}_c \\ \hat{\bar{y}} = \bar{C}\hat{\bar{x}} \end{cases} \tag{5.33}$$

The estimation error $\tilde{\bar{x}} = \bar{x} - \hat{\bar{x}}$, has the dynamics:

$$\dot{\tilde{\bar{x}}} = (\bar{A} - L\bar{C})\tilde{\bar{x}} + \tilde{\Phi}(\hat{x})$$
$$\tilde{\Phi}(\hat{x}) = P^{-1}(\Phi(x) - \Phi(\hat{x}))$$

Then the Lyapunov function candidate is defined as the function V, with a positive definite and symmetric matrix R, where $R \in \mathbb{R}^{5\times 5}$.

$$V = \tilde{\bar{x}}^T R \tilde{\bar{x}} \tag{5.34}$$

This implies that its derivative is expressed as:

$$\dot{V} = \tilde{\bar{x}}^T[(\bar{A} - L\bar{C})^T R + R(\bar{A} - L\bar{C})]\tilde{\bar{x}} + \tilde{\bar{x}}^T R\tilde{\Phi} + \tilde{\Phi}^T R\tilde{\bar{x}} < 0 \tag{5.35}$$

We take into account that the following Jacobian relation exists (and can be easily proven): $Jac(P^{-1}\Phi(x)\ ) = P^{-1}Jac(\Phi(x) - \Phi(\hat{x}))$,

therefore, by oversimplifying the notations we will consider

$$\sum H_{min,max} = \left[\left(\sum_{i,j}^{n_x,n_x} H_{ij}^{\max}\delta_{ij}^{\max}\right) + \left(\sum_{i,j}^{n_x,n_x} H_{ij}^{\min}\delta_{ij}^{\min}\right)\right],$$

we will therefore find $\tilde{\Phi}(\hat{x})$ expressed as:

$$\tilde{\Phi}(\hat{x}) = P^{-1}(\Phi(x) - \Phi(\hat{x})) = P^{-1}\left[\sum H_{min,max}\right](x - \hat{x})$$

Yet we are interested in $\tilde{\bar{x}} = \bar{x} - \hat{\bar{x}}$, therefore:

$$\tilde{\Phi}(\hat{x}) = P^{-1}\left[\sum H_{min,max}\right]PP^{-1}(x - \hat{x}),$$

and therefore:

$$\tilde{\Phi}(\hat{x}) = \left\{P^{-1}\left[\sum H_{min,max}\right]P\right\}\tilde{\bar{x}}.$$

This way we bring forth the notation: $\overline{(A + \bar{H}_{ij}^{max})} = P^{-1}(A + \bar{H}_{ij}^{max})P$, or $\overline{(A+\bar{H}_{ij}^{\min})} = P^{-1}(A+\bar{H}_{ij}^{\min})P$ (the same when we have $\bar{A}$). Now we can rewrite the final system of LMIs as:

$$\begin{cases} R(\overline{\bar{A}+\bar{H}_{ij}^{max}}) + (\overline{A+\bar{H}_{ij}^{max}})^T R - \bar{C}^T L^T R - RL\bar{C} < 0 \\ R(\overline{\bar{A}+\bar{H}_{ij}^{min}}) + (\overline{A+\bar{H}_{ij}^{min}})^T R - \bar{C}^T L^T R - RL\bar{C} < 0 \\ R > 0 \end{cases} \tag{5.36}$$

5.3.3.3 *Applying robustness to the observer*

Starting from the attached theory previously presented, we will have the system:

$$\begin{cases} \dot{x} = Ax + \Phi(x) + g(y,u) + Fc + W_1 w(t) \\ y = Cx + W_2 w(t) \end{cases} \tag{5.37}$$

where $W_2 = \begin{pmatrix} 0 & 0 & 0 & 0.05 & 0 \\ 0 & 0 & 0 & 0 & 0.05 \end{pmatrix}$ $W_1 = \begin{pmatrix} 0 & 0 & 0 & 0.05 & 0 \\ 0 & 0 & 0 & 0 & 0 \end{pmatrix}$

Therefore we have perturbed the supply manifold mass dynamics (generated by a potential falw in the supply manifold chamber). Also measurement perturbations have been added.

If we make the notations: $\bar{x} = P^{-1}x$, $\bar{y} = y$, $\bar{C} = CP$, $\bar{g} = P^{-1}g$, $\bar{A} = P^{-1}(A)P$, $(\bar{F}_c) = P^{-1}F_c$, $(\bar{W}_1) = P^{-1}W_1$, $(\bar{W}_2) = W_2$, we will obtain the LMIs 5.38 for all $i, j = 1..n$:

$$\begin{cases} \begin{pmatrix} \left[\bar{H}_{ij}^{\max} + \bar{A}\right]^T R - \bar{C}^T K^T + R\left[\bar{H}_{ij}^{\max} + \bar{A}\right] - K\bar{C} + I & \left(R\bar{W}_1 - K\bar{W}_2\right) \\ \left(R\bar{W}_1 - K\bar{W}_2\right)^T & -\lambda^2 I \end{pmatrix} < 0 \\ \begin{pmatrix} \left[\bar{H}_{ij}^{\min} + \bar{A}\right]^T R - \bar{C}^T K^T + R\left[\bar{H}_{ij}^{\min} + \bar{A}\right] - K\bar{C} + I & \left(R\bar{W}_1 - K\bar{W}_2\right) \\ \left(R\bar{W}_1 - K\bar{W}_2\right)^T & -\lambda^2 I \end{pmatrix} < 0 \\ R > 0 \end{cases} \tag{5.38}$$

5.3.3.4 *Numerical Results*

The observer has been implemented in Matlab/Simulink environment. The inputs of the system are: Electrical current step like variations, and step like variations of the Surface nozzle from the return manifold.

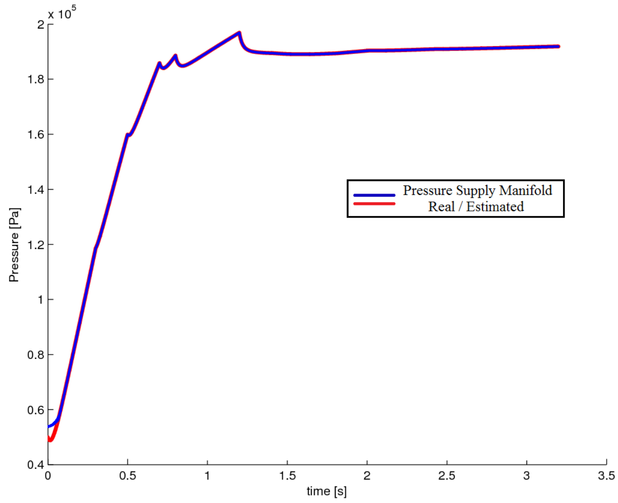

Figure 5.11: Evolution of the Pressure in the Supply Manifold

The evolution of the pressure in the supply manifold in figure 5.3.3.4 shows the system's robustness to perturbation. We can better see in figure 5.12, a comparison of the estimation error between the robust and non-robust case. This confirms the correctness of the results.

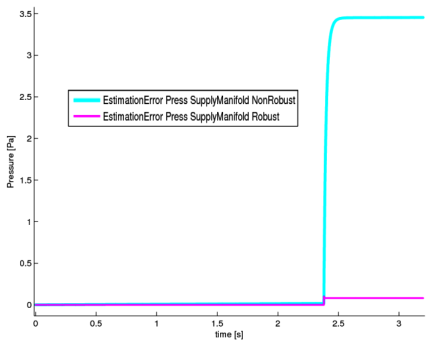

Figure 5.12: Supply Manifold pressure estimation, in robust and non-robust cases

The cathode mass estimation proves to be the most difficult as it is also affected by sensor perturbations that propagate from the supply manifold. The moment when the perturbation is applied is specifically chosen to be the most demanding. We see in figure 5.13 that the perturbation is activated when the mass is rapidly accumulating, thus making the estimation harder. In figure 5.14 we see the estimation error of this mass. Still the perturbation could not be eliminated completely but the remaining error is insignificant (the numerical order of the error being 10^{-4}).

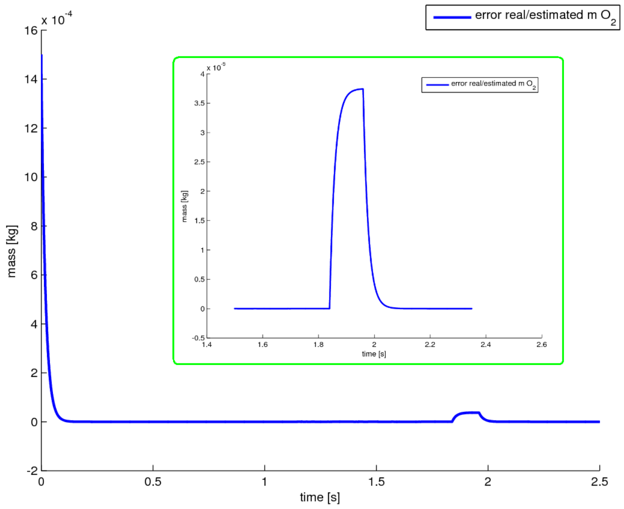

Figure 5.13: Cathode mass evolution

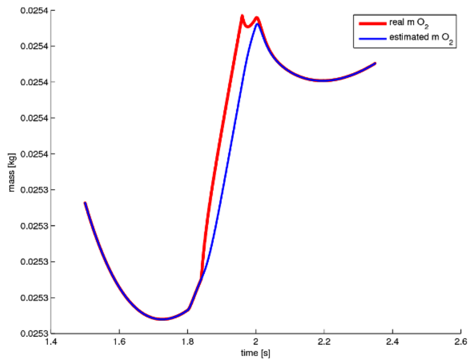

Figure 5.14: Cathode mass estimation error

In conclusion, in the presence of initial state difference and perturbations, we could see that even the most affected states have been correctly estimated.

5.3.4 The embedded solution

The AMESim Fuel cell model built is presented in 5.15. Using the Matlab LMI solver for the previous LMIs applied to the system at hand, we obtain the observer gains which are implemented on the Arduino board, by means of discretization. At this point in order to check the performance we will use different initial values for the observer states

$$\hat{x}(0) = \begin{bmatrix} 0.0563 & 0.0019 & 0.0380 & 387419.1 & 170226 & 144894.8 \end{bmatrix}^T \tag{5.39}$$

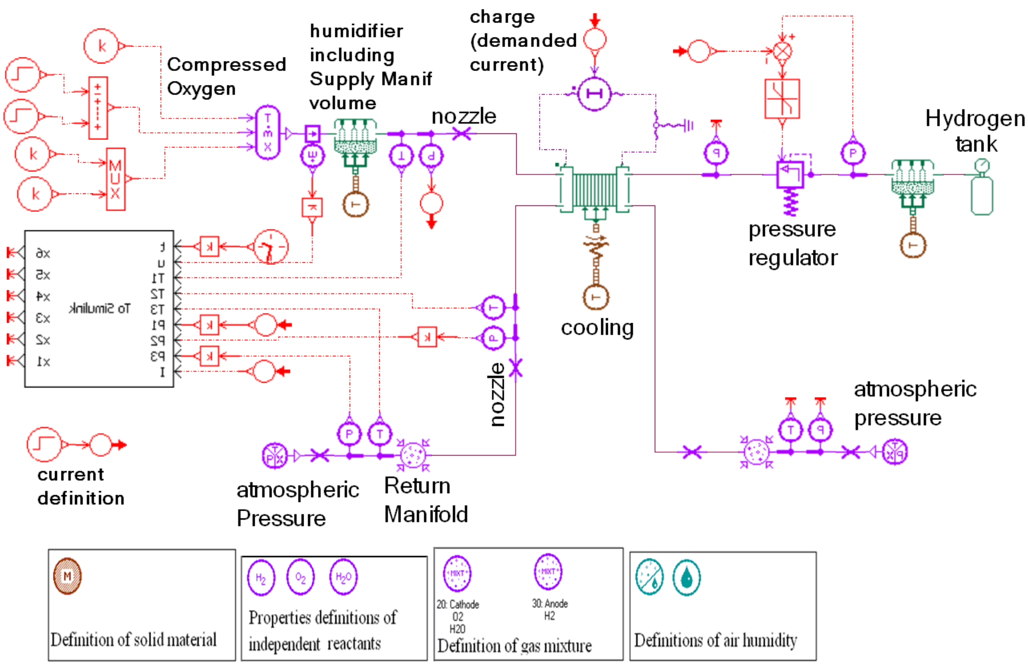

Figure 5.15: The Amesim model of the PEM FC

The simulation between AMESim, Simulink and the Arduino in real time gives us the response in the following figures.The observer appears inactive in the first few seconds due to the initialization time of the devices and the communication. By following the evolution of the estimation error in Figure 5.16, 5.17 one can notice that the stability is not asymptotic, but bounded, of course the bounds being sufficient to respond to requirements. Also one can notice that indeed in the beginning, the observer manifests oscillations before stabilizing, but the settling time is still in an acceptable interval. One can observe in Figure

5.18, at a time around 7 seconds for example, that there is a communication loss, yet the observer manages to re-adapt the estimated values to the real ones. The few seconds delay at the beginning is just due to the initialization procedure of the embedded system.

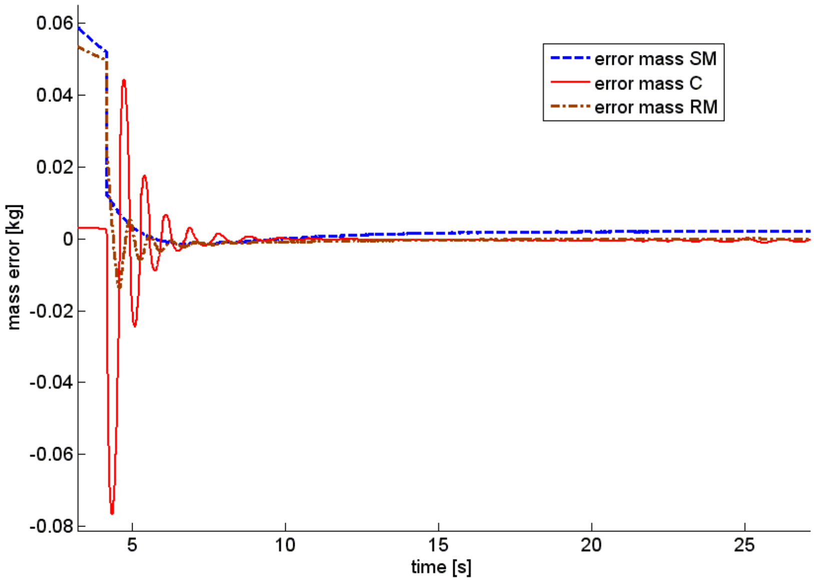

Figure 5.16: Unmeasured premise variables observer error(difference between real and estimated value) for the gas masses of the oxygen supply of the PEMFC

The main problem with this particular embedded system is that the dynamic of the valve is fast and that, for a sample time of more than 5ms, oscillations appear. Considering that we have 6x6 and 6x4 matrices, an 8 bit microcontroller arrives at a minimum sampling time of 10-15ms. Therefore we need to use the Arduino DUE, a 32 bit processor, which has 96kBytes of RAM. Furthermore, the Arduino DUE has a 84 MHz clock, allowing to do the floating point calculations for the oxygen supply in 4ms.

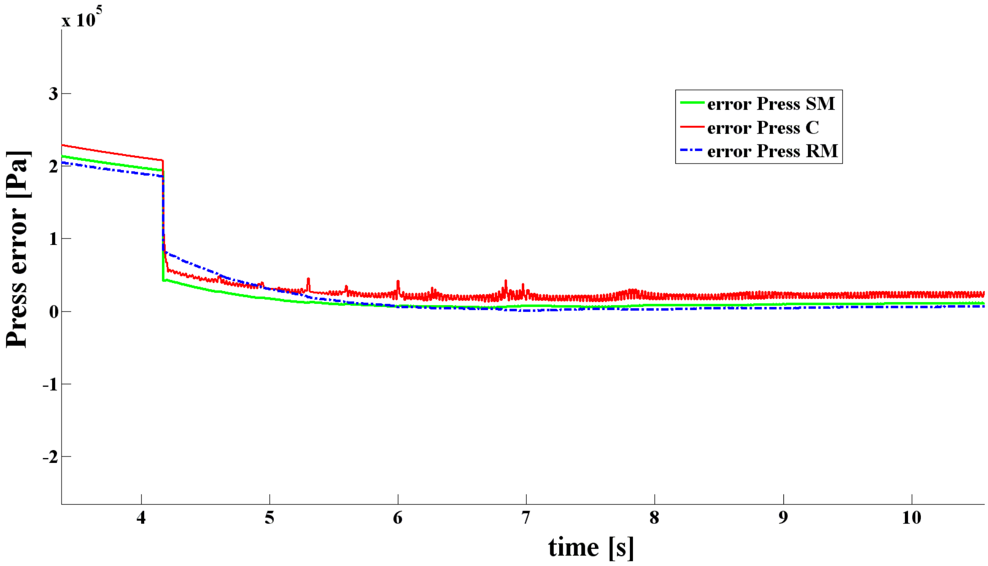

Figure 5.17: Pressure estimation error of the oxygen supply of the PEMFC

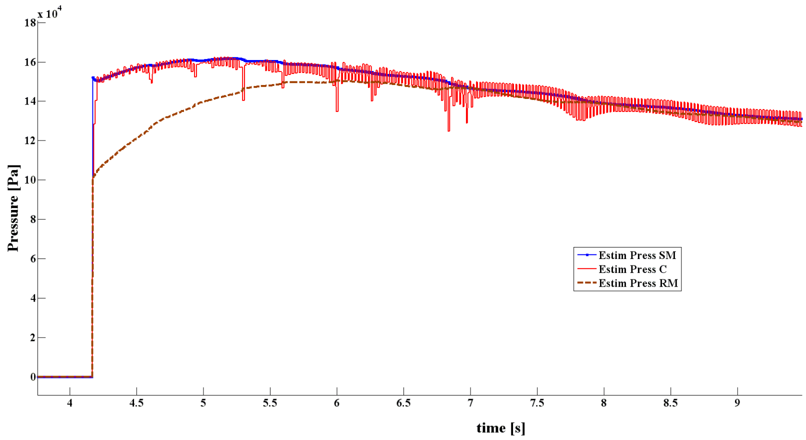

Figure 5.18: Real time observer values for the pressures of the oxygen supply of the PEMFC

5.4 Fuel Cell diagnosis

In this section we will focus on the Diagnostic process for fuel cells. In the Introductory chapter we have presented the state of the art related directly to observer based diagnosis in order to show the motivation for our work. Here we will first present the Fault process in general for fuel cells, and afterward we will briefly detail other existing approaches for FD. Therefore we will start by talking about Knowledge based methods that dominate the research field, and after we will detail in short alternative model based techniques.

5.4.1 Fault trees analysis of FCS

Figure 5.19 shows the faults tree schematic of a part of the FCS. In our case, we have not taken account of faults of battery, converters, storage, etc.. There are three classes of failure at high level for the global system: failure of hydrogen circuit, compressor failure and failure of fuel cell stack. In each class,several types of faults were shown at the second level and causes of failures at the third level in figure 5.19. From this fault tree, we can see that the hydrogen circuit is sensitive to leak faults of hydrogen and capping. Two possible failures can affect the compressor on the mechanical and electrical part. In addition, there is also a failure of the controller which controls the energy demand from the process and a hydraulic failure due to the reduction of the effect of compressibility. Inside the FC, it is shown that the distribution of water in the channel of the membrane may cause drying or flooding. In addition to water generated by the electrochemical reaction, the temperature of the fuel cell can affect drying and flooding faults. Because of the existence of parasitic reaction, it is possible to detect contamination of the feed gas by N2, CO or CO2 especially in stack systems that use hydrogen produced from a fuel reformer or for systems operating in an environment polluted.

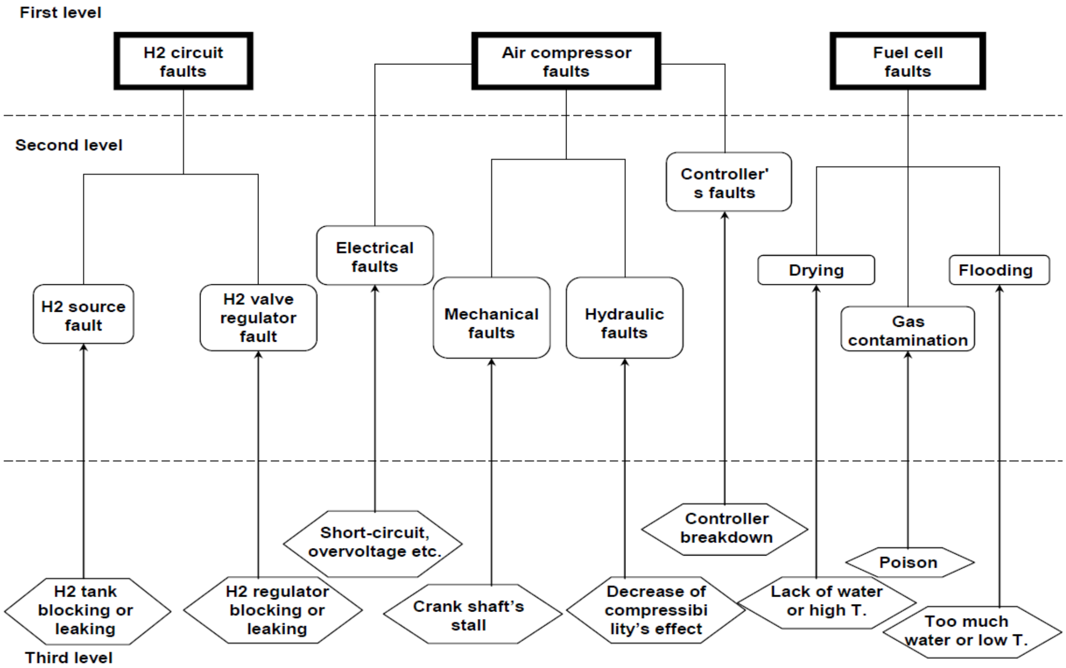

Figure 5.19: Fault trees of Fuel Cell Stack System

5.4.2 Knowledge based approaches for FCS

5.4.2.1 *Diagnostic by Signal Processing Approach*

Acoustic emission (AE) technique for real time survey of the evolution of the hydration state of the membrane in PEMFCs has been used by Legros et al Legros et al. (2009). The aim of this study is to determine if the phenomena linked to water management (hydration, dehydration, flooding) are acoustically active, and if this AE activity is significant. Reference Stumper et al. (2005) presented a novel diagnostic test method which allows the determination of the distribution of water in the membrane across the active area by the combination of galvanostatic discharge with current mapping. In Teranishi et al. (2006), liquid water distribution in the flow field of fuel cell was obtained by using magnetic resonance imaging. A method based on images by neutron radiography is used by Pekula et al. (2005). Partial flooding is detected in the fuel cell with help of visualization of the liquid water inside the flow channel and gas diffusion media in real operating conditions. Authors in Kramer et al. (2005) developed a similar methodology used by Pekula et al. (2005) to detect drying and flooding. This technique is powerful but requirement of a neutron source with a high fluence rate limits its wide application. Other techniques can be used as optical diagnostics used in many research works in order to delineate the origin and development of flooding with high spatial and temporal resolution.

5.4.2.2 *Diagnostic by Artificial Intelligence Approach*

The AI approach does not require a model of the system, generally looking at a system from an input-output perspective, as a black box. In Nitsche et al. (2004), an approach using artificial neural networks to alleviate the task of on-board diagnostic for FC vehicles was presented. As one example of AI based methods used, expert systems are applied by Liu and Wang (2003) dealing with the detection and diagnosis of faults when they develop in different parts of a PEMFC system. In this paper, the diagnosis algorithm is based on a basic model utilizing on-line expert systems. Fuzzy logic which needs a fuzzy model is one of the predominant approaches used in AI. In Hissel et al. (2004), a diagnosis-oriented model in Sugeno type of a FC power generator dedicated to automotive applications is proposed. A genetic algorithm was used for tuning of the fuzzy diagnosis model. Through this method, the accumulation of water and nitrogen in the anode compartment in case of a dead-end mode use of the FC was diagnosed as well as the drying of the proton exchange membrane localized by the configuration of threshold.

5.4.2.3 *Diagnostic by Experimental Approach*

Experimental diagnostic approaches for FCS have already become mature and systematic. Most of these approaches are based on physicochemical phenomena inside the FC. References WU et al. (2008a), WU et al. (2008b) provides a review of diagnostic methods using experimental measurements. In WU et al. (2008a), electrochemical techniques such as the polarization curve, current interruption, and Electrochemical Impedance Spectroscopy (EIS) are presented. EIS consists in applying a very small amplitude signal (current) over a wide range of frequency and to register the response. The ratio of the variation voltage and current gives the magnitude of the impedance and the phase shift. Based on the published papers, the majority of AC impedance studies of PEMFC cells involve in situ measurements because they offer the most pertinent data on PEMFC. In WU et al. (2008b), several physical/chemical methods are presented for PEMFC diagnostic: Pressure drop measurement, Gas chromatography. In that case, the permeating of reactant gas can be detected. In Liu et al. (2005), the authors used dependence between current density and formation of water in FC to analyze the effect on the fuel cell's performance. Other approaches for the diagnostic of FC use characterization of electric components based on spectrometric impedance Brunetto et al. (2004). Even if this methodology provides good results for the detection of flooding in FC, its implementation is still complex and costly. Therefore, a method using a simpler instrumentation was proposed by Barbir et al. Barbir et al. (2005). They use load losses measurements in the stack as a diagnostic tool to detect flooding. Ref. Yuan et al. (2007) studied the 500W Ballard Mark V PEMFC stack with electrical impedance spectroscopy for diagnostic problem. The developed method is based on effect analysis of temperature, flow rate, and humidity on the stack impedance spectra. In the second part of this paper, individual cells of the same fuel cell stack were studied with AC impedance approach. Two methods were utilized for measuring the impedance spectroscopy of the individual cells. The results demonstrate that the AC impedance method is a sensitive technique for detection of the degree of membrane hydration which could be an indicator for flooding and drying in FCs. Voltage measurement is one of the most interesting method as it appears to be the only variable allowing a measurement at the cell level while still being non intrusive. In Hissel et al. (2004), the diagnostic solely depends on the processing of steady-state current/voltage data. This proves to be efficient as far as fault detection is concerned, but leads to an indetermination when it comes to fault isolation since flooding and drying out both cause a voltage drop. Thus, when considering a FC in a given state with no available history, fault isolation is impossible.

Besides of AC impedance approach, the pressure drop can also be as diagnostic tool for FCS. The measure of the differential pressure drop between the inlet and outlet of gas channel could be used in order to diagnose liquid water accumulation Chen and Zhou (2008), Ito et al. (2008), Hsieh et al. (2011). Barbir et al. (2005) also conducted preliminary studies on pressure drop as a diagnostic based on physic-tool for water flooding in PEMFC. A plot of cell potential against current density under a set of constant operating conditions, known as a polarization curve, is the standard electrochemical technique for characterizing the performance of FC. Therefore, failures can be detected and isolated from that information. A non-steady state polarization curve was obtained using a rapid current sweep in Lim and Haas (2006). Any changes of parameters such flow rate, temperature, and relative humidity could become diagnostic signals for water state management. An appropriate humidity Hyun and Kim (2004) can also prevent irreversible degradation of internal composition such as the catalyst or the membrane. A good indicator of the humidification state is the membrane resistance Yuan et al. (2006) that can be obtained by measuring the voltage and the current variations in high frequency. Hinaje et al. (2009) proposes a method for checking the humidification state of the membrane by exploiting the connection of a boost converter to the fuel cell. One of the most important advantages of experimental diagnostic approaches consists in detailing deep insight into the mechanisms that cause performance losses and spatial non uniform distribution. Therefore, experimental approaches are in situ diagnostic tools thus bad suited for online FDD. Most of the experimental approaches can only be realized in off-line conditions. Isolation performances depend on deep expertise or pattern recognition and learning of normal and faulty operating modes. To minimize the drawback of experimental method, in Fouquet et al. (2006), is showed how a model-based approach coupled with EIS measurements could help identify a set of parameters exhibiting a much greater sensitivity and selectivity to flooding and drying than the voltage does.

5.4.3 Model based approaches for FCS

As developed before, the isolation performances of model based methods do not need historical data in normal and in abnormal situations, thus every fault mode has to be represented. In many real processes, especially for FCS, realization of such modes experimentally are hard to be envisaged. This is why FDD model based approaches can be an alternative. The principle of Model Based Diagnosis (MBD) consists in checking the consistency of observed behavior with analytical model in fault detection phase while isolating the component that is in fault isolation phase. Generally, two parts (residual generation and residual evaluation) can be contained in the model based diagnosis. The purpose of the residual generator is to generate the residual signals and the purpose of the residual evaluator is to evaluate the residuals and generate a fault decision (Gertler (1998), Patton et al. (2000)). All of MBD diagnostic approaches can generally be regrouped into four classes: analytical redundancy relation (ARR) or parity space, observers and parameter identification and stochastic approaches . In consulted literature, few papers deal with model based FDI for Fuel Cell stack systems, just in the recent years their number increased.

5.4.3.1 *Diagnostic by ARRs*

Material redundancy (use of several sensors which measure the same variable) is widely used in industry, but this method allows detecting only sensor fault and is costly. Analytical Redundancy Relation (ARR) is an equation that is deduced from analytical model which use solely known variables (measured). ARRs must be consistent in absence of faults with physical operating modes. It utilizes the information embodied in the mathematical model of a system for fault detection and isolation. The actual behavior of the system is compared to that expected on the basis of the model; deviations are indications of faults (or disturbances, noise or modeling errors). The parity equation method is the direct implementation of the analytical redundancy concept.

In Yang et al. (2008), a fault diagnosis and accommodation system with a hybrid model for fuel cell power plant was presented. Faults in this paper were diagnosed by using analytical redundancy method, where the actual plant was compared with a neural network augmented nominal model, which served as a reference on how the state and output variables should behave in normal situations. The ARRs in the fault detection are sometimes given as form of test quantities. In Ingimundarson et al. (2005), two hydrogen leakage test quantities were presented and compared. These two test quantities were created by the model for the anode based on mass balances. Traditionally, the residuals deduced from ARRs are static and sensible to faults to be detected. Recently, a new model based FDD methodology based on the relative fault sensitivity has been presented and tested in Escobet et al. (2009). The innovation of this methodology is based on the characterization of the relative residual fault sensitivity. Recently, Aitouche et al. (2011) presented a FDI of PEMFCS based on nonlinear ARRs. Residuals are generated by an extended parity space approach in order to detect and isolate the input voltage drop of compressor, over current of FC, pressure drop in supply manifold and pressure in the return manifold.

5.4.3.2 *Diagnostic by Parameter identification*

The parameter identification method for FDD design consists in comparing identified or estimated parameters of the FC system with observed ones. In Forrai et al. (2005), some parameter estimation methods for a PEM fuel cell based on current interrupt test and a system identification approach have been presented. Because of the association between major losses (activation and ohmic) and flooding or drying faults, the detection and isolation of these faults could be done through the parameter identification of voltage variation caused by major losses. However, there are few papers for FC diagnosis based on parameter identification approach

5.4.3.3 *Diagnostic by Stochastic Approach*

For stochastic diagnostic approaches, the residual signals are random processes whose statistic analysis can sometimes be difficult. Therefore, databases which record the fault effects and probabilistic methods such as the Bayesian-Score and Markov Chain Monte Carlo (MCMC) with a graphical–probabilistic structure are needed. In Riascos et al. (2007), four types of faults in PEMFCs are considered. The diagnosis is executed at a specific moment, only if abnormal evolution of any variable is monitored; the idea is to associate this evolution with symptoms of incipient faults. The Bayesian-Score K2 and MCMC algorithms were implemented for the construction of a network structure which defines the cause-effect relationship among the variables. While these two probabilistic methods capture the numerical dependence among these variables. In Riascos et al. (2008), the algorithm is was applied on line in order to detect faults. Another stochastic diagnosis for fuel cell system was presented in Hernandez et al. (2006). By using cell voltage probability density functions as clustering parameter, different working conditions including several induced failure modes are characterized. From this characterization, normal operation and failure zones are defined either by arbitrary selection of a given region or by natural clustering of experimental results.

5.4.3.4 *Structural analysis for Fuel Cells*

The challenges for FDD in fuel cells consist in that the model is of a high complexity, in it occurring several kind of processes (electrical, mechanical, electro-chemical, etc) and the numerical values are not always known. This is why structural model (based on existence or not of the links between variables and the relations) is well suited. The basic tool for structural analysis is based on the concept of matching on a bipartite graph Blanke et al. (2006). Few works deal with structural analysis applied to fuel cell systems. In Yang et al. (2009), it is shown how the structural monitorability (ability to detect and isolate faults) and the fault signatures can be deduced directly from FCSS multi-energy bond graph model with no need for any numerical calculation. Therefore, before industrial design, an optimal sensor placement to provide which faults can be detected and or isolated and how to make them monitorable can be proposed. The structural monitorability show that drying, flooding, contamination by gas pipe, compressor faults and some sensor faults (velocity, current, air mass flow) are detectable and isolable. To isolate other faults, it is necessary to add sensors, i.e., for hydrogen leakage. The efficiency of the structural methods depends mainly on the model's accuracy and has to be validated experimentally.

5.4.3.5 *Diagnostic by Observers*

Finally we encounter the observer based approaches, the object of our work, and presented in the introductory chapter. We will now develop further on the idea of FD in fuel cells using Takagi Sugeno methods.

5.4.4 Takagi-Sugeno PI observer for the FCS

The fault tree analysis by means of RRA has been done in a previous work in the laboratory (Aitouche et al. (2011)), therefore here this aspect is neglected. Also we will focus on only a particular fault case described further in the text. We thus consider a sensor fault and we will develop a PI observer as described before in order to estimate some of the system parameters and also to estimate the fault. The estimation of the fault being very useful in order to properly respond to the fault, or even if it is the case to construct Fault Tolerant control methods.

The FC system on which we apply the algorithm is the gaseous model, where the system states are respectively, the supply manifold gaseous mass, the cathode gaseous mass, the return manifold gaseous mass, the supply manifold pressure, the cathode pressure, the return manifold pressure: $x = \begin{bmatrix} m_{sm} & m_{cs} & m_{rm} & p_{sm} & p_{cs} & p_{rm} \end{bmatrix}^T$.

We have considered as unmeasured parameter (therefore parameter to be estimated) the mass in the cathode. The sensor fault acts upon the

Supply manifold sensor. This choice is made, as the Supply manifold pressure propagates to the cathode as well as the Return manifold. The fault starts at 5 seconds in the simulation and lasts for 10 seconds. The fault is presented in 5.20. One can see the fault amplitude is significant. This function has a bounded second derivative.

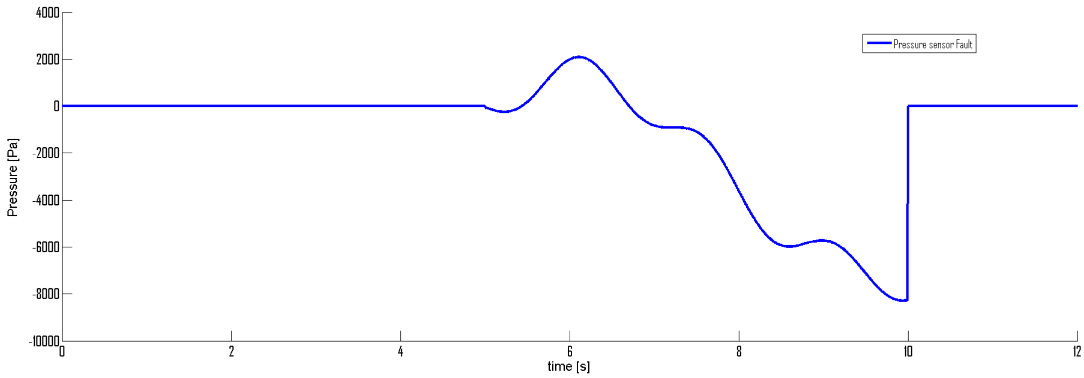

Figure 5.20: Fault in Supply Manifold Pressure Sensor

We present the estimation of the fault in parallel to the real fault, in figure 5.21. The estimation presents a small delay in estimation, but an overall good behavior. The delay may be caused by the dynamics of the observer. The minimization of the L_2 norm in the construction of the observer will increase the precision of the response, but will reduce the dynamics. The response is to be expected considering that we have made also suppositions of boundedness, thus a small estimation error is predicted.

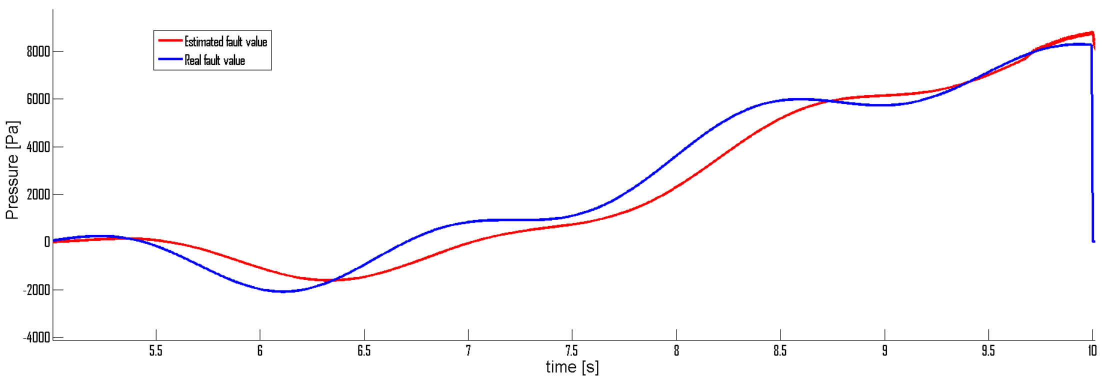

Figure 5.21: Fault estim/real in the Supply Manifold pressure sensor

Finally we show the estimation of the Cathode mass in 5.22. Even if we also estimate the fault, the estimation of the mass is good. We see some perturbation when the fault occurs between seconds 5 and 10 but with a minimal error (a zoom is shown in 5.23).

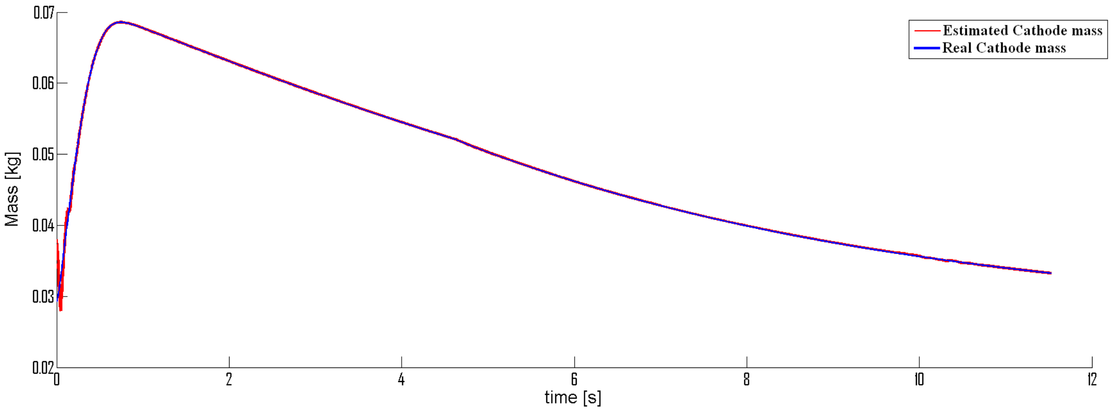

Figure 5.22: Cathode mass estimation

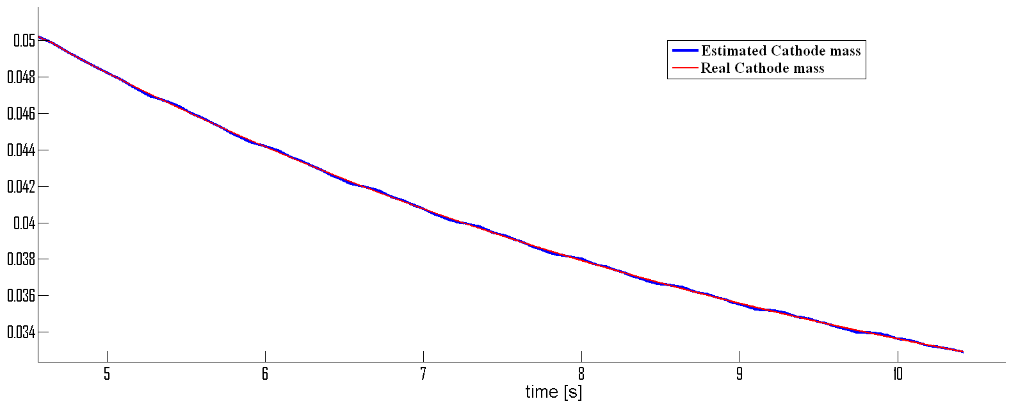

Figure 5.23: Cathode mass estimation

5.4.5 Advanced Takagi-Sugeno PI observer applied to FCS

As in the previous case, the fault considered is only a sensor fault. The estimation of the fault being very useful in order to properly respond to the fault, or even if it is the case to construct Fault Tolerant control methods. The estimation of some system states is also done in parallel to the fault estimation.

The FC system on which we apply the algorithm is the gaseous model, where the system states are respectively, the supply manifold gaseous mass, the cathode gaseous mass, the return manifold gaseous mass, the supply manifold pressure, the cathode pressure, the return manifold pressure: $x = \left[\begin{array}{cccccc} m_{sm} & m_{cs} & m_{rm} & p_{sm} & p_{cs} & p_{rm} \end{array}\right]^T$.

We have considered as unmeasured parameters (therefore parameters to be estimated), the Mass and Pressure in the cathode. The sensor fault acts upon the Supply manifold sensor (fault to be estimated).

The additive fault in the supply manifold pressure sensor is considered to be of a polynomial form having a degree of 2: $2{\cdot}10^4(-3.954392409(t-0.5)^2 + 15.77609428(t-0.5) - 14.69162381)$. To this, a bounded perturbation is superimposed (more precisely the bounded 3rd derivative of the polynomial). The value of this last derivative of the fault is presented in figure 5.24. The fault acts from second 2 for an interval of 1 second.

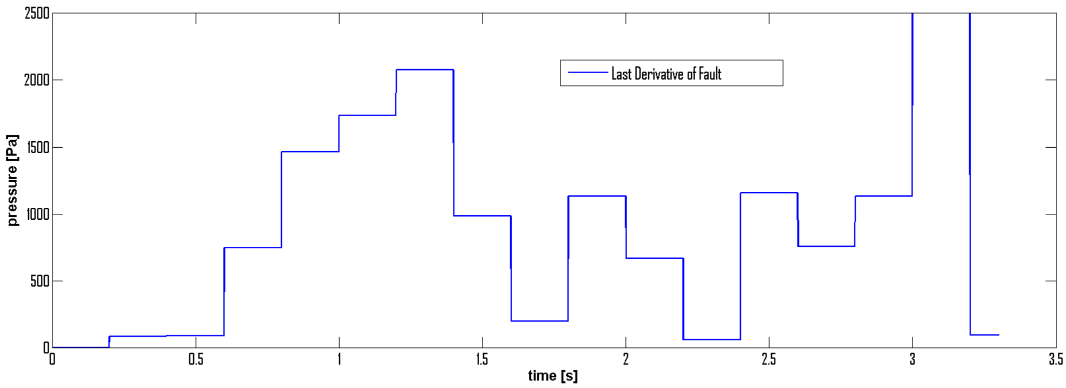

Figure 5.24: The 3 rd derivative of the fault

Thus, the entire fault is clear in figure 5.25, alongside with the estimation of the fault. Here the previous noise can be clearly seen acting at seconds 2.2s, 2.4s, 2.6s and 2.8s. The estimation shows a good performance even when this noise has a high value. The effect of the fault on the pressure sensor is clearly visible in the figure 5.26. The fault visibly affects the measurement between seconds 2s and 3s. Even the perturbation is obvious at seconds 2.2s and 2.4s. A zoom on the faulty interval is shown in figure 5.27.

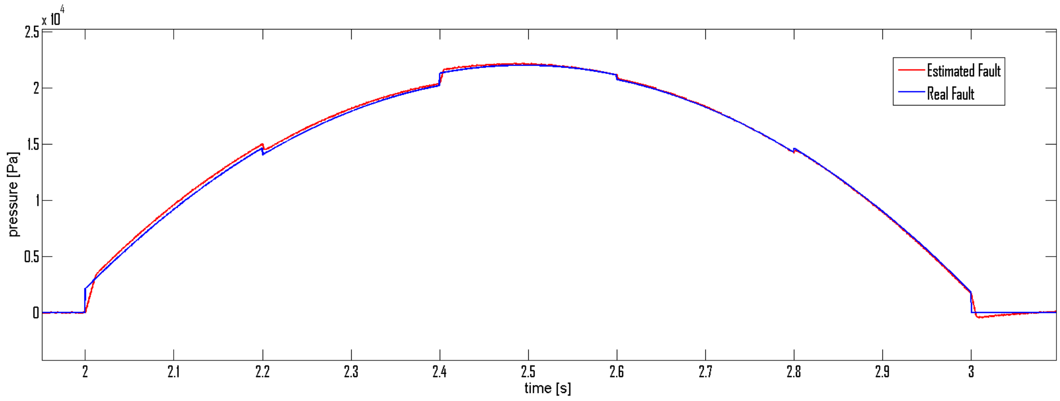

Figure 5.25: Real and estimated fault acting on the SM pressure

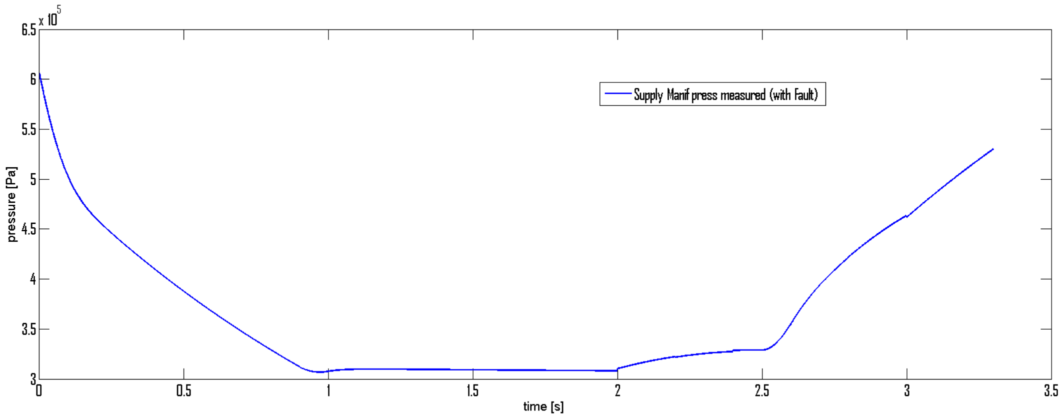

Figure 5.26: SM pressure affected by the fault

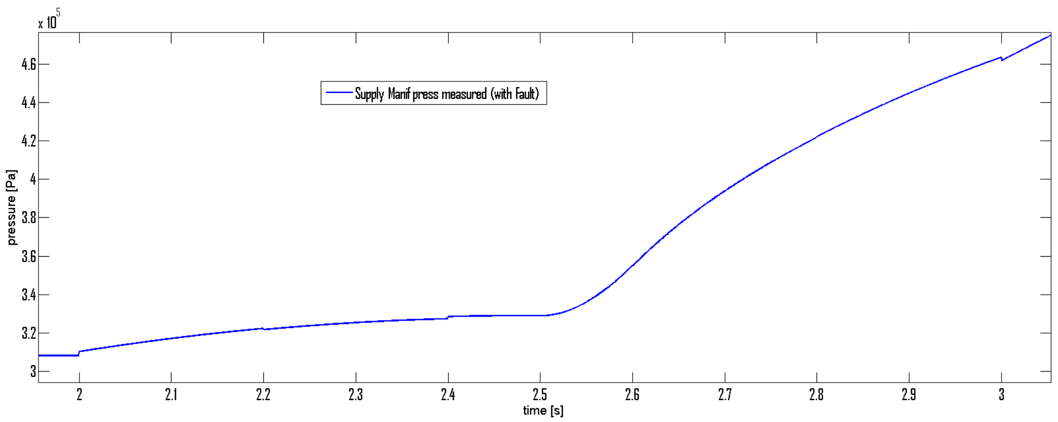

Figure 5.27: SM pressure affected by the fault

Concerning the estimation of the states describing the amplitude of the cathode mass and cathode pressure, these are shown in, respectively, figure 5.28 and figure 5.29. Here, the estimation errors are presented.

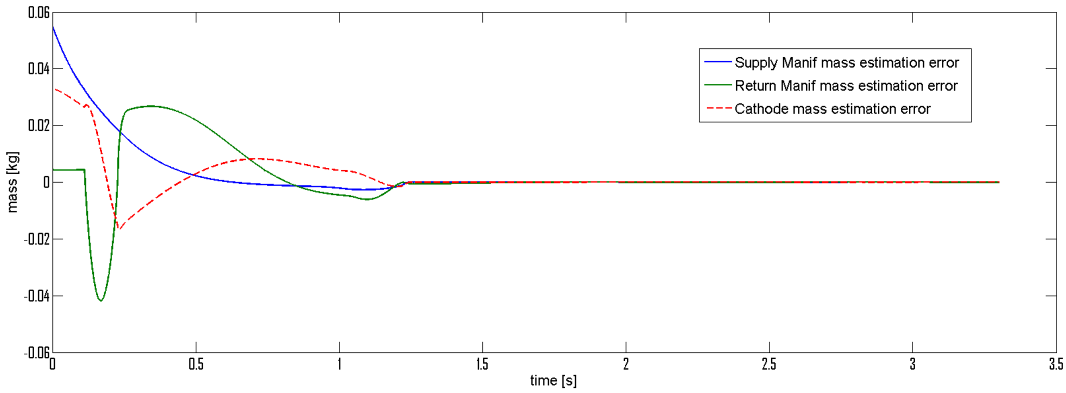

Figure 5.28: Cathode side mass estimation error dynamics

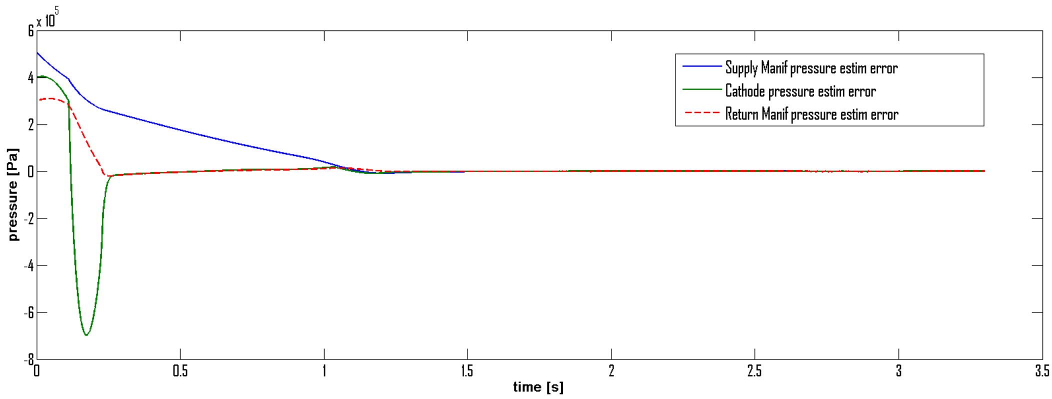

Figure 5.29: Cathode side pressure estimation error dynamics

These estimation errors reflect the evolution of the masses and pressures that have the dynamics shown in figure 5.30 and figure 5.31.

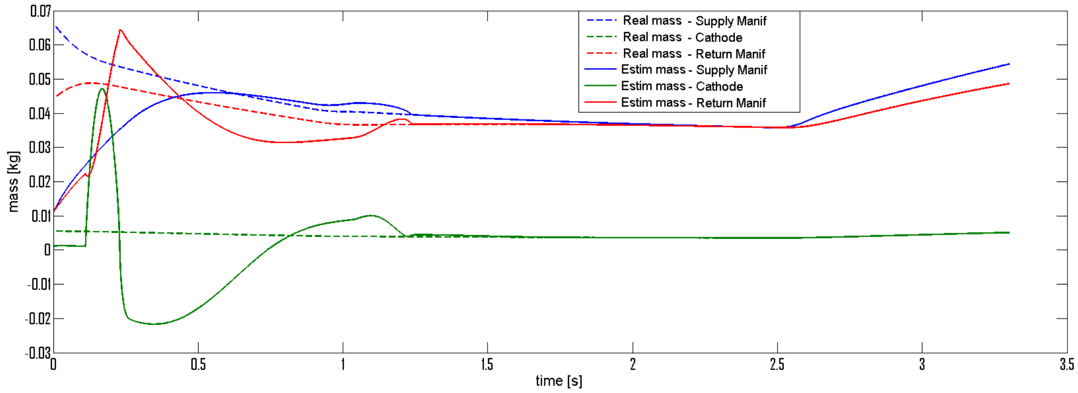

Figure 5.30: Cathode side mass estimated / real

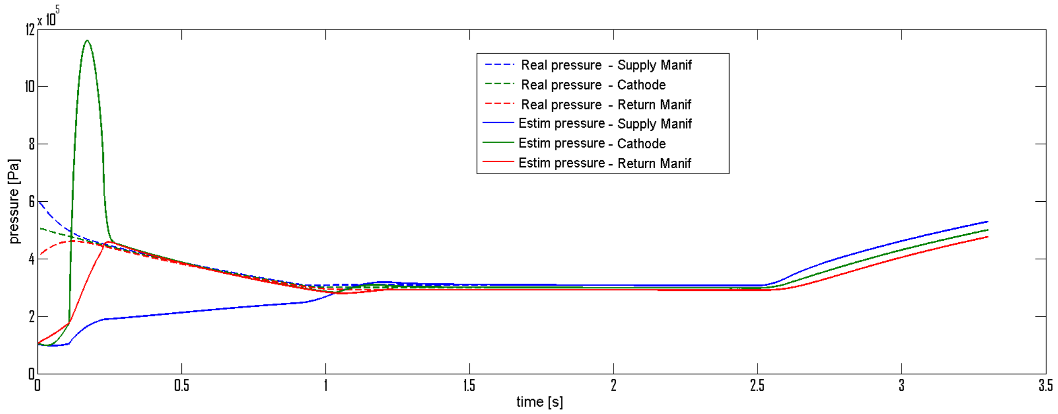

Figure 5.31: Cathode side pressure estimated / real

It has been considered that the observer's initial pressures start at atmospheric values. In order to implement numerically the LMI, one has to find best values for the LMI matrices and variables. For example, the α value, has to be experimentally and manually chosen so that a balance between response time and overshoot is attained (the value at which we settled was 0.07). More precisely, looking at figure 5.31, the cathode pressure estimation has an overshoot that will increase even further if the α coefficient that controls the exponential character of the stability, is further reduced. On the other hand, if this coefficient is bigger, the overshoot reduces but the estimation time increases. Also one has to take into consideration, that when the imposed response performances become stricter, the resulted behavior will act on another interval for the z variables (premise variables - or the nonlinear terms) because the nonlinearity may increase.

By the same logic, conditions have to be imposed also on other parameters of the optimization, as the matrices P or R. We have settled for $R < 2$ and $P > 0.15$ (these notations signifying that the eigenvalues are respectively smaller than 2 and bigger than 0.15).

Concerning the auxiliary compensation terms that are present in this method, they act as sliding terms, thus producing significant chattering if the observer is not well configured or the sampling time is too low, this has to be resolved apriori, otherwise the observer may exit the estimated sector of values for the nonlinearities. Therefore these terms may induce some instantaneous high/low values for the nonlinear terms, thus the $z_{Max} and z_{min}$ have to be chosen appropriately.

The last observation that we will make is that the optimization results (for solving the LMIs) differ according to the solver, in this case the Matlab 'lmilab' solver being chosen.

5.5 Conclusions

In this chapter, we have developed a set of observers (based on the Takagi Sugeno method as well as the Mean value based theorem) for determining parameters inside a PEM Fuel Cell which is able to estimate the pressures and mass flow rates. The chapter also shows the potential of Takagi-Sugeno modeling to be applied on small scale processing units for observers, achieving good sampling time and real-time constraints. Thus, such solution can be embedded on mobile devices supplied by a FC system, as a vehicle for example, being more economically viable than the usual ECU.

The real-time interface between AMESim, Matlab/Simulink and an Arduino connected by Ethernet that we developed represents a proper way to test any FC related embedded system and ensures that the observers behave as intended before using them on a real system. Using this connection allows to test any possible loss in the communication and design of the observer.

In this context, as the gaseous medium is of a faster dynamic than mechanical processes, this proves the potential of the embedded approach in strenuous numerical constraints. Despite the memory restriction, the calculations remain fast and the limiting factor for real-time can be improved by parallel calculus as T-S is well adapted for it. Also this model contains two interesting aspects: the high number of states and nonlinearities and also the high difference in magnitude of the parameters implied in the model (Pressures vary around 10^5 and Masses vary around 10^{-3}); this brings a generality to the estimation method so that it can be extended to a model of a higher degree of complexity.

The last PI observer, although it shows good results, comes with the requirement of faster processing power, as the sampling time is smaller than that of a normal observer because of the sliding terms.

Chapter 6

Conclusions and Perspectives

6.1 Conclusions 153

6.2 Perspectives 155

B.1 **The test bench** 163

B.2 **Performing the tests** 165

B.3 **Analysis of tests** 165

B.3.1 *General results* 166

B.3.2 *Influence of the temperature on the electrical power* 166

B.3.3 *Influence of the hydrogen supply pressure* 166

B.3.4 *Influence of the air excess* 168

B.3.5 *Program development* 169

6.1 Conclusions

The thesis analyzes observer and diagnosis design methods for PEM fuel cells using Takagi-Sugeno theory. The main aim of the research is to develop observers for estimation and diagnosis of embedded fuel cells, operating in the framework of the European project i-MOCCA (PN-7-022-BE, Inter-regional Mobility and Competence Centres in Automation) being funded by INTERREG IV A 2 seas Programme and the Ministry of Education and Research, France.

The mass flow rates of reactant gases (air, oxygen and hydrogen mass flow rates in the inlet and return manifold) play an important role in the reliable and efficient operation of Fuel Cell System (FCS). Their precise and exact estimation is necessary and important for maintenance of chemical reactions in the cathode and anode chambers. The Takagi-Sugeno techniques are employed for the design of observer to estimate those variables. The simulation results show robustness and fast convergence of observer estimates to nominal values. The observers can replace the mass flow sensors which results in getting rid of expensive and hard to install instrumentation for measurement of mass flow rates.

Fuel Cell System emerged in the recent years as the next potential power source as supported by many research documents and journals. In the introduction, a literature review regarding the problem of estimation and diagnosis of FCS has been identified.

There are three research objectives in this thesis. The first focuses upon modeling, estimation and diagnostics in a nonlinear framework using a Takagi-Sugeno approach. The dynamic nonlinear model of PEMFCs is proposed, which considers the auxiliary components and therefore is more accurate. In terms of estimation approach for PEMFCs, a nonlinear approach is developed to design observer based on the nonlinear TS model in order to achieve more robust estimation. By using this estimation to develop algorithms for diagnosis, the fuel cell stack life can be prolonged and can be protected. The second topic on embedding nonlinear algorithms, acts upon the potential of using small scaled embedded systems for complex tasks, thus reducing cost and physical size of the automatic system. More precisely the use of the Takagi-Sugeno approach in embedded applications is researched. In the Fuel Cell context, embedded FC systems are promising energy sources for portable applications, particularly in transportation. Solutions of embedded observers have been provided and show the effectiveness of our approach. The last topic works upon the development of a testing and validation procedure for the embedded algorithms applied to the FCS, in a Hardware In the Loop architecture, based on the professional software AMESim.

The conditions for meeting the stability and robustness criteria for the observers, have been formulated into systems of LMIs. The number of LMIs involved is reduced as much as possible. The proposed algorithm combines different merits:

- The stability and robustness analysis for the Fuel Cell throughout this thesis is based on the TS fuzzy plant model.
- The observer gains are obtained by solving simple optimization problems presented as LMIs.
- The capability for dealing with disturbances is taken into account.
- The analysis results and design methodologies of the robust observers presented in this thesis have been extended to plants with the premise variables unmeasurable.
- Increased robustness over conventional observers is aimed, by means of PI Observers.
- The interesting aspect of estimating the fault as well as some states is investigated.
- Embedded algorithms have been implemented and a HIL validation procedure is analyzed.

6.2 Perspectives

Based on this work, many perspectives can be envisioned, as for example one can improve by trying different fuel cell models, that affect other aspects of the FC system, either related to water content, to fuel intake, to temperature or to the electrical part.

Also concerning the Embedding of nonlinear algorithms, incipient work has been done with testing other microcontrollers and also ARM processor based microprocessors (to ease the effort there exists electronic development boards that include all the auxiliary hardware components as the Arduino Tre). Also other types of algorithms can be tested, for example treating TS fault estimation using more advanced sliding mode methods.

These embedded algorithms can also be tested in a more in depth way for a better evaluation. One aspect that was envisioned during the thesis as a perspective was to try FPGAs (Field-Programmable Gate Arrays) solutions as well or hybrid microcontroller-FPGAs solutions, thus the parallel distribution of code can be optimized even further for the Takagi-Sugeno code. Of course validating the potential of distributed calculus in TS solutions can be first tested on a stationary numerical system as an ordinary desktop computer, by using the CUDA (Compute Unified Device Architecture) architecture of regular NVIDIA graphical processing cores.

Concerning the TS algorithms, reduction of conservativeness of solutions is imperative. For example many researchers concentrate on non-quadratic Lyapunov functions, yet these are still limited to certain types of systems, or like the integral Lyapunov functions that can be applied only if the system is path independent. Some solutions that can develop further from the thesis is the solution used for the dynamical TS observer, that leaves place for improvement, at the same time showing a high potential. Also diagnostic techniques based on Sliding Mode TS need to be further developed.

Appendices

Appendix A

Significance of Fuel Cell parameters

The significance of parameters that appear in the FC model are presented in the following three figures:

		Variable	Description
η_{cp}	Compressor efficiency	Ra	Gas constant (J/mol.K)
$C_{D,rm}$	Discharge coefficient nozzle		
p_{sm}	Pressure supply manifold (Pa)	R	Gas constant (J/kg.K)
p_{rm}	Pressure return manifold (Pa)	T_{atm}	Air temperature (K)
w_{cp}	Compressor speed (rad/s)	T_{rm}	Temperature return manifold(K)
I_{st}	Current in the stack (A)	$T_{cp,out}$	Ai outputted temperature (K)
T_{st}	Temperature in the stack (K)	P_{atm}	Air pressure (Pa)
γ	specific heat capacity of gas		

Figure A.1: List 1 of Fuel Cell Parameters

		Variable	Description
V_{ca}	Cathode volume (m^3)	C_p	Specific heat capacity of air (J/kg.K)
V_{an}	Anode volume (m^3)	F	Faraday number
V_{rm}	Return manifold volume (m^3)	M_{02}	Molar masse of Oxygen (kg/mol)
V_{sm}	Supply manifold volume (m^3)	M_{H2}	Molar masse of Hydrogen(kg/mol)
W_{cp}	Compressor mass flow (kg/s)	$k_{sm,out}$	Supply manifold outlet flow constant (kg/s.Pa)
η_{cp}	Compressor efficiency	$k_{rm,out}$	Return manifold outlet flow constant (kg/s.Pa)
τ_{cm}, τ_{cp}	Torques of motor and compressor (N.m)	$A_{T,rm}$	Return manifold nozzle area (m^2)

Figure A.2: List 2 of Fuel Cell Parameters

Notations of constants employed in this paper are shown in A.1.

		Variable	Description
R_v	Vapor gas constant	R_{H_2}	Hydrogen gas constant
R_{O_2}	Oxygen gas constant	$C_{d,an}$	Hydrogen purge nozzle discharge coefficient
M_v	Molar mass of vapor	$W_{sm,out}$	Mass flow exiting the supply manifold[kg/s]
k_{term}	Constants representing the linearization coefficient describing a valve[kg/(s*Pa)]	$W_{ca,out}$	Mass flow exiting the cathode[kg/s]
$W_{rm,out}$	Mass flow exiting the return manifold[kg/s]	$W_{O_2,ca,in}$	Mass flow of oxygen entering the cathode[kg/s]
$W_{H_2,reacted}$	Mass flow of oxygen reacted inside the anode[kg/s]	$\bar{R}$	Universal gas constant
$W_{O_2,reacted}$	Mass flow of oxygen in the cathode that reacts with the electrons and ions to form vapor	$W_{v,ca,gen}$	Mass flow of generated water inside the cathode

Figure A.3: List 3 of Fuel Cell Parameters

$$
\begin{aligned}
cst6 &= \frac{A_{an} C_{d,an} \sqrt{\gamma} \left(\frac{2}{\gamma+1}\right)^{\frac{\gamma+1}{2\cdot(\gamma-1)}}}{\sqrt{\bar{R}\cdot T_{atm}}} \\
cst5 &= \frac{K K_1 R_{H_2} T_{st}}{V_{an}} \\
cst4 &= \frac{M_v}{M_{O_2}} \\
cst3 &= \frac{R_a \cdot T_{st}}{V_{rm}} \\
cst2 &= \frac{R_{O_2} \cdot T_{st}}{V_{ca}} \\
cst1 &= \frac{R_v \cdot T_{st}}{V_{ca}}
\end{aligned}
\tag{A.1}
$$

The concrete values that were chosen for the FC parameters are presented in the table (A).

Table A.1: Parameter values of the FC

Symbol	Value	Symbol	Value
γ	1.4	A_{Tc}	600 mm^2
R_a	259.8 $\frac{J}{kg.K}$	A_{Trm}	600 mm^2
C_{Dsm}	0.2	V_{sm}	20 L
A_{Tsm}	550 mm^2	V_c	1 L
V_{sm}	20 L	V_{rm}	20 L
C_{Dsm}	0.2	$T_{sm_{in}}$	353.15 K
C_{Dc}	0.2	$P_{sm_{in}}$	5 bar
C_{Drm}	0.075	$T_{rm_{out}}$	273.15 K
A_{Tsm}	550 mm^2	$P_{sm_{out}}$	1.013 bar

The constant notations for the Mean Value FC model is as follow:

$$
\begin{aligned}
f_{cst1} &= \frac{R_{O_2} T_{st}}{V_{ca}} \\
f_{cst2} &= k_{sm,out} \frac{R_{O_2} T_{st}}{V_{ca}} + k_{ca,out} \frac{R_{O_2} T_{st}}{V_{ca}} \\
f_{cst3} &= 0.0009225603 \cdot 2.1 \cdot 10^{-3} \\
f_{cst4} &= 2.4870103138421 \cdot 2.1 \cdot 10^{-3} \\
f_{cst5} &= \frac{\mathrm{R_{H2} T_{st}}}{\mathrm{V_{an}}} \cdot 2.1 \cdot 10^{-6} \\
f_{cst6} &= \frac{R_a T_{rm} k_{ca,out}}{V_{rm}} \\
f_{cst7} &= \frac{\gamma R_a}{V_{sm}} W_{cp} T_{atm} \\
f_{cst8} &= k_{sm,out} \frac{\gamma R_a}{R} \\
f_{cst9} &= \frac{k_{sm,out} R_{O_2} T_{st} \gamma R_a}{V_{ca} R} \\
f_{cst10} &= \frac{R_a T_{rm}}{V_{rm}} \frac{C_{D,rm}}{\sqrt{\bar{R} T_{rm}}} \left(\frac{2\gamma}{\gamma - 1} \right)^{\frac{1}{2}} p_{atm}^{\frac{1}{\gamma}} \\
f_{cst11} &= \frac{f_{cst7}}{\eta_{cp} \cdot p_{atm}^{\frac{\gamma-1}{\gamma}}}
\end{aligned}
\tag{A.2}
$$

Appendix B

Physical Fuel Cell platform

The Fuel Cell stack platform is a Heliocentris FC-42. Different tests were made on the platform, by changing the variables one at a time.

Figure B.1: Heliocentris FC-42 platform

The system consists of a hydrogen Fuel Cell that accepts air as secondary gaseous source, that includes a cooling a humidifying unit (both the temperature of the Fuel Cell and the humidity can be controlled). The values are read and set by a software already provided by the developer.

B.1 The test bench

The system is composed of the following:

Auxiliary components module

This module contains all auxiliary components like the compressor, humidifier, cooler and all the actuators. Here the pressures of hydrogen and oxygen are set. It receives the commands from the Command Module and it is directly connected to the DC load.

The controller

The controller unit is the unit that sets the values of the parameters for the platform and also the unit that communicates the parameter values to the computer.

The Fuel Cell

The Fuel cell is a 360W stack, protected to inverse current by integrated diodes.

The hydrogen tank

From all the types of hydrogen tanks, metal hydride based tanks were chosen, being easy to use, and with a high degree of safety, at the expense of lower energy per weight ratio if compared to direct hydrogen storage (in gas or liquid form). Two types of tanks are used, one smaller at 10 bars and another one bigger at 100 bars.

DC controllable load module

In order to simulate the consumer, a controllable DC load has been added to the system. It can receive references for either Current or Voltage or Power.

B.2 Performing the tests

In order to do the tests, the parameters have been varied one at a time. This being the only way to effectively test the Fuel Cell behavior. In our tests, we've tried to highlight the factors of inertia of the redox reaction of the FC, meaning the factors that affect the performance and the amount of generated electricity. These factors are two in number:

1. The temperature
2. The concentration of reactive components (hydrogen and air)

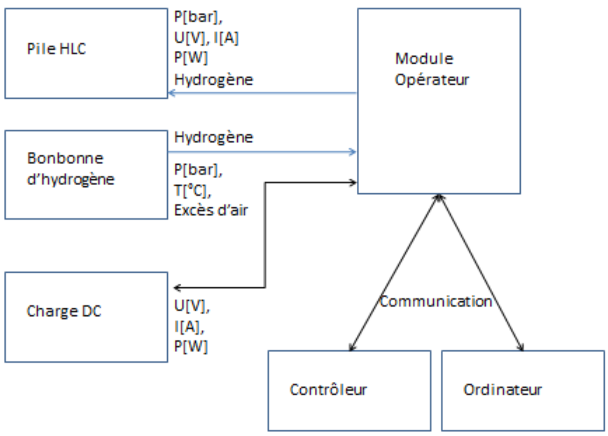

Figure B.2: Block view of the platform with characteristic parameters

B.3 Analysis of tests

There are different functioning modes for the Fuel cell. We were interested only in driving it based on the electrical load. The first test (test1), was done using the big hydrogen tank. The second one (test2), was realized with the small hydrogen tank, with a 10 bar initial pressure, showing a capacity lasting 30 minutes.

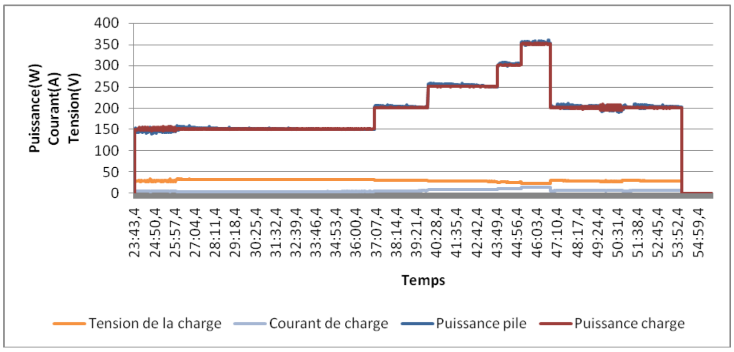

Figure B.3: (low capacity H2 tank) Time evolution of FC/load power, voltage and current

B.3.1 *General results*

The produced power follows very well the power demanded by the load. We can also observe the evolution of the current and voltage compared to the power dynamics.

B.3.2 *Influence of the temperature on the electrical power*

Initially, the FC starts at ambient temperature. During the warming up period, the current and voltage oscillate intensely around their reference values, stabilizing only after the warming up period ends, in around 12 minutes. The periodic sudden variations are due to the purge process that repeats with a specific frequency.

B.3.3 *Influence of the hydrogen supply pressure*

Maximum anode input pressure equals 344 mbar, minimum anode input pressure equals 331 mbar at the beginning of the simulation. The regular descent of the pressure is caused by the emptying of the Hydrogen tank, that lasts at around 30 minutes.

We can observe that the difference between the demanded power and the power obtained begins to increase once the input pressures reduces;

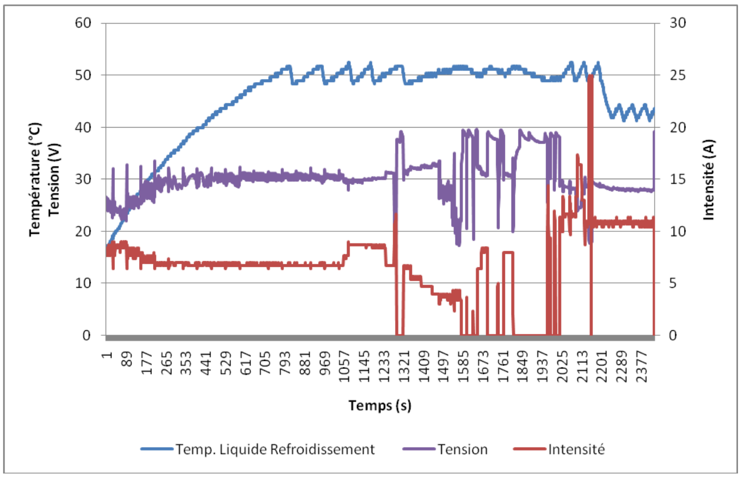

Figure B.4: (high capacity H2 tank) Voltage, temperature and current dynamics

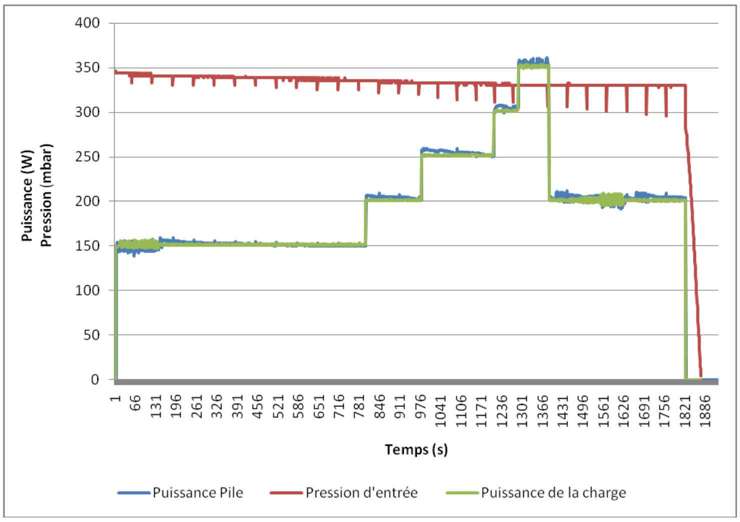

Figure B.5: (small H2 tank) Power and hydrogen Pressure

it is not a significant error, but it is visible especially in the interval 1366s-1821s.

Here we see even better the irregular, periodic points on the red Pressure (hydrogen input pressure) curve. These are the moments the fuel cell purges, happening at each 54 seconds.

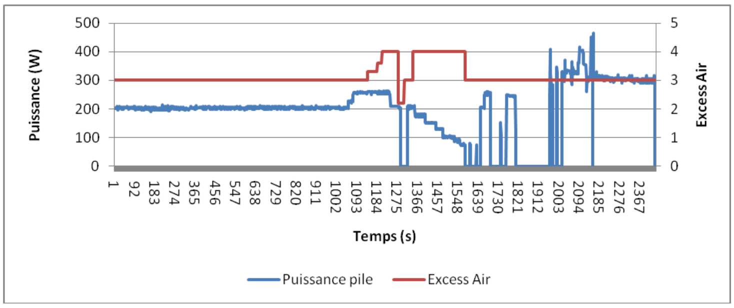

Figure B.6: (big H2 tank) FC power and air excess

B.3.4 *Influence of the air excess*

The graphic shows the power evolution in time while the air pressure varies. The excess means it is more or less than the hydrogen pressure (the number of times). In multiple periods the power goes to 0. This happens because the Fuel cell disconnects as the security measures activate, as the FC is starved of oxygen. This first happens at t=1293s. Therefore, an excess values of less than 2.2 will starve the Fuel cell. Usually an equal pressure in H2 and Oxygen should be enough, yet we can deduce that the optimization mechanism sets a very large value for the Hydrogen pressure, therefore the oxygen needs to compensate.

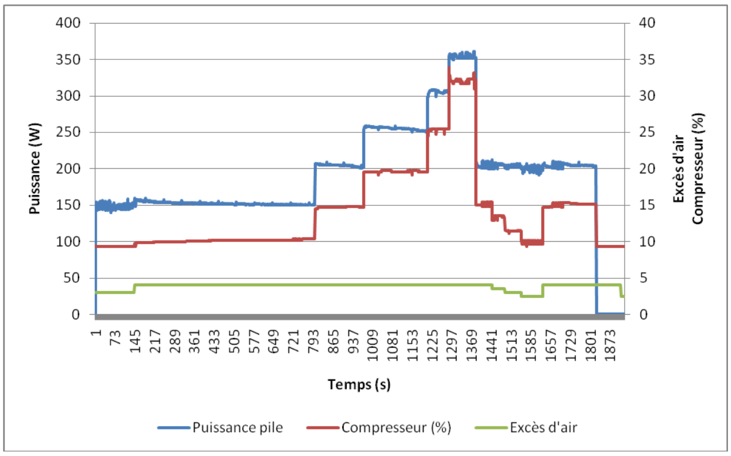

Figure B.7: (small H2 tank) FC power and air excess

Under this test, we can see very well the influence of the excess air ratio (without arriving in fault situation because of starvation). For 0 < t < 200 s, we observe that the power oscillates very strongly around the reference for an excess in air of 3. At t=148 s, we increase the excess air ratio to 4 and observe an amelioration in terms of power response stability. It has to be noted that the temperature was already at working parameters since the beginning of the simulation, therefore the temperature has no negative influence. Finally, for 1440 < t < 1700 s, we reduce the air excess and obtain a constant degradation of the power.

As a final conclusion, we can have a large air excess ratio with no problem. The only restriction is the high power consumption by the compressor. If the hydrogen is at a limit nominal value, then an air excess ratio of less that $2.2P_a$ is never enough.

B.3.5 *Program development*

The program is made in Labview. The constraint of this particular Fuel Cell is the dedicated labview software for data acquisition for which the source code is not accessible. On top of this basic program, one can manipulate the received data like in the following program.

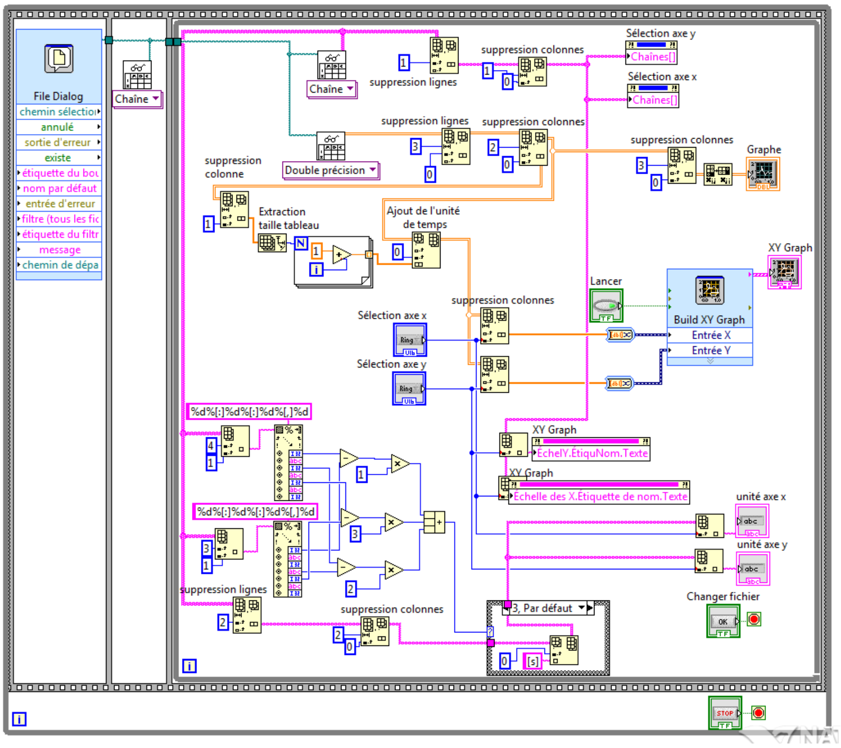

Figure B.8: Labview program

DAQ FC-42 Evaluation Kit

Date [DD.MM.YY]	Time [hh:mm:ss,000]	U FC [V]	I FC [A]	P FC [W]	T1 [°C]	TS [°C]	T2 [°C]	Excess	P1 H2 [bar]	P2 H2 [mbar]	Compr [%]	Cooler [ON/OFF]	Load
12.12.12	14:23:02,514	26,65	7,70	205,00	17,30	52,00	12,60	3,00	6,60	336,00	11,26	0,00	24,75
12.12.12	14:23:03,514	25,22	8,00	201,00	16,90	52,00	12,60	3,00	6,60	336,00	11,70	0,00	24,77
12.12.12	14:23:04,513	24,51	8,40	205,00	17,30	52,00	12,60	3,00	6,60	336,00	12,28	0,00	26,20
12.12.12	14:23:05,513	25,73	8,00	205,00	17,30	52,00	12,60	3,00	6,60	336,00	11,70	0,00	26,65
12.12.12	14:23:06,513	24,10	8,40	202,00	17,30	52,00	13,00	3,00	6,60	336,00	12,28	0,00	25,00
12.12.12	14:23:07,513	25,43	8,00	203,00	17,30	52,00	12,60	3,00	6,60	336,00	11,70	0,00	24,98
12.12.12	14:23:08,513	24,00	8,40	201,00	17,30	52,00	13,00	3,00	6,60	336,00	12,28	0,00	26,07
12.12.12	14:23:09,513	25,73	8,00	205,00	17,30	52,00	13,00	3,00	6,60	336,00	11,70	0,00	26,85
12.12.12	14:23:10,513	26,34	7,70	202,00	17,30	52,00	13,00	3,00	6,60	336,00	11,26	0,00	24,98
12.12.12	14:23:11,513	25,73	8,00	205,00	17,30	52,00	13,00	3,00	6,60	336,00	11,70	0,00	24,32
12.12.12	14:23:12,513	24,10	8,70	209,00	17,30	52,00	13,00	3,00	6,60	336,00	12,72	0,00	25,50
12.12.12	14:23:13,513	24,31	8,40	204,00	17,30	52,00	13,00	3,00	6,60	336,00	12,28	0,00	26,10
12.12.12	14:23:14,513	25,02	8,40	210,00	17,80	52,00	13,00	3,00	6,60	336,00	12,28	0,00	26,27
12.12.12	14:23:15,513	25,43	8,00	203,00	17,80	52,00	13,00	3,00	6,60	336,00	11,70	0,00	25,20
12.12.12	14:23:16,513	25,63	7,70	197,00	17,80	52,00	13,00	3,00	6,60	336,00	11,26	0,00	24,18
12.12.12	14:23:17,514	25,93	7,70	199,00	17,80	52,00	13,00	3,00	6,60	336,00	11,26	0,00	23,73
12.12.12	14:23:18,514	25,73	7,70	198,00	17,80	52,00	13,00	3,00	6,60	336,00	11,26	0,00	24,02
12.12.12	14:23:19,514	24,41	8,40	205,00	17,80	52,00	13,00	3,00	6,60	336,00	12,28	0,00	24,55
12.12.12	14:23:20,514	24,20	8,40	203,00	18,20	52,00	13,00	3,00	6,60	336,00	12,28	0,00	25,12
12.12.12	14:23:21,513	23,59	8,70	205,00	18,20	52,00	13,00	3,00	6,60	336,00	12,72	0,00	25,37
12.12.12	14:23:22,513	24,20	8,40	203,00	18,20	52,00	13,40	3,00	6,60	336,00	12,28	0,00	26,02
12.12.12	14:23:23,513	24,51	8,40	205,00	18,20	52,00	13,00	3,00	6,60	336,00	12,28	0,00	26,20
12.12.12	14:23:24,513	24,10	8,70	209,00	18,20	52,00	13,40	3,00	6,60	336,00	12,72	0,00	25,62
12.12.12	14:23:25,513	24,31	8,40	204,00	18,20	52,00	13,00	3,00	6,60	336,00	12,28	0,00	25,75
12.12.12	14:23:26,513	24,20	8,40	203,00	18,70	52,00	13,40	3,00	6,60	336,00	12,28	0,00	25,68
12.12.12	14:23:27,513	24,31	8,40	204,00	18,70	52,00	13,40	3,00	6,60	336,00	12,28	0,00	25,87
12.12.12	14:23:28,513	24,31	8,40	204,00	18,70	52,00	13,40	3,00	6,60	336,00	12,28	0,00	26,20
12.12.12	14:23:29,513	24,00	8,70	208,00	18,70	52,00	13,40	3,00	6,70	336,00	12,72	0,00	25,52
12.12.12	14:23:30,513	22,58	9,00	203,00	18,70	52,00	13,40	3,00	6,60	336,00	13,15	0,00	24,40
12.12.12	14:23:31,513	22,98	9,00	206,00	19,20	52,00	13,40	3,00	6,60	336,00	13,15	0,00	22,80
12.12.12	14:23:32,513	32,04	6,40	205,00	18,70	52,00	13,40	3,00	6,60	336,00	9,45	0,00	32,15
12.12.12	14:23:33,513	25,02	8,00	200,00	19,20	52,00	13,40	3,00	6,60	336,00	11,70	0,00	25,45
12.12.12	14:23:34,514	26,65	7,70	205,00	19,20	52,00	13,40	3,00	6,60	336,00	11,26	0,00	24,48
12.12.12	14:23:35,514	23,19	9,00	208,00	19,20	52,00	13,40	3,00	6,60	336,00	13,15	0,00	25,32
12.12.12	14:23:36,514	24,20	8,40	203,00	19,70	52,00	13,40	3,00	6,60	336,00	12,28	0,00	26,05
12.12.12	14:23:37,514	25,43	8,00	203,00	19,70	52,00	13,40	3,00	6,60	336,00	11,70	0,00	26,15
12.12.12	14:23:38,514	25,73	7,70	198,00	19,70	52,00	13,40	3,00	6,70	336,00	11,26	0,00	24,93
12.12.12	14:23:39,513	25,63	8,00	205,00	19,70	52,00	13,40	3,00	6,70	336,00	11,70	0,00	23,30
12.12.12	14:23:40,513	24,61	8,40	206,00	19,70	52,00	13,40	3,00	6,60	336,00	12,28	0,00	23,87
12.12.12	14:23:41,513	24,81	8,00	198,00	19,70	52,00	13,80	3,00	6,60	336,00	11,70	0,00	24,75
12.12.12	14:23:42,513	24,00	8,40	201,00	19,70	52,00	13,40	3,00	6,70	336,00	12,28	0,00	25,15
12.12.12	14:23:43,513	24,00	8,70	208,00	19,70	52,00	13,80	3,00	6,60	336,00	12,72	0,00	25,75
12.12.12	14:23:44,513	24,20	8,40	203,00	20,10	52,00	13,80	3,00	6,60	336,00	12,28	0,00	26,10
12.12.12	14:23:45,513	24,51	8,40	205,00	20,10	52,00	13,80	3,00	6,60	336,00	12,28	0,00	26,18
12.12.12	14:23:46,513	24,31	8,40	204,00	20,10	52,00	13,80	3,00	6,60	336,00	12,28	0,00	25,62
12.12.12	14:23:47,513	23,90	8,70	207,00	20,10	52,00	13,80	3,00	6,60	336,00	12,72	0,00	25,35
12.12.12	14:23:48,513	24,31	8,40	204,00	20,10	52,00	13,80	3,00	6,60	336,00	12,28	0,00	25,95
12.12.12	14:23:49,513	24,31	8,40	204,00	20,10	52,00	13,80	3,00	6,60	336,00	12,28	0,00	26,00

Figure B.9: Data received by the dedicated software

This will give us tables of data found in Annex B.9. This data can be then manipulated (ex: to obtain graphics):

The difficulty of this Fuel Cell platform lies in the fact that the serial communication protocol is proprietary, and the only communication possible is by means of the dedicated software provided with the device.

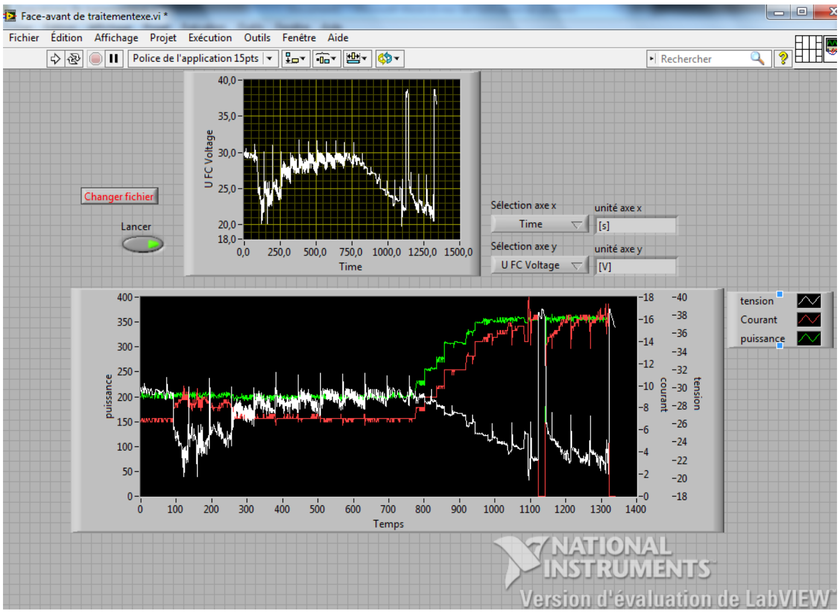

Figure B.10: Obtained graphics from the data

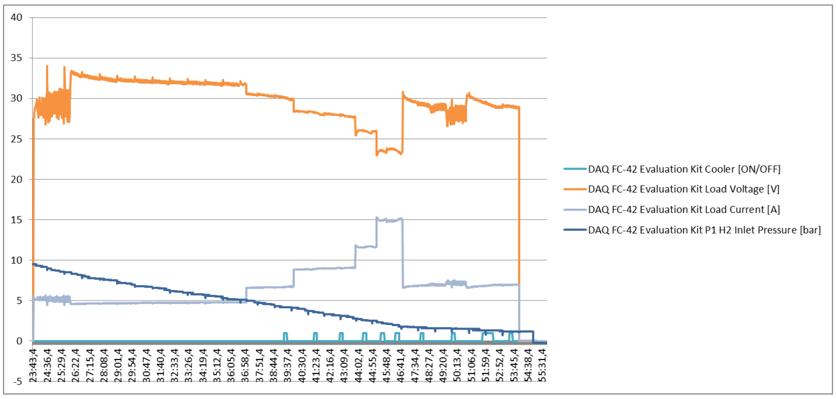

Figure B.11: Block view of fuel cell stack with auxiliary elements

Appendix C

Chapter Embedded

The values for the parameters in the three tank system are:

$$\begin{cases} Cp = 1.57 \cdot 10^{-6}\, m^3.s^{-1}.Pa^{-1/2} \\ \rho = 1000\, kg.m^{-3} \\ g = 9.81\, kg.m.s^{-2} \\ S = 0.0164\, m^2 \\ Qp = 10^{-4}\, m^3.s^{-1} \end{cases} \tag{C.1}$$

The TS representation of the three tank system has the following minimal/maximal premise variable values:

$$\begin{array}{l} z_{1_{\min}} = 0.5 \ ; \ z_{1_{\max}} = 2.5 \ ; \ z_{2_{\min}} = 2 \ ; \\ z_{2_{\max}} = 10 \ ; \ z_{3_{\min}} = 1.6 \ ; \ z_{3_{\max}} = 2.6 \end{array} \tag{C.2}$$

The obtained observer gains (and the other parameters found from the solution of the optimization problem) for the three tank system are:

$$
\begin{aligned}
L_1 &= \begin{bmatrix} 1.4887 \\ 6.2326 \end{bmatrix} \; L_2 = \begin{bmatrix} 13.4161 \\ -60.8919 \end{bmatrix} \\
L_3 &= \begin{bmatrix} 1.4887 \\ -6.3514 \end{bmatrix} \; L_4 = \begin{bmatrix} 13.4161 \\ -61.0108 \end{bmatrix} \\
L_5 &= \begin{bmatrix} 1.4293 \\ -6.2326 \end{bmatrix} \; L_6 = \begin{bmatrix} 13.3567 \\ -60.8919 \end{bmatrix} \\
L_7 &= \begin{bmatrix} 1.4293 \\ -6.3514 \end{bmatrix} \; L_8 = \begin{bmatrix} 13.3567 \\ -61.0108 \end{bmatrix}
\end{aligned} \tag{C.3}
$$

$$
P = \begin{bmatrix} 804.2900 & 175.5070 \\ 175.5070 & 63.1366 \end{bmatrix} \tag{C.4}
$$

$$
\begin{aligned}
Q_1 &= \begin{bmatrix} 103.4952 \\ -132.2248 \end{bmatrix} \; Q_2 = \begin{bmatrix} 103.4952 \\ -1489.8872 \end{bmatrix} \\
Q_3 &= \begin{bmatrix} 82.6354 \\ -139.7289 \end{bmatrix} \; Q_4 = \begin{bmatrix} 82.6354 \\ -1497.3913 \end{bmatrix} \\
Q_5 &= \begin{bmatrix} 55.6985 \\ -142.6547 \end{bmatrix} \; Q_6 = \begin{bmatrix} 55.6985 \\ -1500.3171 \end{bmatrix} \\
Q_7 &= \begin{bmatrix} 34.8387 \\ -105.1588 \end{bmatrix} \; Q_8 = \begin{bmatrix} 34.8387 \\ -1507.8212 \end{bmatrix}
\end{aligned} \tag{C.5}
$$

The communication timing for the serial protocol is defined in C.1.

The configuration of the matlab blocks of the type 'Packet Input/Output', that manages the communication with outside devices is presented in C.2.

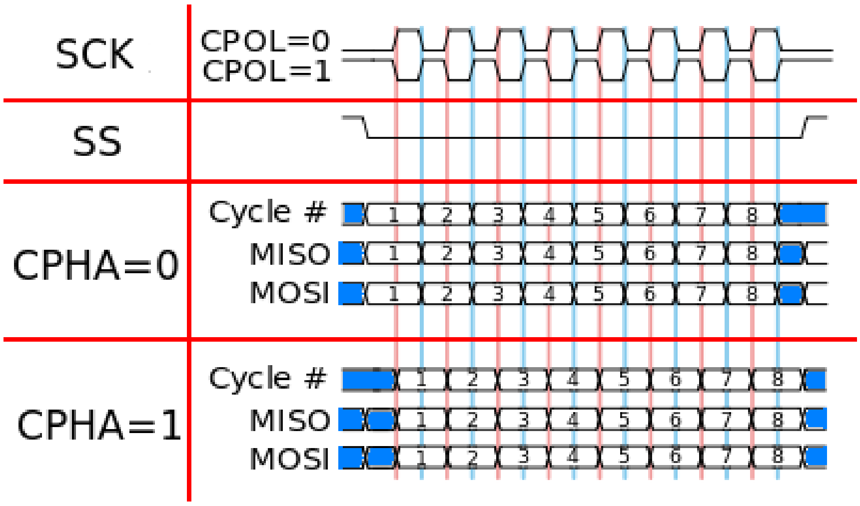

Figure C.1: Communication timing

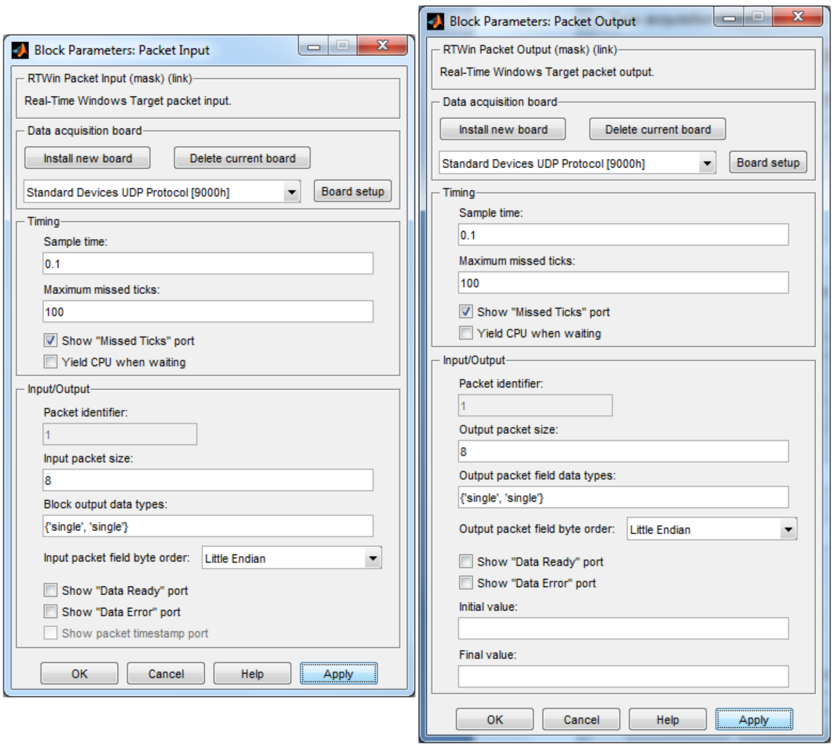

Figure C.2: Interface for the Packet Input block || Interface for the Packet Output block

Bibliography

Abdollahi, F., Talebi, H., and Patel, R. (2006). A stable neural network-based observer with application to flexible-joint manipulators. *Neural Networks, IEEE Transactions on*, 17(1):118–129.

Aitouche, A., Olteanu, S. C., and Ould Bouamama, B. (2012). Survey and analysis of diagnostic of fuel cell stack systems survey and analysis of diagnostic of fuel cell stack systems. In Zaragoza, A., editor, *8th IFAC Symposium on Fault Detection, Supervision and Safety of Technical Processes*. Elsevier BV.

Aitouche, A., Yang, Q., and Ould Bouamama, B. (2011). Fault detection and isolation of pem fuel cell system based on nonlinear analytical redundancy. *The European Physical Journal Applied Physics*, 54.

Alwi, H. and Edwards, C. (2013). Robust fault reconstruction for linear parameter varying systems using sliding mode observers. *Int. J. Robust. Nonlinear Control*, 24(14):1947–1968.

Amin, Bambang, R. T., Rohman, A. S., Dronkers, C. J., Ortega, R., and Sasongko, A. (2014). Energy management of fuel cell/battery/supercapacitor hybrid power sources using model predictive control. *IEEE Transactions on Industrial Informatics*, 10(4):1992–2002.

Aouaouda, S., Chadli, M., and Bouhali, O. (2013). Observer-based fault tolerant tracking control for vehicule lateral dynamics. In *2013 International Conference on Control, Decision and Information Technologies (CoDIT)*. Institute of Electrical & Electronics Engineers (IEEE).

Arcak, M., Gorgun, H., Pedersen, L., and Varigonda, S. (2004). A nonlinear observer design for fuel cell hydrogen estimation. *IEEE Transactions on Control Systems Technology*, 12(1):101–110.

Barbir, F. (2012). *PEM Fuel Cells: Theory and Practice*. Academic Press.

Barbir, F., Gorgun, H., and Wang, X. (2005). Relationship between pressure drop and cell resistance as a diagnostic tool for PEM fuel cells. *Journal of Power Sources*, 141(1):96–101.

Benallouch, M., Outbib, R., Boutayeb, M., and Laroche, E. (2008). A result on state estimation of nonlinear systems with application to fuel cell stacks. In *17th IFAC World Congress*, page CDROM, Seoul, South Korea.

Bergsten, P. and Palm, R. (2000). Thau-luenberger observers for TS fuzzy systems. In *Ninth IEEE International Conference on Fuzzy Systems. FUZZ- IEEE 2000 (Cat. No.00CH37063)*. Institute of Electrical & Electronics Engineers (IEEE).

Blanke, M., Kinnaert, M., Lunze, J., and Staroswiecki, M. (2006). *Diagnosis and Fault-Tolerant Control*. Springer Science Business Media.

Bonato, V., Marques, E., and Constantinides, G. A. (2007). A floating-point extended kalman filter implementation for autonomous mobile robots. In *2007 International Conference on Field Programmable Logic and Applications*. IEEE.

Bourdon, T., Saussol, L., and Varoquié, B. (2007). Integration of physical amesim® engine model in hardware in the loop environment, dedicated to engine control unit testing. *SAE Technical Paper Series*.

Boyd, S., Ghaoui, L. E., Feron, E., and Balakrishnan, V. (1994). *Linear Matrix Inequalities in System and Control Theory*. Society for Industrial & Applied Mathematics (SIAM).

Brunetto, C., Tina, G., Squadrito, G., and Moschetto, A. (2004). PEMFC diagnostics and modelling by electrochemical impedance spectroscopy. In *Proceedings of the 12th IEEE Mediterranean Electrotechnical Conference (IEEE Cat. No.04CH37521)*. Institute of Electrical & Electronics Engineers (IEEE).

Busawon, K. and Kabore, P. (2000). On the design of integral and proportional integral observers. In *Proceedings of the 2000 American Control Conference. ACC (IEEE Cat. No.00CH36334)*. Institute of Electrical & Electronics Engineers (IEEE).

Chadli, M. (2010). An LMI approach to design observer for unknown inputs takagi-sugeno fuzzy models. *Asian Journal of Control*, pages n/a–n/a.

Chadli, M., Akhenak, A., Ragot, J., and Maquin, D. (2008). On the design of observer for unknown inputs fuzzy models. *IJAAC*, 2(1):113–125.

Chen, J. and Patton, R. J. (1999). *Robust Model-Based Fault Diagnosis for Dynamic Systems*. Springer US.

Chen, J. and Zhou, B. (2008). Diagnosis of PEM fuel cell stack dynamic behaviors. *Journal of Power Sources*, 177(1):83–95.

Chen, W. and Saif, M. (2007). Design of a TS based fuzzy nonlinear unknown input observer with fault diagnosis applications. In *2007 American Control Conference*. Institute of Electrical & Electronics Engineers (IEEE).

Darouach, M., Zasadzinski, M., and Xu, S. J. (1994). Full-order observers for linear systems with unknown inputs. *IEEE transactions on automatic control*, 39(3):606–609.

de Lira, S., Puig, V., and Quevedo, J. (2010). Robust LPV model-based sensor fault diagnosis and estimation for a PEM fuel cell system. In *2010 Conference on Control and Fault-Tolerant Systems (SysTol)*. Institute of Electrical & Electronics Engineers (IEEE).

De Lira, S., Puig, V., Quevedo, J., and Husar, A. (2011). Lpv observer design for pem fuel cell system: Application to fault detection. *Journal of Power Sources*, 196(9):4298–4305.

Debenjak, A., Gašperin, M., Pregelj, B., Atanasijević-Kunc, M., Petrovčič, J., and Jovan, V. (2013). Detection of flooding and drying inside a pem fuel cell stack. *Strojniški vestnik-Journal of Mechanical Engineering*, 59(1):56–64.

Ding, S. X. (2013). *Model-Based Fault Diagnosis Techniques*. Springer London.

Djemili, I., Boulkroune, B., Aitouche, A., and Cocquempot, V. (2012). Nonlinear unknown input observer for intake leakage estimation in diesel engines. In *2012 20th Mediterranean Conference on Control & Automation (MED)*. Institute of Electrical & Electronics Engineers (IEEE).

Edwards, C., Spurgeon, S. K., Tan, C. P., and Patel, N. (2007). Sliding-mode observers. In *Mathematical Methods for Robust and Nonlinear Control*, pages 221–242. Springer Science Business Media.

Enrique, J., Castillo-Toledo, B., Ramirez-Cordova, C. J., and Eugenio (2008). Takagi-sugeno fuzzy observer for a switching bioprocess: Sector nonlinearity approach. In *New Developments in Robotics Automation and Control*. InTech.

Escobet, T., Feroldi, D., de Lira, S., Puig, V., Quevedo, J., Riera, J., and Serra, M. (2009). Model-based fault diagnosis in PEM fuel cell systems. *Journal of Power Sources*, 192(1):216–223.

Fiter, C., Hetel, L., Perruquetti, W., and Richard, J.-P. (2012). A state dependent sampling for linear state feedback. *Automatica*, 48(8):1860–1867.

Forrai, A., Funato, H., Yanagita, Y., and Kato, Y. (2005). Fuel-cell parameter estimation and diagnostics. *IEEE Transactions on Energy Conversion*, 20(3):668–675.

Fouquet, N., Doulet, C., Nouillant, C., Dauphin-Tanguy, G., and Ould-Bouamama, B. (2006). Model based PEM fuel cell state-of-health monitoring via ac impedance measurements. *Journal of Power Sources*, 159(2):905–913.

Gao, Z., Ding, S. X., and Ma, Y. (2007). Robust fault estimation approach and its application in vehicle lateral dynamic systems. *Optimal Control Applications and Methods*, 28(3):143–156.

Georg, S., Müller, M., and Schulte, H. (2014). Wind turbine model and observer in takagi-sugeno model structure. *Journal of Physics: Conference Series*, 555:012042.

Gertler, J. (1998). *Fault Detection and Diagnosis in Engineering Systems*. CRC Press.

Ghorbel, H., El Hajjaji, A., Souissi, M., and Chaabane, M. (2014). Robust tracking control for takagi–sugeno fuzzy systems with unmeasurable premise variables: Application to tank system. *Journal of Dynamic Systems, Measurement, and Control*, 136(4):041011.

Golabi, A., Beheshti, M., and Asemani, M. (2013). Dynamic observer-based controllers for linear uncertain systems. *Journal of Control Theory and Applications*, 11(2):193–199.

Goldberg, D. (1991). What every computer scientist should know about floating point arithmetic. *ACM Computing Surveys*, 23(1):5–48.

Gorgun, H., Arcak, M., and Barbir, F. (2005a). A voltage-based observer design for membrane water content in PEM fuel cells. In *Proceedings of the 2005, American Control Conference, 2005*. Institute of Electrical & Electronics Engineers (IEEE).

Gorgun, H., Arcak, M., Varigonda, S., and Bortoff, S. (2005b). Observer designs for fuel processing reactors in fuel cell power systems. *International Journal of Hydrogen Energy*, 30(4):447–457.

Hafaifa, A., Laaouad, F., and Laroussi, K. (2010). Fuzzy logic approach applied to the surge detection and isolation in centrifugal compressor. *Aut. Conrol Comp. Sci.*, 44(1):53–59.

Hernandez, A., Hissel, D., and Outbib, R. (2006). Fuel cell fault diagnosis: A stochastic approach. In *2006 IEEE International Symposium on Industrial Electronics*. Institute of Electrical & Electronics Engineers (IEEE).

Hinaje, M., Sadli, I., Martin, J.-P., Thounthong, P., Raël, S., and Davat, B. (2009). Online humidification diagnosis of a PEMFC using a static DC–DC converter. *International Journal of Hydrogen Energy*, 34(6):2718–2723.

Hissel, D., Péra, M., and Kauffmann, J. (2004). Diagnosis of automotive fuel cell power generators. *Journal of Power Sources*, 128(2):239–246.

Hosseini, M., Shamekhi, A. H., and Yazdani, A. (2012). Modeling and simulation of a pem fuel cell (pemfc) used in vehicles. *SAE Technical Paper Series*.

Hsieh, S.-S., Her, B.-S., and Huang, Y.-J. (2011). Effect of pressure drop in different flow fields on water accumulation and current distribution for a micro PEM fuel cell. *Energy Conversion and Management*, 52(2):975–982.

Hyun, D. and Kim, J. (2004). Study of external humidification method in proton exchange membrane fuel cell. *Journal of Power Sources*, 126(1-2):98–103.

Ichalal, D., Marx, B., Ragot, J., and Maquin, D. (2007). Conception d'observateurs pour un modèle de Takagi-Sugeno à variables de décision non mesurables. In *8ème conférence internationale des Sciences et Techniques de l'Automatique, STA'2007*, page CDROM, Sousse, Tunisia.

Ichalal, D., Marx, B., Ragot, J., and Maquin, D. (2009). An approach for the state estimation of takagi-sugeno models and application to sensor fault diagnosis. In *Proceedings of the 48h IEEE Conference on Decision and Control (CDC) held jointly with 2009 28th Chinese Control Conference*. Institute of Electrical & Electronics Engineers (IEEE).

Ichalal, D., Marx, B., Ragot, J., and Maquin, D. (2010). Fault tolerant control for takagi-sugeno systems with unmeasurable premise variables by trajectory tracking. In *2010 IEEE International Symposium on Industrial Electronics*. Institute of Electrical & Electronics Engineers (IEEE).

Ingimundarson, A., Stefanopoulou, A., and McKay, D. (2005). Model based detection of hydrogen leaks in a fuel cell stack. In *Proceedings of the 44th IEEE Conference on Decision and Control*. Institute of Electrical & Electronics Engineers (IEEE).

Ingimundarson, A., Stefanopoulou, A. G., McKay, D., et al. (2008).

Model-based detection of hydrogen leaks in a fuel cell stack. *Control Systems Technology, IEEE Transactions on*, 16(5):1004–1012.

Ito, K., Ashikaga, K., Masuda, H., Oshima, T., Kakimoto, Y., and Sasaki, K. (2008). Estimation of flooding in PEMFC gas diffusion layer by differential pressure measurement. *Journal of Power Sources*, 175(2):732–738.

Jamel, W., Khedher, A., Bouguila, N., and Othman, K. B. (2010). State estimation via observers with unknown inputs: Application to a particular class of uncertain takagi-sugeno systems. *Studies in Informatics and Control*, 19(3):219–228.

Jung, W. S., Han, S. H., and Ha, J. (2004). A fast BDD algorithm for large coherent fault trees analysis. *Reliability Engineering & System Safety*, 83(3):369–374.

Kang, G., Lee, W., and Sugeno, M. (1998). Design of tsk fuzzy controller based on tsk fuzzy model using pole placement. In *Fuzzy Systems Proceedings, 1998. IEEE World Congress on Computational Intelligence., The 1998 IEEE International Conference on*, volume 1, pages 246–251 vol.1.

Kazmi, I. H., Bhatti, A. I., and Iqbal, S. (2009). A nonlinear observer for PEM fuel cell system. In *2009 IEEE 13th International Multitopic Conference*. Institute of Electrical & Electronics Engineers (IEEE).

Kendoul, F., Lara, D., Fantoni, I., and Lozano, R. (2007). Real-time nonlinear embedded control for an autonomous quadrotor helicopter. *Journal of Guidance, Control, and Dynamics*, 30(4):1049–1061.

Khedher, A., Benothman, K., Maquin, D., and Benrejeb, M. (2010). An approach of faults estimation in takagi-sugeno fuzzy systems. In *ACS/IEEE International Conference on Computer Systems and Applications - AICCSA 2010*. Institute of Electrical & Electronics Engineers (IEEE).

Kim, E.-S., Kim, C.-J., and Eom, K.-S. (2007). Nonlinear observer design for pem fuel cell systems. In *Electrical Machines and Systems, 2007. ICEMS. International Conference on*, pages 1835–1839. IEEE.

Kim, J., Lee, J., and Cho, B. H. (2013). Equivalent circuit modeling of pem fuel cell degradation combined with a lfrc. *IEEE Trans. Ind. Electron.*, 60(11):5086–5094.

Kirubakaran, A., Jain, S., and Nema, R. (2009). A review on fuel cell technologies and power electronic interface. *Renewable and Sustainable Energy Reviews*, 13(9):2430–2440.

Kramer, D., Zhang, J., Shimoi, R., Lehmann, E., Wokaun, A., Shinohara, K., and Scherer, G. G. (2005). In situ diagnostic of two-phase flow phenomena in polymer electrolyte fuel cells by neutron imaging. *Electrochimica Acta*, 50(13):2603–2614.

Legros, B., Thivel, P.-X., Bultel, Y., Boinet, M., and Nogueira, R. P. (2009). Electrochemical impedance and acoustic emission survey of water desorption in nafion membranes. *Electrochemical and Solid-State Letters*, 12(7):B116.

Lendek, Z., Guerra, T. M., Babuška, R., and Schutter, B. D. (2011). *Stability Analysis and Nonlinear Observer Design Using Takagi-Sugeno Fuzzy Models*. Springer Berlin Heidelberg.

Lendek, Z., Lauber, J., Guerra, T.-M., Babuška, R., and De Schutter, B. (2010). Adaptive observers for ts fuzzy systems with unknown polynomial inputs. *Fuzzy Sets and Systems*, 161(15):2043–2065.

Li, Z., Outbib, R., Hissel, D., and Giurgea, S. (2014). Data-driven diagnosis of {PEM} fuel cell: A comparative study. *Control Engineering Practice*, 28(0):1 – 12.

Lim, C. and Haas, H. (2006). Diagnostic method for an electrochemical fuel cell and fuel cell components. US Patent App. 10/935,723.

Liu, W. and Wang, X. G. (2003). Fault diagnosis of a pem fuel cell system by sp model and on-line expert systems techniques. In Hamza, M. H., editor, *Modelling and Simulation*, pages 188–191. IASTED/ACTA Press.

Liu, Z., Mao, Z., Wu, B., Wang, L., and Schmidt, V. M. (2005). Current density distribution in PEFC. *Journal of Power Sources*, 141(2):205–210.

Luenberger, D. (1971). An introduction to observers. *IEEE Transactions on Automatic Control*, 16(6):596–602.

Lukic, S., Cao, J., Bansal, R., Rodriguez, F., and Emadi, A. (2008). Energy storage systems for automotive applications. *IEEE Trans. Ind. Electron.*, 55(6):2258–2267.

Maquin, D. (2009). State estimation and fault detection for systems described by takagi-sugeno nonlinear models. In *Proceedings of the 10th International Conference on Sciences and Techniques of Automatic Control and Computer Engineering*, pages 20–22.

Marquez, R., Guerra, T., Kruszewski, A., and Bernal, M. (2013). Improvements on non-pdc controller design for takagi-sugeno models. In *Fuzzy Systems (FUZZ), 2013 IEEE International Conference on*, pages 1–7.

Martinez-Guerra, R. and Diop, S. (2004). Diagnosis of nonlinear systems using an unknown-input observer: an algebraic and differential approach. *IEE Proceedings-Control Theory and Applications*, 151(1):130–135.

Marx, B., Koenig, D., and Ragot, J. (2007). Design of observers for takagi–sugeno descriptor systems with unknown inputs and application to fault diagnosis. *IET Control Theory & Applications*, 1(5):1487–1495.

Marx, B., Ragot, J., Maquin, D., and Ichalal, D. (2010). State estimation of takagi-sugeno systems with unmeasurable premise variables. *IET Control Theory & Applications*, 4(5):897–908.

Matraji, I., Laghrouche, S., and Wack, M. (2011). Cascade control of the moto-compressor of a pem fuel cell via second order sliding mode. *IEEE Conference on Decision and Control and European Control Conference*.

Maurya, M. R., Rengaswamy, R., and Venkatasubramanian, V. (2006). A signed directed graph-based systematic framework for steady-state malfunction diagnosis inside control loops. *Chemical Engineering Science*, 61(6):1790–1810.

Nesterov, Y. and Nemirovskii, A. (1994). *Interior-Point Polynomial Algorithms in Convex Programming*. Society for Industrial & Applied Mathematics (SIAM).

Nitsche, C., Schroedl, S., and Weiss, W. (2004). Onboard diagnostics concept for fuel cell vehicles using adaptive modelling. In *IEEE Intelligent Vehicles Symposium, 2004*. Institute of Electrical & Electronics Engineers (IEEE).

Olteanu, S. C., Aitouche, A., and Belkoura, L. (2014). Advances in p.e.m. fuel cell stack observer design using a takagi-sugeno approach with unmeasurable premise variables. *Springer Proceedings in Energy*, pages 117–130.

Olteanu, S. C., Aitouche, A., Oueidat, M., and Jouni, A. (2012). PEM fuel cell modeling and simulation via the takagi-sugeno fuzzy model. In *2012 International Conference on Renewable Energies for Developing Countries (REDEC)*. Institute of Electrical & Electronics Engineers (IEEE).

Omran, H., Hetel, L., Richard, J.-P., and Lamnabhi-Lagarrigue, F. (2013). Stabilité des systèmes non linéaires sous échantillonnage apériodique. *Journal Européen des Systèmes Automatisés*, 47(4-8):467–482.

Ouyessaad, H., Chafouk, H., and Lefebvre, D. (2013). Doubly fed induction generator fault diagnosis using unknown input takagi-sugeno observer. In *2013 International Conference on Control, Decision and Information Technologies (CoDIT)*. Institute of Electrical & Electronics Engineers (IEEE).

Patton, R. J., Frank, P. M., and Clark, R. N., editors (2000). *Issues of Fault Diagnosis for Dynamic Systems*. Springer Science Verlag London.

Pearce, C., Guckenberg, M., Holden, B., Leach, A., Hughes, R., Xie, C., Hassett, M., Adderley, A., Barnes, L., Sherriff, M., and Lewin, G. (2014). Designing a spatially aware, automated quadcopter using an android control system. In *Systems and Information Engineering Design Symposium (SIEDS), 2014*, pages 23–28.

Pekula, N., Heller, K., Chuang, P., Turhan, A., Mench, M., Brenizer, J., and Ünlü, K. (2005). Study of water distribution and transport in a polymer electrolyte fuel cell using neutron imaging. *Nuclear Instruments and Methods in Physics Research Section A: Accelerators, Spectrometers, Detectors and Associated Equipment*, 542(1-3):134–141.

Petrone, R., Zheng, Z., Hissel, D., Péra, M., Pianese, C., Sorrentino, M., Becherif, M., and Yousfi-Steiner, N. (2013). A review on model-based diagnosis methodologies for pemfcs. *International Journal of Hydrogen Energy*, 38(17):7077–7091.

Phanomchoeng, G., Rajamani, R., and Piyabongkarn, D. (2011). Nonlinear observer for bounded jacobian systems, with applications to automotive slip angle estimation. *Automatic Control, IEEE Transactions on*, 56(5):1163–1170.

Pilloni, A., Pisano, A., and Usai, E. (2015). Observer-based air excess ratio control of a PEM fuel cell system via high-order sliding mode. *IEEE Trans. Ind. Electron.*, 62(8):5236–5246.

Pisano, A., Salimbeni, D., Usai, E., Rakhtala, S., and Noei, A. (2013). Observer-based output feedback control of a pem fuel cell system by high-order sliding mode technique. In *Control Conference (ECC), 2013 European*, pages 2495–2500.

Poschke, F., Georg, S., and Schulte, H. (2014). Fault reconstruction using a takagi-sugeno sliding mode observer for the wind turbine benchmark. In *2014 UKACC International Conference on Control (CONTROL)*. Institute of Electrical & Electronics Engineers (IEEE).

Pukrushpan, J. T., Stefanopoulou, A. G., and Peng, H. (2004). Control of fuel cell power systems. *Advances in Industrial Control*.

Rajamani, R. (1998). Observers for lipschitz nonlinear systems. *IEEE Transactions on Automatic Control*, 43(3):397–401.

Rallières, O. (2011). *Modelisation and characterization of fuel cell and PEM electrolyzer*. Theses, Institut National Polytechnique de Toulouse - INPT.

Riascos, L. A. M., Simoes, M. G., and Miyagi, P. E. (2007). A bayesian network fault diagnostic system for proton exchange membrane fuel cells. *Journal of Power Sources*, 165(1):267–278.

Riascos, L. A. M., Simoes, M. G., and Miyagi, P. E. (2008). On-line fault diagnostic system for proton exchange membrane fuel cells. *Journal of Power Sources*, 175(1):419–429.

Rincon-Pasaye, J. J., Martinez-Guerra, R., and Soria-Lopez, A. (2008). Fault diagnosis in nonlinear systems: An application to a three-tank system. In *2008 American Control Conference*. IEEE.

Salim, R. I., Noura, H., and Fardoun, A. (2013). A review on fault diagnosis tools of the proton exchange membrane fuel cell. In *2013 Conference on Control and Fault-Tolerant Systems (SysTol)*. Institute of Electrical & Electronics Engineers (IEEE).

Schutz, D., Legat, C., and Vogel-Heuser, B. (2014). MDE of manufacturing automation software — integrating SysML and standard development tools. In *2014 12th IEEE International Conference on Industrial Informatics (INDIN)*. IEEE.

Shamma, J. and Cloutier, J. R. (1992). A linear parameter varying approach to gain scheduled missile autopilot design. In *American Control Conference, 1992*, pages 1317–1321.

Sinha, N. K., editor (1986). *Microprocessor-Based Control Systems*. Springer Netherlands.

Slotine, J.-J., Hedrick, J., and Misawa, E. (1986). On sliding observers for nonlinear systems. In *American Control Conference, 1986*, pages 1794–1800.

Sontag, E. D. (1995). On the input-to-state stability property. *Systems & Control Letters*, 24:351–359.

Spiegel, C. (2008). *PEM fuel cell modeling and simulation using Matlab*. Academic Press/Elsevier, Amsterdam Boston.

Steiner, N. Y., Hissel, D., Moçotéguy, P., and Candusso, D. (2011). Non intrusive diagnosis of polymer electrolyte fuel cells by wavelet packet transform. *International Journal of Hydrogen Energy*, 36(1):740–746.

Stumper, J., Löhr, M., and Hamada, S. (2005). Diagnostic tools for liquid water in PEM fuel cells. *Journal of Power Sources*, 143(1-2):150–157.

Sugeno, M. and Kang, G. (1988). Structure identification of fuzzy model. *Fuzzy Sets and Systems*, 28(1):15 – 33.

Takagi, T. and Sugeno, M. (1985). Fuzzy identification of systems and its applications to modeling and control. *Systems, Man and Cybernetics, IEEE Transactions on*, SMC-15(1):116–132.

Tanaka, K. and Wang, H. O. (2001). *Fuzzy Control Systems Design and Analysis*. John Wiley & Sons, Inc.

Teranishi, K., Tsushima, S., and Hirai, S. (2006). Analysis of water transport in PEFCs by magnetic resonance imaging measurement. *Journal of The Electrochemical Society*, 153(4):A664.

Thau, F. E. (1973). Observing the state of non-linear dynamic systems†. *International Journal of Control*, 17(3):471–479.

Thomas, C. (2009). Fuel cell and battery electric vehicles compared. *International Journal of Hydrogen Energy*, 34(15):6005–6020.

Trumpf, J. (2007). Observers for linear time-varying systems. *Linear Algebra and its Applications*, 425(2-3):303–312.

Turner, W., Parten, M., Vines, D., Jones, J., and Maxwell, T. (1999). Modeling a pem fuel cell for use in a hybrid electric vehicle. In *Vehicular Technology Conference, 1999 IEEE 49th*, volume 2, pages 1385–1388 vol.2.

Utkin, V. I. (1978). *Sliding Modes and their Application in Variable Structure Systems*. MIR Publishers.

VADIM, I. U. (1977). Survey paper variable structure systems with sliding modes. *IEEE Transactions on Automatic control*, 22(2).

Venkatasubramanian, V., Rengaswamy, R., Kavuri, S. N., and Yin, K. (2003). A review of process fault detection and diagnosis. *Computers & Chemical Engineering*, 27(3):327–346.

Vepa, R. (2012). Adaptive state estimation of a PEM fuel cell. *IEEE Transactions on Energy Conversion*, 27(2):457–467.

Walcott, B. and Zak, S. (1987). State observation of nonlinear uncertain dynamical systems. *IEEE Transactions on Automatic Control*, 32(2):166–170.

Wang, H., Tanaka, K., and Griffin, M. (1995). Parallel distributed compensation of nonlinear systems by takagi-sugeno fuzzy model. In *Proceedings of 1995 IEEE International Conference on Fuzzy Systems. The International Joint Conference of the Fourth IEEE International Conference on Fuzzy Systems and The Second International Fuzzy Engineering Symposium*. Institute of Electrical & Electronics Engineers (IEEE).

WU, J., YUAN, X., WANG, H., BLANCO, M., MARTIN, J., and ZHANG, J. (2008a). Diagnostic tools in PEM fuel cell research: Part i electrochemical techniques. *International Journal of Hydrogen Energy*, 33(6):1735–1746.

WU, J., ZIYUAN, X., WANG, H., BLANCO, M., MARTIN, J., and ZHANG, J. (2008b). Diagnostic tools in PEM fuel cell research: Part IIPhysical/chemical methods. *International Journal of Hydrogen Energy*, 33(6):1747–1757.

Yacine, Z., Ichalal, D., Oufroukh, N. A., Mammar, S., and Djennoune, S. (2012). Nonlinear vehicle lateral dynamics estimation with unmeasurable premise variable takagi-sugeno approach. *2012 20th Mediterranean Conference on Control & Automation (MED)*.

Yang, Q., Aitouche, A., and Bouamama, B. (2009). Structural analysis for fault detection and isolation in fuel cell stack system. In Howlett, R., Jain, L., and Lee, S., editors, *Sustainability in Energy and Buildings*, pages 239–254. Springer Berlin Heidelberg.

Yang, W., Lee, K. Y., Junker, S. T., and Ghezel-Ayagh, H. (2008). Fault diagnosis and accommodation system with a hybrid model for fuel cell power plant. In *2008 IEEE Power and Energy Society General Meeting - Conversion and Delivery of Electrical Energy in the 21st Century*. Institute of Electrical & Electronics Engineers (IEEE).

Youssef, T., Chadli, M., Karimi, H., and Zelmat, M. (2014a). Design of unknown inputs proportional integral observers for TS fuzzy models. *Neurocomputing*, 123:156–165.

Youssef, T., Karimi, H. R., and Chadli, M. (2014b). Faults diagnosis based on proportional integral observer for TS fuzzy model with unmeasurable premise variable. In *2014 IEEE International Conference on Fuzzy Systems (FUZZ-IEEE)*. Institute of Electrical & Electronics Engineers (IEEE).

Yuan, X., Sun, J. C., Wang, H., and Zhang, J. (2006). AC impedance diagnosis of a 500w PEM fuel cell stack. *Journal of Power Sources*, 161(2):929–937.

Yuan, X., Wang, H., Colinsun, J., and Zhang, J. (2007). AC impedance technique in PEM fuel cell diagnosis—a review. *International Journal of Hydrogen Energy*, 32(17):4365–4380.

Zander, J., Schieferdecker, I., and Mosterman, P. J. . (2011). *Model-Based Testing for Embedded Systems (Computational Analysis, Synthesis, and Design of Dynamic Systems)*. CRC Press.

Zemouche, A. and Boutayeb, M. (2007). A new observer design method for a class of lipschitz nonlinear discrete-time systems with time-delay. extension to hinf performance analysis. In *Decision and Control, 2007 46th IEEE Conference on*, pages 414–419.

Zemouche, A. and Boutayeb, M. (2012). Observers design for discrete-time lipschitz nonlinear systems. state of the art and new results. In *Decision and Control (CDC), 2012 IEEE 51st Annual Conference on*, pages 4780–4785.

Zemouche, A. and Boutayeb, M. (2013). On {LMI} conditions to design observers for lipschitz nonlinear systems. *Automatica*, 49(2):585 – 591.

Zhang, J., Zhang, H., Wu, J., and Zhang, J. (2013). Techniques for pem fuel cell testing and diagnosis. *Pem Fuel Cell Testing and Diagnosis*, pages 81–119.

Zhao, D. (2013). Control of an ultrahigh speed centrifugal compressor for the air management of fuel cell systems. *Thesis*.

Abstract: The thesis contributes to the observer and diagnosis design for Polymer Electrolyte Membrane Fuel Cells using Takagi-Sugeno theory. There are three research objectives in this thesis. First is focused on modeling, estimation and diagnostics. The dynamic nonlinear model of PEMFCs is proposed, which considers the auxiliary components. In terms of parameter estimation for PEMFCs, a nonlinear approach is developed to design observers based on the nonlinear Takagi-Sugeno model in order to achieve a more robust estimation. The observers can replace the mass flow sensors which results in getting rid of expensive and cumbersome to install instrumentation for measurement of mass flow rates. By using such observers to develop algorithms for diagnosis, the fuel cell stack's life can be prolonged. A simple method of diagnostic based on PI observer for state and sensor fault detection has been investigated. The second topic on embedding nonlinear algorithms, acts upon the potential of using small scaled embedded systems for complex tasks, thus reducing cost and physical size of the automatic system. More precisely the use of the Takagi-Sugeno approach in embedded applications is investigated. Different solutions for embedded observers have been provided. The last topic was the testing of these embedded solutions for fuel cell system in a Hardware In the Loop architecture, based on the professional software AMESim and Matlab for a Windows operating system. A real Fuel Cell has been used in order to configure the validation tests.

Keywords: *state estimation, fault estimation, nonlinear observer, Takagi-Sugeno, fuel cell, embedded system, LMI, HIL validation.*

Résumé: La thèse contribue à la conception des observateurs et au diagnostic pour les piles à combustible de type 'membrane échangeuse de protons' en utilisant la théorie Takagi-Sugeno. Il y a trois objectifs de recherche dans cette thèse. La première est axée sur la modélisation, l'estimation et le diagnostic basés sur une représentation Takagi-Sugeno. Le modèle dynamique non linéaire de la pile est proposé, en considérant les composants auxiliaires. En termes d'estimation de paramètre, une approche est développée pour concevoir des observateurs basés sur des modèles non linéaires afin de parvenir à une estimation plus robuste. Les observateurs peuvent remplacer les capteurs de débit massique dont l'instrumentation est chère et difficile d'implémenter pour la mesure du débit massique. En utilisant de tels observateurs pour développer des algorithmes pour le diagnostic, la durée de vie de l'empilement de piles à combustible peut être prolongée. Une méthode de diagnostic basée sur un observateur PI pour l'estimation d'état et de défaut du capteur a été étudiée. Le deuxième objectif sur des algorithmes non linéaires embarqués, agit sur le potentiel de l'utilisation de systèmes embarqués de petite échelle pour des tâches complexes, réduisant ainsi le coût et la taille physique du système. Plus précisément, l'utilisation de l'approche de Takagi-Sugeno dans les applications embarquées a été développée. Différentes solutions pour les observateurs embarqués ont été fournies. Le dernier objectif concerne les tests de ces algorithmes embarqués pour des piles à combustible dans une architecture HIL, avec le logiciel professionnel AMESim et Matlab dans un environnement d'exploitation Windows. Une pile à combustible réelle a été utilisée pour configurer les test de validation.

Mots clés: *estimation d'état, estimation de défaut, Pile à Combustible, observateur non-linéaire, Takagi-Sugeno, système embarqué, LMI, validation HIL.*

